DETECTION OF DNA METHYLATION OF MULTIPLE TUMOR SUPRESSOR P16^{INK4A} GENE BY POLYTHIOPHENE BASED OPTICAL SENSOR

A Thesis Submitted to
the Graduate School of Engineering and Sciences of
İzmir Institute of Technology
in Partial Fulfillment of the Requirements for the Degree of

MASTER OF SCIENCE

in Biotechnology

by
Hakan KAYA

December 2018
İZMİR

We approve the thesis of **Hakan KAYA**

Examining Committee Members:

Assoc. Prof. Dr. Ümit Hakan YILDIZ
Department of Chemistry, İzmir Institute of Technology

Prof. Dr. Canan VARLIKLI
Department of Photonics, İzmir Institute of Technology

Assist. Prof. Dr. Altuğ KOÇ
Department of Medical Genetics, Dokuz Eylül University

05 December 2018

Assoc. Prof. Dr. Ümit Hakan YILDIZ
Supervisor, Department of Chemistry
İzmir Institute of Technology

Prof. Dr. Nuran ELMACI IRMAK
Co-Supervisor, Department of Chemistry
İzmir Institute of Technology

Assoc. Prof. Dr. Engin ÖZÇİVİCİ
Head of the Department of Bioengineering

Prof. Dr. Aysun SOFUOĞLU
Dean of the Graduate School of Engineering and Science

ACKNOWLEDGMENT

First of all, I would like to express my sincere appreciation to my supervisor Assoc. Prof. Dr. Ümit Hakan YILDIZ for his professional guidance, suggestions, encouragement, understanding and endless patience not only throughout this study but also for other situations.

I would like to thank to my co-supervisor Prof. Dr. Nuran ELMACI IRMAK for her beneficial suggestions, guidance and valuable comments for this study. I am also thankful to Asist. Prof. Dr. Ahu ARSLAN YILDIZ for her valuable comments, suggestions and patience for this study.

I wish to express my thankfulness to my co-workers, Sezer ÖZENLER and Müge YÜCEL for their encourage and help during my throughout thesis study. I wish also thank to Mustafa Umut MUTLU, Soner KARABACAK and the rest of Biomimetics and BioSens & BioApps groups for their good friendship, helps and supports.

Finally, I want to express my deepest gratitude and love to my parents Arife KAYA, Turan KAYA and my sister Pınar KAYA YILMAZ for their understanding and encouragement that they have showed in every stage of my life, including this thesis. I would not be able to finish my study without these people.

ABSTRACT

DETECTION OF DNA METHYLATION OF MULTIPLE TUMOR SUPRESSOR P16^{INK4A} GENE BY POLYTHIOPHENE BASED OPTICAL SENSOR

DNA methylation is epigenetic events commonly occurs in mammalian genome starting from formation of embryo to the end of life. Especially, hypermethylation in tumor suppressor genes, corresponds the cancer growth and detection of DNA methylation in these genes crucial for the diagnosis of cancer. Water soluble polythiophenes are frequently used for the detection of biomolecules through the optoelectronic properties.

In this study, detection of DNA methylation of multiple tumor suppressor p16^{INK4A} gene via polythiophene based optical sensor was achieved. Newly designed, synthesized and characterized poly(1-(3-((4-methylthiophen-3-yl) oxy) propyl)-1,4-diazabicyclo [2.2.2] octan-1-ium bromide) was used during characterization of DNA sequences and detection of DNA methylation. The target sequence position is +137 to +156 in p16^{INK4A} gene which have three potential CG dinucleotide to be methylated. Detection of DNA methylation based on sodium bisulfite treatment, complementary sequence of unmethylated ssDNA and the conformational change of water soluble polythiophene. In our fluorometric analysis, unmethylated sequence/complementary successfully hybridized and dsDNA I_o/I ratio is under the 1.40 while the methylated sequence/complementary hybridization failed due to different base content and remain as ssDNA and, I_o/I ratio is higher than 1,60. The novelty of work is detection mechanism is PCR and FRET free with a range of 300 ng to 700 ng sample requirement.

Characterization of homopurines, homopyrimidines, methylated and unmethylated sequence with cationic polythiophenes also accomplished. PolyG (10), polyG (20) and polyA (10) yielded a no signal in UV-VIS region while the polyA (20) yielded a 100 nm red shift. Furthermore, PolyC (10), PolyC (20), PolyT (10), PolyT (20) yielded three vibrionic peaks at 505 nm, 545 nm and 595 nm with different intensities and unique isosbestic points. All 10 bases long homopyrimidine and homopurine have a unique quencher character with cationic polythiophene. Lastly, conformational change of polythiophene investigated with computational methods and heptamer used as a model.

ÖZET

POLİTİYOFEN TABANLI OPTİK SENSÖR İLE ÇOKLU TÜMÖR BASKILAYICI p16INK4A GENİNDEKİ DNA METİLASYONU TAYİNİ

DNA metilasyonu, embriyonun oluşmasından başlayarak yaşamın sonuna kadar kadar memeli genomunda yaygın olarak görülen epigenetik olaylardır. Özellikle tümör basklıyacı genlerde oluşan hipermetilasyonlar kanser büyümesine neden olurlar ve bu genlerdeki DNA metilasyon tespiti kanser teşhisi için kritiktir. Suda çözünen tiyofenler optoelektronik özelliklerinden dolayı biyomoleküllerin tayininde sıklıkla kullanılmaktadır.

Bu çalışmada, politiyofen tabanlı optic sensor ile çoklu tümör baskılayıcı $p16^{INK4A}$ genindeki DNA metilasyonu tayini başarılı bir şekilde yapıldı. Dizayn edilen, sentezlenen ve karakterizasyonu yapılan poly(1-(3-((4-metiltiyofen-3-il) oksi) propil)-1,4-diazabisiklo [2.2.2] oktan-1-yum bromür) DNA sekanslarının karakterizasyonunda ve DNA metilasyon tayininde kullanıldı. $p16^{INK4A}$ genindeki üç tane potansiyel metillenebilir CG dinükleotidi bulunan hedef sekansın pozisyonu +137 ile +156 arasındadır. DNA metilasyonun tayininin temeli, sodium bisulfit işlemine, metillenmemiş sekansın tamamlayıcı sekansına ve politiyofenin konformasyonal değişimine dayanmaktadır. Yapılan florometrik analizler sonucunda, metillenmemiş sekans/tamamlayıcı sekans ile başarılı bir şekilde hibridize oldu ve çift sarmal DNA I_o/I oranı 1.40 değerinin altında bulundu. Metilli sekans/tamamlayıcı sekansın hibridizasyonu farklı baz içeriği yüzünden başarısız oldu ve tek sarmal DNA olarak kaldı ve I_o/I oranı 1.60 değerinin üzerinde bulundu. Bu çalışmanın yenilikçi tarafı, PCR ve FRET bağımsız tayin metodu olup 300 ng ile 700 ng aralığında örnek miktarın tayin için yeterli olmasıdır.

Aynı zamanda katyonik tiyofen ile homopürin, homopirimidin, metilli sekans ve metilsiz sekansıların karakterizasyonları başarı ile gerçekleştirildi. PolyG (10), polyG (20) and polyA (10) için UV-VIS bölgesinde sinyal değişimi gözlemlenmezken polyA (20) 100 nm lik bir kırmızı kaymaya neden oldu. Buna ek olarak, PolyC (10), PolyC (20), PolyT (10), PolyT (20) için farkı şiddete ve eşsiz isosbestik noktasına sahip olan 505 nm, 545 nm ve 595 nm de üç sinyal gözlemlendi. Politiyofenin konformasyonal değişimi hesaplamalı metodlarla araştırılarak yedimer model olarak seçilmiştir.

TABLE OF CONTENTS

LIST OF FIGURES

Figure **Page**

LIST OF TABLES

Table **Page**

CHAPTER 1

INTRODUCTION

1.1. Conjugated Polythiophenes

Discovery of polyacetylene lead the new class of π-conjugated conducting polymer[1]. An important step for π-conjugated conducting polymers, is the oxidative electropolymerization of polypyrole[2]. Then different heteroaromatic molecules use as a target molecules for the electropolymerization such as thiophene[3], furan, indole[4], carbazole, azulene, pyrene[5], benzene[6] and fluorene[7]. To considered five membered aromatic heterocycles, thiophene has the most aromatic structure compared to pyrrole and furan Polythiophene rapidly became a main promising and model polymer for the futuristic works among the numerous conductive polymers (Figure 1). For this reason, over the past few decades polythiophene focused for both academicals and industrial works. Conjugated polythiophene is candidate for the lots of next generation electronic and optical devices due to low cost, ease of processing, thermal stability, tunable electronic properties and optical gaps. These unique physical and chemical properties of polythiophene is ensure the use in different fields such as field effective transistors (FET)[8], organic light emitting diodes (OLED)[9], photovoltaic devices[10], solar cells[11] and biosensors[12].

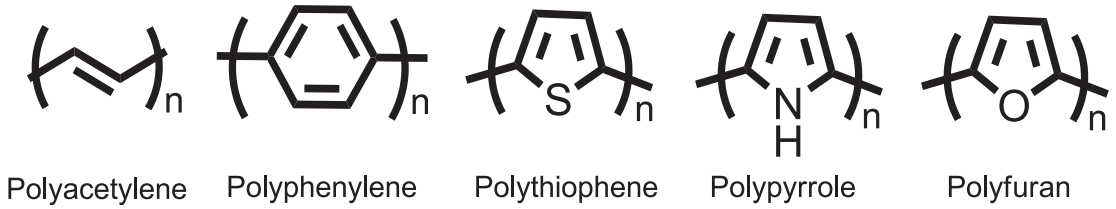

Figure 1. Structure of conductive polymers

"There are five factors tune the band gap of polythiophene and these are; bond length alteration, resonance effect, substitute group, dihedral angle between monomer units and intramolecular interaction" (*Wang et all*. 2014, Figure 2)[13]. Originally four

factors shown in Figure 2, affect the π electron delocalization along the backbone of polythiophene except the resonance effect. Resonance effect in polythiophene chain labelled as formation of polaron (radical cation) and bipolaron (radical dication) which abstraction of one electron from the HOMO level and abstraction of two electron from the HOMO level, respectively. Nominately the optoelectronic properties of polythiophene originated from the delocalization of π electron along the carbon backbone[14]. Optoelectronic properties of polythiophene proportional to substitute group of the ring which substitute group affect the position of the monomer unit in the space. The optoelectronic properties of thiophene also tuned through doping. Doping of the thiophene proceed three different ways which are chemically, electrochemically and presence of the external electric field[15-17]. The band gap of the polythiophene can be tuned with both substituted group and the dopant level from the 3 eV to 1eV[18, 19].

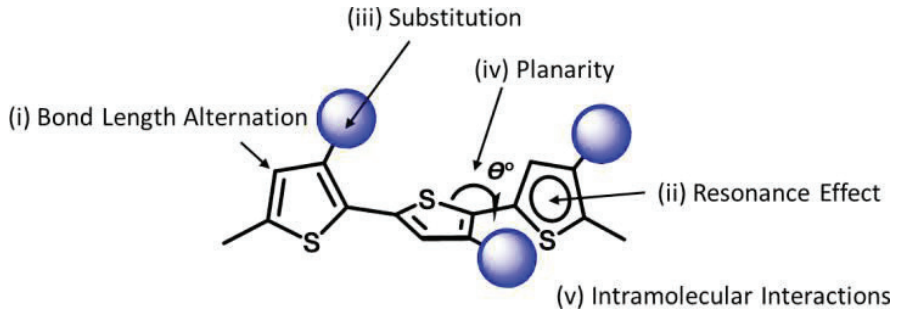

Figure 2. Determination of band gap of polythiophene with 5 factors

There are many methods available for the substitution of thiophene ring[20]. These substitution methods were applied both α and β position of thiophene ring. Mostly thiophene ring substituted at β position and polymer chain elongated at α position. In the nature of the thiophene, α position 100 times reactive then the β position of ring. However, regularity of polymer chain is crucial for the electrical device materials. Therefore, almost all polythiophene materials substituted at β position of ring. Figure 3 shows the α and β position of both unsubstituted and substitute thiophene ring. In unsubstituted thiophene α position named as 2' and 5' while the 2' and 5' also named as head (H) and tail (T) to considering substituted thiophene (R_1= functional group or CH_3, R_2=H or CH_3). β position of both unsubstituted and substituted thiophene ring named as 3' and 4' position.

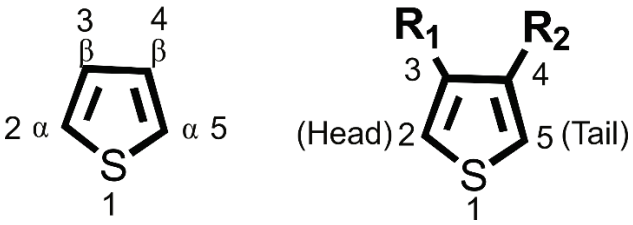

Figure 3. Unsubstituted and substituted thiophene ring positions

Thiophene substitution reaction proceed through electrophilic addition, nucleophilic addition or radical reaction. Electrophilic addition is historical with the nature of the thiophene while nucleophilic addition and radical reaction developed with the modern thiophene chemistry. The structure of polythiophene affect the physical properties of polymer and it determines the interchain overlap with elimination of structural defect. Also, substitute group of thiophene magnitude or reduce the π electron delocalization along the backbone and enhance the π-π stacking in two dimensions. Countless theoretical studies have been performed to examine the electrical properties of thiophene derivatives. In these works, effect of both substitute group and dopant level of polythiophene investigated[20-22]. Generally, short oligomers chosen as model molecule to predict the electrical and optical properties of polythiophenes with the computational methods. To considered short oligomers, alteration of structure or conformation are not expensive and ease of computing. Furthermore, monolayer structure of oligothiophene used in theoretical modelling with methods; density functional theory (DFT)[23], first-principle calculations[24] and periodic boundary conditions (PBC)[25]. All type of theoretical methods aimed to explore the optoelectronic properties of polythiophene with the different structure and conformation while some of studies focused on the relationship between theoretical calculation and experimental[26].

1.2. Coupling of Thiophene

Two main different routes are available for the synthesis of polythiophene that electrochemical and chemical synthesis[27]. In early stage, electrochemical synthesis of polythiophene is mostly used in many research. However undesirable polymer and oligomer, α-β coupling produce a defective chain. To achieve the α-α coupling of substitute and unsubstituted polythiophene several chemical synthetic routes were reported. Condensation polymerization with using metal catalyst have been reported by Yamamoto[28], Lin and Dudek[29]. Both method have a low final molecular weight of

polymer. Then, Suzuki[30], Negishi[31], Kumada[32] and Stille[33] metal mediated coupling reaction have been reported. Substitution of thiophene with an alkyl group reveals the new phenomenon which is regioregularity of polymer. Regioregularity is the idea of the all thiophene ring coupled with the same HT content. Rieke coupling yield the 98,5% regioregular polymer chain[34]. McCullough coupling route yield a 100% HT content of polythiophene[35]. Current metal mediated coupling reaction yield a regioregular and regioirregular polymerization with lots of disadvantages such as prefunctionalization of monomers, extra preparation steps, additional purification and harsh condition to yield an active monomer. Different aspect of the polymerization of thiophene reported by Sugimoto in 1984 with using $FeCl_3$[36]. This oxidative polymerization was not yield a regioregular polythiophene. In the contrary the product of polymerization by using $FeCl_3$ yield a regioirregular polymers. Regioirregular polymer chains contain all probable coupling type that head to tail (HT), tail to tail (TT) and head to head (HH) (Figure 4). To yield a regioregular polymer slow addition of ferric chloride have been studied and accomplished 94% HT content[37].

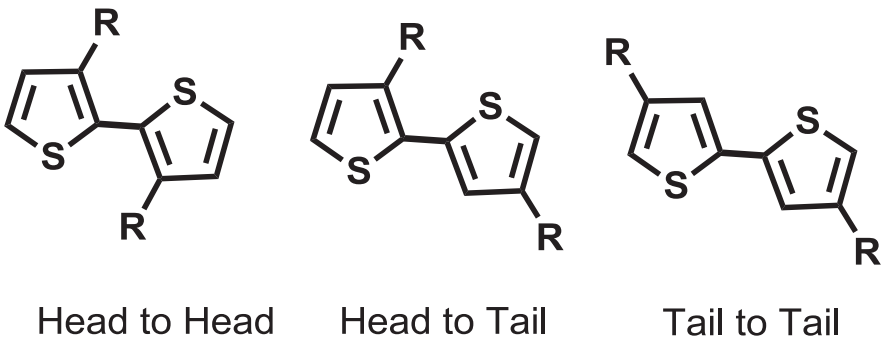

Figure 4. Coupling type of monomer units

To eliminate the disadvantages of the metal mediated coupling reaction direct arylation polymerization (DArP) developed which is cost-effective and efficient method. Recently, DArP become a promising alternative synthetic route of polymerization of π-conjugated polymers[38-44]. New alternative methods of polymerization of π-conjugated systems still studying to achieve the control of regioregularity of the polymer chain. Regioregularity is the essential properties of the polythiophene chain while designing the electrical devices. Metal mediated coupling reaction developed to yield a regioregular polymer chain and yield a desired coupling type different than HT content. The coupling type of two monomer units also affect the positions of monomer units in space, π delocalization through the carbon backbone. Briefly, coupling type of two monomer units

in polymer chain have a great influence in the band gap of the π-conjugated systems. Represented regioirregular and regioregular polymer chain shown in Figure 5.

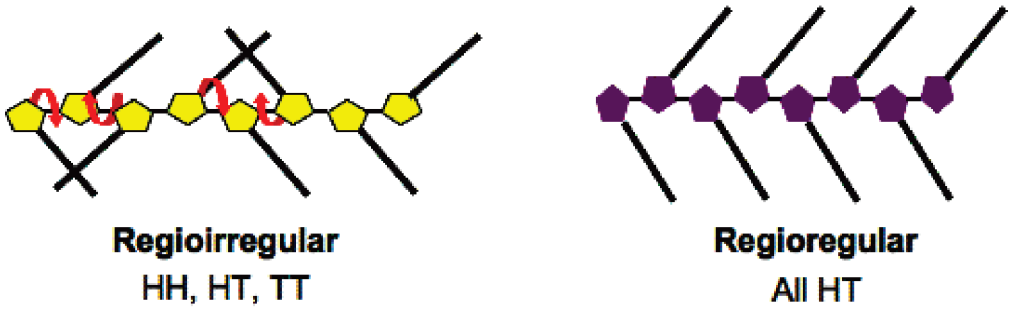

Figure 5. Represented regioregular and regioirregular polymer chain[45]

1.3. Optical Properties of Cationic Polythiophenes

Highly sensitive optical response of polythiophene provide a variety of application in many fields[46-48]. Especially in biological and analytical applications conjugated cationic polythiophene focused due to the unique solubility and optical properties. Substitution of thiophene with a cationic functional group such as quaternary ammonium salts and substituted phosphonium enhance the solubility and processability. Introduction of substituent group to the thiophene ring actualized 3' or both 3' and 4' positions. Furthermore, addition of substituent group affects the optical properties with a distortion of π-conjugation. The optical properties of cationic polythiophenes highly dependent on their regioregularity, backbone conformations, and aggregation states in solutions or solid states[49-51]. Mostly, Electronic and chemical structure of π-conjugated backbones have a great influence on photophysical properties of polythiophene. The similar π-conjugated backbones with a different substituted functional group have a similar optical property. A strong absorption of polythiophene in the visible range of the spectrum generally dominated by π-π* transition from highest occupied molecular orbital (HOMO) to lowest unoccupied molecular orbital (LUMO). Therefore, π electrons in conjugated cationic polythiophene are crucial for their band structure. The energy differences between HOMO and LUMO defined as band gap shown in equation.

$$E_{gap} = E_{LUMO} - E_{HOMO}\ (ev)$$

Polythiophene have a thermochromic, surfactochromic, solvatochromic, photochromic and biochromic properties with corresponding fluorescence properties

change in the presence of external stimuli[52-55]. The self-assembly property of charged polythiophenes give the outstanding performance to sense ionic or polar biomolecules. Not only cationic polythiophene focused in these type of works but also anionic or zwitterionic polythiophene synthesized[56, 57]. The significant optical properties of water soluble cationic conjugated polythiophene create a new area such as monitoring biological molecules[58], cell imaging[59] detection and sequencing nucleic acids[60]. Monitoring of DNA hybridization or nucleic acid detection with conjugated polythiophene based on the conformational change and the aggregation states of the polymers with the help of absorption and emission spectroscopy. There are 2 different polythiophene conformation in space that twisted and planar. In twisted conformation, all dihedral angle between monomer units distorted and different than 180° or 0°. In the contrary, planar conformation of polythiophene all monomer units in the same plane and dihedral angle between monomer units equal to 0° or 180°.

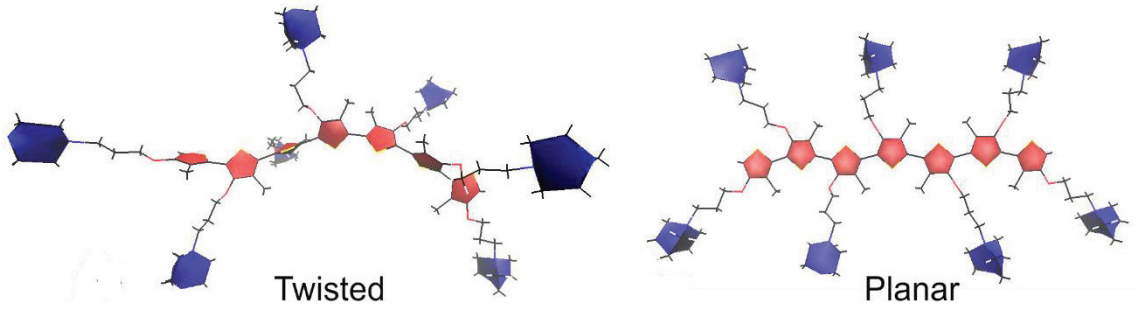

Figure 6. Twisted and planar conformation of 3-alkoxy-4-methylthiophene

The polythiophene chain with a regioirregular synthesis oriented randomly and unspecific shape. The cationic functional group of random coiled polythiophene chains interact with the negatively charged phosphate group of the DNA sequences. The conformation of the cationic polythiophene changes with the electrostatic and hydrophobic interaction between polythiophene and DNA sequences. In addition to conformational change, π-π aggregation observed in polythiophenes backbone. This conformational change and aggregation also proportional to the nature of the DNA sequences. DNA sequences as a single stranded (ssDNA) ensure the conformational change of the polymers twisted to planar. The conformation of the polythiophene remain twisted (same or different dihedral angle than random coiled polymer chain) while interacted with the double strand DNA (dsDNA). Conjugated cationic polythiophene have great features to monitor the ssDNA and dsDNA. Furthermore, the base content and

length of the DNA sequences affect the conformation and aggregation state of polymer. Detection of biomolecules with the water soluble polythiophene proportional to the conformational change and the formation of aggregation which resulting the colorimetric and fluorometric detection[50, 51, 61].

1.4. DNA Methylation and Detection

Genetics and epigenetics are study of heritable changes in gene activity or functions. In genetics, direct alteration of DNA sequence such as deletion, insertion, mutation and translocation change the function or gene activity while the this change of function and gene activity reversible and proceed without change in DNA sequence in epigenetics[62]. Methylation is the most commonly occurring epigenetic event in the mammalian genome which methyl group are added to different DNA molecules at different positions. DNA methylation is covalent modification that does not change the sequence while this modification influenced on gene activity. DNA methylation is crucial in the regulation of gene transcription, X-chromosome activity, chromatin compaction, genomic imprinting and carcinogenesis[63-67]. There are 3 main types of methylated base in DNA which are C5-methycytosine, N4-methylcytosine and N6-methyladenine. The widespread methylation is addition of the methyl group to the 5' position of the cytosine residue. The addition of methyl groups to the 5' of cytosine catalysed by DNA methyl transferases (DNMT) while the methyl group transferred from the S-adenosyl methionine (Figure 7).

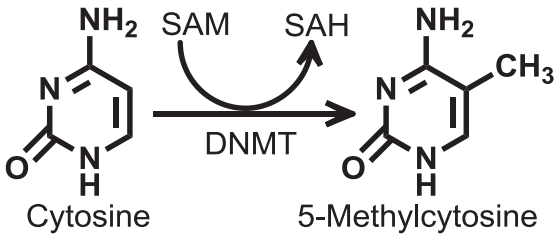

Figure 7. Methylation of cytosine

There are 3 essential DNMTs in mammalian and these are DNMT1, DNMT3a and DNMT3b[68-70]. DNMT1 has automatic semiconservative mechanism due to maintains the existing DNA methylation pattern during DNA replication. DNMT3a and DNMT3b categorized as *de novo* methyl transferases which responsible for addition of methyl group to the unmodified DNA. High percentage of DNA methylation occurs on cytosine

which neighbouring the guanine nucleotide and called CpG dinucleotide. CpG dinucleotide spread out across the genome and 70% of dinucleotides are methylated except for the CpG islands (CGIs)[71, 72]. Clusters of CpG dinucleotides named as CpG islands and predominantly unmethylated. Approximately 50% of all the genes in human have CGIs and these are present on both housekeeping gene and tightly regulated developmental genes. CGIs generally present at near the transcription start site of gene and TATA box less promoter region[73-75]. CGIs enhanced the binding to transcription start site due to GC richness of transcriptional factor binding sites. CGIs in promoter region usually hypomethylated and hypermethylation of CGIs result in transcriptional silencing. In the contrary, hypermethylation of CGIs in non-promoter region silences the parasitic genetic elements. Hypomethylation is the decreasing number of methylated base while the hypermethylation is the increasing number of methylated base. Figure 8 Shows the effect of the methylation of CGIs in promoter and non-promoter region.

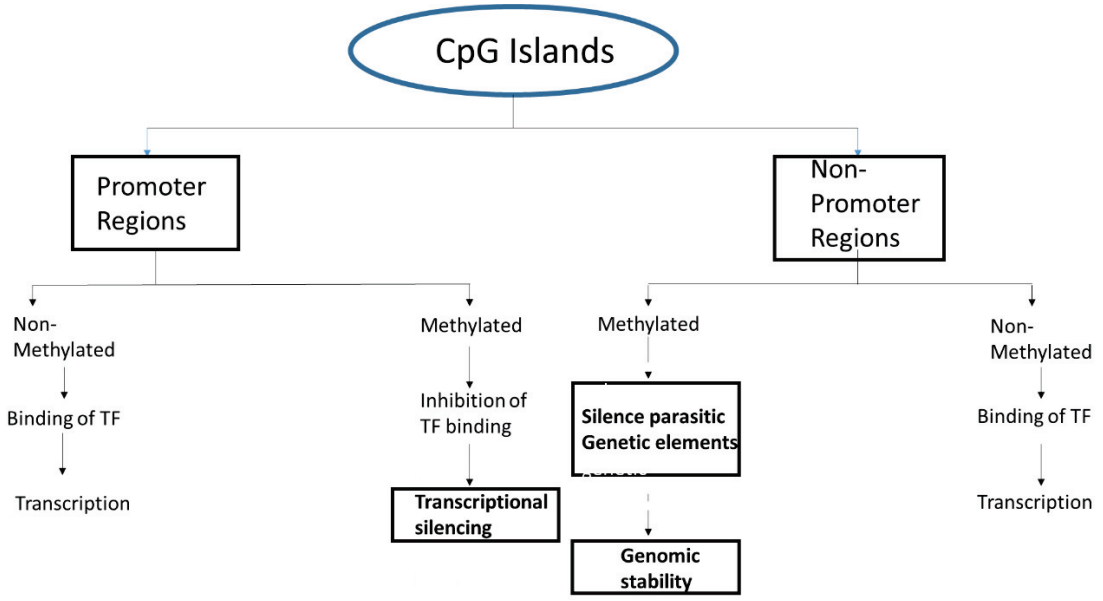

Figure 8. Methylation of CpG Islands in promoter and non-promoter region

Hypomethylation and hypermethylation are observed in almost all cancer types cells[76-78]. Presence of hypomethylation in centromeric repeat sequences responsible for genomic instability and activating oncogenes[79]. Increment of Hypermethylation in gene with promoter associated CGIs responsible for repression of tumor suppressors[80]. $p16^{INK4a}$ named as a multiple tumor suppressor gene with a cytogenic location 9p21.3 and 1200 base pair long. The functions of p16 gene are, bind the protein CDK4 and CDK6,

helps regulate the cell and control growing and cell division. Any silencing with methylation on p16 corresponds the occurrence of different types tumor depending on the location such as lung carcinoma, melanoma brain tumor and lymphoma[81, 82]. To consider the relationship between carcinogenesis and metastasis with DNA methylation, detection of DNA methylation is crucial to diagnosis of cancers[83]. There are three main technique available to detect the DNA methylation and these are bisulfite treatment, methylation anti-body recognition and methylation-sensitive restriction enzyme digestion[84-86]. Detection of DNA methylation achieved with many different methods relying on these three techniques such as radioactive label-based protocols[87], next-generation sequencing[88, 89], matrix-assisted laser desorption ionization mass spectrometry[90], capillary electrophoresis[91, 92] and methylation sensitive high-resolution melting (MS-HRM) analysis[93]. Methylation-specific polymerase chain reaction (MSP) analysis with bisulfite treatment is widespread method in detection. In recent years, fluorometric and colorimetric sensors become popular due to several practical advantages such as portability, simplicity, effectiveness and low detection limit. However, all colorimetric and fluorometric methods to detect the DNA methylation including polymerase chain reaction (PCR) method, fluorescence resonance energy transfer (FRET) or enzyme activity[87, 94, 95].

Here in this thesis, cationic conjugated polythiophene synthesized and detection of DNA methylation via cationic polythiophene have been aimed with monitoring UV-VIS and fluorescence spectrophotometer. Detection mechanism of DNA methylation should be PCR, enzyme and FRET free. At the same time, different DNA sample characterization via cationic polythiophene is aimed to understand the nature of the polymer-DNA complexes.

CHAPTER 2

MATERIALS & METHODS

2.1. Materials

1-Methyl-2-pyrrolidinone anhydrous, (99.5% Sigma Aldrich) Sodium methoxide (95%, powder, Sigma Aldrich), methanol (ACS reagent, ≥99.8%, Sigma Aldrich), copper(II) bromide (99%, Sigma Aldrich) and 3-Bromo-4-methylthiophene (95%, Sigma Aldrich) were used for synthesis of Synthesis of 3-Methoxy-4-methylthiophene (precursor 1). 3-Bromo-1-propanol (97%, Sigma Aldrich), sodium bisulfate anhydrous (Sigma Aldrich) and Toluene (ACS reagent ≥99.7%, Sigma Aldrich) were used for synthesis of 3(3-Bromo) propoxy-4-methylthiophene (precursor 2). Sodium bromide (99%, Sigma Aldrich), diethyl ether (99.5% Sigma Aldrich), magnesium sulfate (97%, Sigma Aldrich), hexane (95%, Sigma Aldrich) and Silica gel (pore size 60 Å, 60-100 mesh, Merck) were used for purification of precursor 1 (PC1) and precursor 2 (PC2). 1,4-diazabicyclo [2.2.2] octane (≥99%, Sigma Aldrich), 1,4-dimethylpiperazine (98%, Sigma Aldrich), N-allyl-N-methylprop-2-en-1-amine (99%, Sigma Aldrich) and tetrahydrofuran (THF, ACS reagent, ≥99.9%, Sigma Aldrich) were used for synthesis of monomers. Iron(III)chloride (Merck) and chloroform anhydrous (≥99%, Sigma Aldrich) were used for polymerization reactions. Chloroform-d (99.8%, Merck) and Deuterium oxide (D_2O, 99.96%, Merck) used for 1H NMR analysis of synthesized precursors, monomers and polymers. Tris(hydroxymethyl)aminomethane (ACS reagent, ≥99.8%, Sigma Aldrich), EDTA (powder, Sigma Aldrich), Hydrochloric acid (ACS reagent, ≥37%, Sigma Aldrich), sodium hydroxide (ACS reagent, ≥97.0%, pellets) used for preparation of Tris-EDTA (TE) buffer solution (pH: 7.4). All synthetic oligonucleotides purchased from Oligomer Biotechnology. Bisulfite Conversion Kit NEB # 3318S purchased from Epimark.

2.2. Synthesis of Monomers

Sodium methoxide (25 wt. %) synthesized from sodium metal in a dry methanol. Because, commercial sodium methoxide is not stable for a long time used.

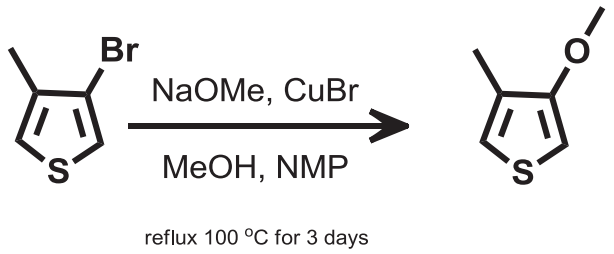

Figure 9. Synthesis of 3-Methoxy-4-methylthiophene (PC1)

Sodium methoxide (0.479 g, 8.85 mmol), methanol (1.8ml) and 1-methyl-2-pyrolidinone (1.0 mL) mixed in a round bottom flask. 3-bromo-4-methylthiophene (0.5 mg, 2.82 mmol) and CuBr (0.25 g, 1.74 mmol) were added to mixture. This mixture was heated to 100°C – 110°C. Water cooled condenser was equipped and temperature fixed at 5°C. The round bottomed flask refluxed for 3 days at 100°C – 110°C. After reaction, mixture cooled to room temperature. 0,1 g sodium bromide dissolved in 4ml diluted water then solution added and stirred for 1 hour. The mixture was filtered and extracted with 10 ml diethyl ether 4-5 times. The organic phase washed with diluted water during extraction step, dried over $MgSO_4$. Solvent was removed from media by rotary evaporator to yield a light-yellow oil. Column chromatography method used as a purification of a light-yellow oil to yield 3-Methoxy-4-methylthiophene (PC1).

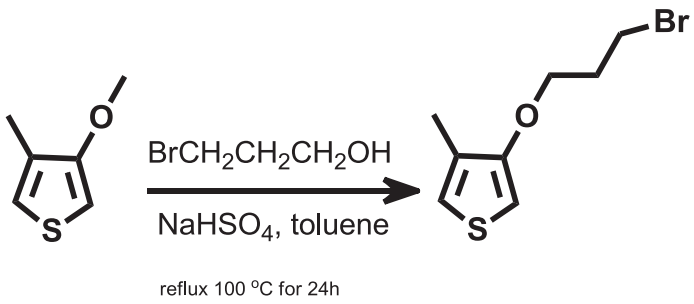

Figure 10. Synthesis of 3(3-Bromo) propoxy-4-methylthiophene (PC2)

To a dry round bottom flask, 3-Methoxy-4-methylthiophene (PC1) (100 mg, 0,78mmol), 3-bromo-1-propanol (150 µl, 1.66 mmol), and $NaHSO_4$ (12.5 mg, 0,1 mmol)

and 2 ml toluene were added. The reaction was heated at 100ºC with water cooled condenser for 24 hours under nitrogen (N_2) atmosphere. The reaction mixture cooled the room temperature and toluene was removed by rotary evaporator. The remaining mixture was extracted with diethyl ether 4-5 times and washed with diluted water. Then dried over $MgSO_4$ and diethyl ether was removed by rotary evaporator. Column chromatography method used as a purification of the crude product to yield a 3(3-Bromo) propoxy-4-methylthiophene (PC2) as a colorless oil. PC2 was used for all types of monomers synthesis.

2.2.1. Synthesis of 1-(3-((4-methylthiophen-3-yl) oxy) propyl)-1,4-diazabicyclo [2.2.2] octan-1-ium bromide (M3)

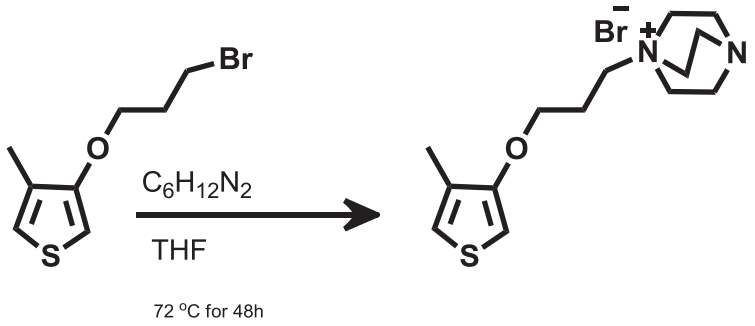

Figure 11. Synthesis of 1-(3-((4-methylthiophen-3-yl) oxy) propyl)-1,4-diazabicyclo [2.2.2] octan-1-ium bromide (M3)

(3-Bromo) propoxy-4-methylthiophene (70 mg, 0.30 mmol), 1,4-diazabicyclo [2.2.2] octane (300 mg, 2,67 mmol) and 2ml THF were mixed in a round bottomed flask. The mixture was stirred at 72ºC for 48h. After cooled down to room temperature the reaction medium poured into falcon and centrifugated at 3000 rpm for 5 minutes. The supernatant was removed and washed again with THF, then centrifugated at 3000 rpm for 10 minutes. The supernatant was removed again, white color precipitate observed and dried under vacuum.

The same synthesis and purification protocols applied for M1 and M2 with different amount of chemicals. Only the M3 synthesis details given. The structure of M1 and M1 shown in Figure 12.

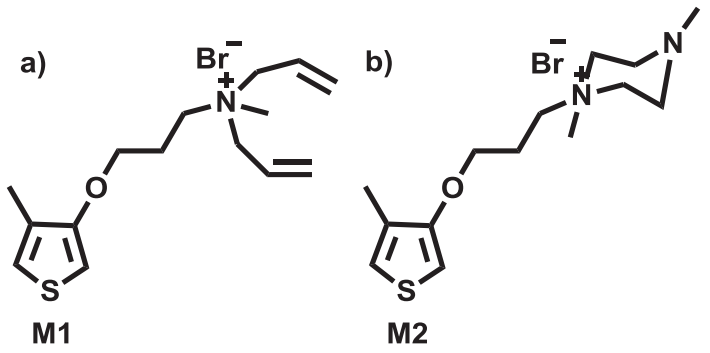

Figure 12. a) N-allyl-N-methyl-N-(3-((4-methylthiophen-3-yl) oxy) propyl) prop-2-en-1-aminium bromide (M1), b) 1,4-dimethyl-1-(3-((4-methylthiophen-3-yl) oxy) propyl) piperazin-1-ium bromide (M2)

2.3. Synthesis of Polymers

Polymerization reaction carried out for PC1, M1, M2 and M3. Only synthesis protocol of PT3 details given. Same protocol applied for the PC1, M1 and M2 with different starting concentration. Figure 13 shows the structure of synthesized polymers.

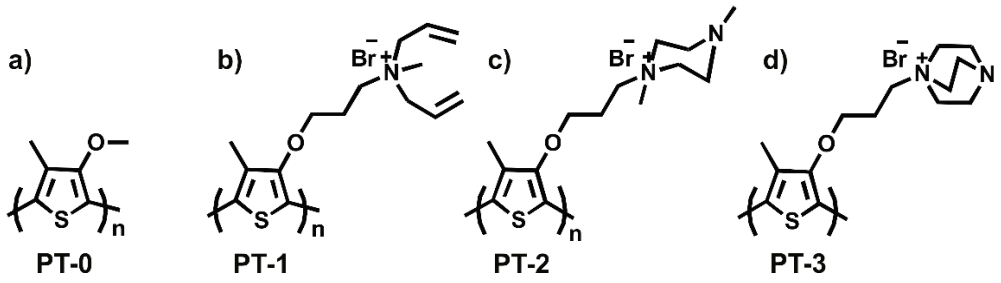

Figure 13. Synthesized Polymers a) Poly(3-Methoxy-4-methylthiophene) (PT0), b) Poly(N-allyl-N-methyl-N-(3-((4-methylthiophen-3-yl) oxy) propyl) prop-2-en-1-aminium bromide) (PT1), c) Poly(1,4-dimethyl-1-(3-((4-methylthiophen-3-yl) oxy) propyl) piperazin-1-ium bromide) (PT2), d) Poly(1-(3-((4-methylthiophen-3-yl) oxy) propyl)-1,4-diazabicyclo [2.2.2] octan-1-ium bromide) (PT3)

2.3.1. Synthesis of Poly(1-(3-((4-methylthiophen-3-yl) oxy) propyl)-1,4-diazabicyclo [2.2.2] octan-1-ium bromide) (PT3)

Approximately 1-(3-((4-methylthiophen-3-yl) oxy) propyl)-1,4-diazabicyclo [2.2.2] octan-1-ium bromide (M3) (20 mg, 0.07 mmol) was dissolved in 1 ml CH_3Cl and Fe_3Cl (40 mg, 0.25 mmol) dissolved in 1,5 ml CH_3Cl. M1 solution added dropwise to

Fe_3Cl solution. Reaction stirred at room temperature for 24h under nitrogen (N_2) atmosphere. Reaction washed with the CH_3Cl and centrifugated at 4000 rpm for 5 minutes. Brownish particle observed and dried under vacuum.

2.4. Preparation of Tris-EDTA(TE) Buffer

TE buffer components are; tris(hydroxymethyl) aminomethane, common pH buffer and chelating agent ethylenediaminetetraacetic acid(EDTA). In molecular biology, RNA and DNA based procedures required TE buffer which solubilize the DNA or RNA while protecting it from degradation. RNA usually requires pH 8.0 and DNA requires pH 7.5, also 8.0 can safely use for solubilizing the DNA. 6,06g tris(hydroxymethyl) aminomethane dissolved in a 50ml mq water to yield a 1M tris stock solution. Solution Cooled to room temperature (because pH of tris-solution is temperature dependent) and pH adjusted as 7.4 by adding concentrated HCl to the solution. To prepare a EDTA stock solution 3,72 g EDTA dissolved in a 20 ml mq water and pH adjusted as 8,0 by adding NaOH pellet (EDTA is not soluble until pH reach 8.0). 5 ml tris solution and 1 ml EDTA solution mixed briefly and diluted adding 494 ml mq water. Final concentration of tris and EDTA, 10mM and 1mM respectively. TE buffer is sterilized by autoclaving to use further preparation of DNA.

2.5. Preparation of DNA samples

All purchased DNAs synthesis scales are 50nmol. Prepared and sterilized TE buffer used for solubilizing to DNA and used materials were sterilized by autoclaving such as pipette, tips and ependorf. Table 1 below show the sequence of strands, molecular weight of DNA, amount of DNA and required TE buffer for the prepare to 100μM DNA solutions.

2.6. Sodium Bisulfite Conversion (SBC)

SBC is used for defining to the target sequence's cytosine is methylated or unmethylated. When reaction over unmethylated cytosine turned to uracil while methylated cytosine remains intact. In this work The EpiMark Bisulfite Conversion Kit NEB # 3318S is used.

Table 1. Properties of DNA sequences

Tittle of Sequences	Sequences of DNA	M.W.of DNA (g/mol)	Amount of DNA (nmol)	TE buffer for 100µM DNA
PolyC (10)	5'CCC CCC CCC C'3	2830	59	588
PolyG (10)	5'GGG GGG GGG G'3	3230	5	51
PolyA (10)	5'AAA AAA AAA A'3	3070	72	720
PolyT (10)	5'TTT TTT TTT T'3	2980	103	1030
PolyC (20)	5'CCC CCC CCC CCC CCC CCC CC'3	5722	63	626
PolyG (20)	5'GGG GGG GGG GGG GGG GGG GG'3	6522	3	27
PolyA (20)	5'AAA AAA AAA AAA AAA AAA AA'3	6202	77	772
PolyT (20)	5'TTT TTT TTT TTT TTT TTT TT'3	6022	92	919
Unmethylated Sequence	5'CAG AGG GTG GGG CGG ACC GC'3	6249	73	733
Methylated Sequence	5'CAG AGG GTG GGG CmeGG ACCme GCme'3	6290	33.8	338
Complementary-2	3'ATC TCC CAC CCC ACC TAA CA'5	5911	82	817
Complementary-1	3'GTC TCC CAC CCC GCC TGG CG'5	5991	61	614

- Sodium metabisulfite
- Solubilization buffer
- Desulphonation reaction buffer
- EpiMark spin column
- Binding buffer
- Wash buffer
- Elution buffer

2.6.1. Reagent Preparation

40 ml of ethanol (99%) is added into a concentrate wash buffer and mixed briefly. Prepared wash buffer stored at room temperature for further reactions. 27 ml

ethanol is added to concentrate desulphonation reaction buffer and mixed briefly. Desulphonation reaction buffer stored at +4 ºC for further reactions. Bisulfite mix prepared by adding 650µl of nuclease free water and 250 µl solubilization buffer to solid sodium metabisulfite. Bisulfite mix vortexed until sodium metabisulfite completely dissolved. Bisulfite mix stored at -20 ºC for further reactions.

2.6.2. Bisulfite Conversion Reaction

Target DNA (50 ng- 2 µg, 10 µl) and 130 µl bisulfite mix, poured into ependorf. Reaction ependorf transferred to a thermocycler and began cycling. Denaturation and incubation steps applied as shown in Table 2.

Table 2. Incubation Times

Cycle Step	**Temperature**	**Time**
Denaturation	95ºC	5 minutes
Incubation	65 ºC	30 minutes
Denaturation	95 ºC	5 minutes
Incubation	65 ºC	60 minutes
Denaturation	95 ºC	5 minutes
Incubation	65 ºC	90 minutes
Hold	20 ºC	12 hours

2.6.3. Desulphonation Reaction and Sample Clean Up

After bisulfite conversion reaction ended, reaction medium transferred into a microcentrifuge tubes. 550 µl of DNA binding buffer added into a microcentrifuge tubes and mixed gently with pipetting. Sample is loaded onto a Epimark spin column. Column was centrifuged at 15000 rpm for 1 minute and flow through was discarded. Then 500 µl wash buffer added, column was centrifuged at 15000 rpm for 1 minute and flow through was discarded. 500 µl desulphonation reaction buffer was added to each column and incubated at room temperature for 15 minutes. Then column was centrifuged at 15000 rpm for 1 minute and flow through was discarded. 500 µl wash buffer added, column was centrifuged at 15000 rpm for 1 minute and flow through was discarded. Wash step was

repeated one more time. Column was centrifuged at 15000 rpm for 1 minute to remove any residual wash buffer from the spin column. Spin column was placed into sterile 1.5 ml microcentrifuge tubes. 20 µl elution buffer was added and incubated for 1 minute. Column was centrifuged at 15000 rpm for 1 minute. Additional 20 µl elution buffer was added and column was centrifuged at 15000 rpm for 30 seconds. Conversion was completed.

2.7. Characterization Tests

Characterization tests was performed for the synthesized monomers, polymers, artificial DNA and treated DNA.

2.7.1. Nuclear Magnetic Resonance (NMR) Analysis

^{1}H NMR spectrum were recorded in the solution of $CDCl_3$ on Varian 400 spectrometers for precursor 1 and precursor 2. ^{1}H NMR spectrum were recorded in the solution of D_2O for M1, M2, M3, PT1, PT2 and PT3.

2.7.2. Mass spectrometry Analysis

Mass spectrometry analysis performed to determine the M1, M2 and M3 molecular weight after synthesized.

2.7.3. UV-VIS Spectrophotometer Analysis

Spectral analysis was performed using a Shimadzu UV-2550 UV-VIS spectrophotometer. Hellma quartz were used for all spectral analysis which have light path 1 mm with width 1 cm and made of quartz SUPRASIL®. Scan range was 200 nm to 800 nm. For the analysis, stock solutions of PT1 and PT2 were prepared as 1.88 mM polymer concentration in water. Stock solutions diluted with TE buffer 1:1 before each analysis performed. Titration starting volume was 200 µl polymer-TE buffer mix. Titration performed with the addition of single stranded DNA (ssDNA) (1µl, 100 µM) systematically into a quartz which have 200 µl polymer-TE buffer mix. This titration protocols were performed for the characterization of PolyC (10), PolyG (10), PolyA (10), PolyTh (10). PolyC (20), PolyG (20), PolyA (20) and PolyTh (20) ssDNA titration with PT1 and PT2. Melting temperature of ssDNA were used as an incubation temperature

while the dsDNA complex was prepared by homopurine and homopyrimidine. PolyA (10) (20 µl, 100 µM) and PolyTh (10) 20 µl, 100 µM) were poured into microcentrifuge tubes, mixed briefly with pipetting and incubated for 15 minutes. PolyA (20) (20 µl, 100 µM) and PolyTh (20) (20 µl, 100 µM) were poured into microcentrifuge tubes, mixed briefly with pipetting and incubated for 15 minutes. Then, dsDNA samples cooled the room temperature. Titration starting volume was 200 µl polymer-TE buffer mix. Titration performed with the addition of dsDNA (1µl, 100 µM) systematically into a quartz which have 200 µl polymer-TE buffer mix. Titration protocol carried out for the characterization of dsAT (10) and dsAT (20) with PT1 and PT2.

Optic characterization of unmethylated sequence, methylated sequence, complementary-1 and complementary-2 performed with PT3. Stock solution of PT3 was prepared as 1.88 mM polymer concentration in water. Stock solution diluted with TE buffer 1:1 before analysis performed. Titration starting volume was 200 µl polymer-TE buffer mix. Titrations performed with the addition of DNA samples into a quartz with different concentrations. 100 µM of ssDNA concentration were used to understand the behavior of the sequences. Titration protocol followed as 1 µl, 100 µM of ssDNA added into quartz and spectra recorded in every addition. 3 µM to 10 µM concentration range were used after SBC conversion to understand the treated ssDNA and dsDNA behavior. Titration protocol followed as 1 µl of 100 µM ssDNA and dsDNA added into quartz and spectra recorded in every addition. Concentration differences of DNA samples for titrations resulted from the limitation of the SBC kit.

2.7.4. Fluorescence Spectrophotometer Analysis

Fluorescence analysis were performed with using Varian Cary Eclipse Fluorescence spectrophotometer. Fluorescence spectrum obtained for PT1, PT2, PT3, PT1-DNA titrations and PT3-DNA titrations with excitation wavelength 395nm. The corresponding wavelength of maximum emission for PT1, PT2 and PT3 at 533 nm, 532 nm and 535 nm respectively. Polymer concentration is 1,88 mM for the characterization of polymer-ssDNA and polymer-dsDNA. Homopurine and homopyrimidine characterized with 100 µM ssDNA added into polymer-TE medium. Detection of DNA methylation experiments carried out with the different DNA concentrations and for every DNA sample concentration determined by nanodrop. Hybridization of dsDNA is the most essential step for the detection of DNA methylation experiments. The most efficient

hybridization protocol is the 5 minutes incubation at 95ºC and 10 minutes incubation with DNA sequence's melting temperature. In addition, cooling the DNA samples to the room temperature should be very slow. For the all fluorescence analysis starting volume is 200 µl polymer-TE solution.

2.7.5. Nanodrop Analysis

Nanodrop analysis applied to determine the ssDNA concentration before and after SBC. 2µl sample is required for the concentration analysis for each sample.

2.8. Computational Methods

Computational methods described as a model chemistry with a unique, unbiased and applicable model for predicting the properties of chemical systems. Combination of theoretical method with a basis set is fundamental of a computational chemistry. Different combinations represent the different approximation to the Schrödinger equation.

2.8.1. Semi-empirical Methods

Semi-empirical methods have been developed to investigate the simple organic molecules. However, semi-empirical methods used in large system optimization due to relatively inexpensive and practical method. There are variety of semi-empirical methods such as AM1, PM3, PM6, PDDG SAM1, INDO and MNDO etc. Molecular geometry and energy approximation of semi-empirical methods good for systems especially in organic compounds. There are few limitations of semi-empirical methods such as poor van der Walls and dispersion intermolecular forces. In the contrary some methods approximation good for the organic system and useful for the further larger systems[96].

2.8.2. Density Functional Theory (DFT) Methods

DFT methods compute the treatment of correlated motions of electron via general functionals of the electron density. The popularity of method increases with the years due to much less expensive than traditional correlated wavefunction methods. DFT functionals divided the electronic energy to the 4 components which are electron-nuclear interaction, the kinetic energy, the Coulomb repulsion and exchange correlation. 4

components of electronic energy computed separately in DFT methods. Furthermore, there are several hybrid methods developed that combine functionals of Hartree-Fock and other methods. Some hybrid methods superior to the traditional methods such as Becke's style hybrid functionals and available in *Gaussian* via B3LYP and B3PW91.

2.8.3. Excited State Calculations

Excited state calculations generally carry out to determine the molecular properties and the corresponding energies. Spectroscopic analysis can perform via excited state calculations. Time dependent density functional theory (TD-DFT) widely used instead of other methods due to quality of result and different response properties of large molecules are possible.

CHAPTER 3

RESULTS & DISCUSSION

3.1. Synthesis and characterization of Monomers

The first step of the synthesis of monomers start with the PC1. After purification steps, the yield is 63%. ^{1}H NMR analysis performed and Figure 15 shows the NMR spectrum of PC1 as a ^{1}H NMR (400 MHz, $CDCl_3$) δ (ppm): 6.82 (1H, d, J= 3.3 Hz), 6.16 (1H, d, J= 3.3 Hz), 3.82 (3H, s), 2.10 (3H, s).

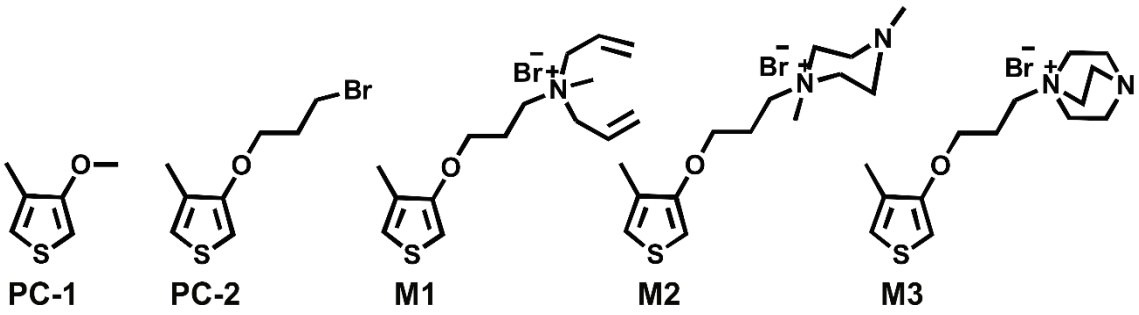

Figure 14. Synthesized precursors and monomers

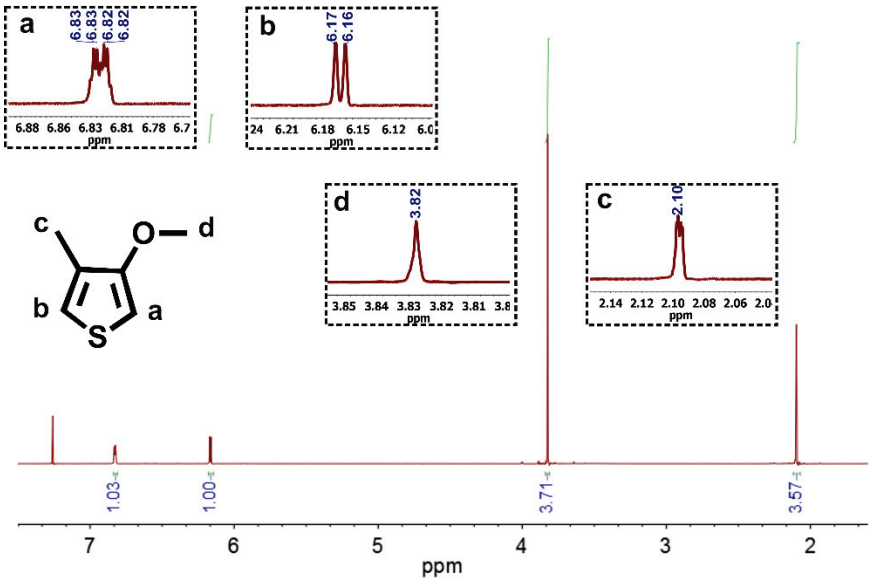

Figure 15. ^{1}H NMR spectrum of PC1

PC2 was a starting material in every monomer synthesis. After purification steps, the yield is 78%. Figure 16 shows the ^{1}H NMR spectrum of the PC2 as a ^{1}H NMR (400 MHz, $CDCl_3$) δ (ppm): 6.84 (1H, d, J= 2.8 Hz), 6.19 (1H, d, J= 3.0 Hz), 4.09 (2H, t, J= 5,9 Hz, 6,2 Hz), 3.61 (2H, t, J= 6.3 Hz, 6,6 Hz), 2.34 (2H, p, J= 5.2 Hz, 5.2 Hz, 6.4 Hz, 5.6 Hz), 2.09 (3H, s).

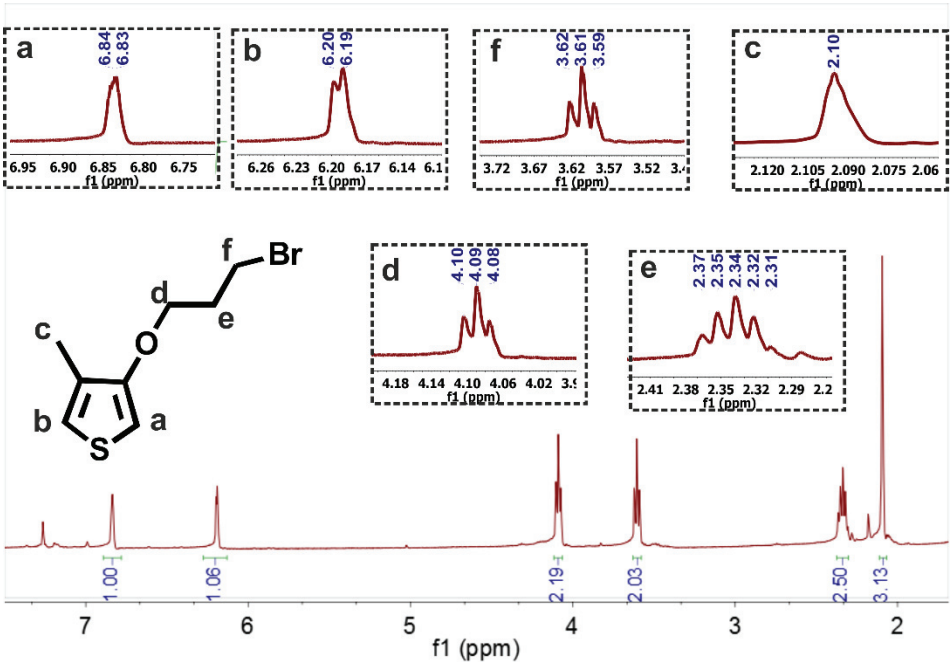

Figure 16. ^{1}H NMR spectrum of PC2

^{1}H NMR analysis and mass analysis were performed for the M3 molecule. The calculated yield is 83% and Figure 17 shows the ^{1}H NMR (400 MHz, D_2O) δ (ppm): 6.88 (1H, m), 6.35 (1H, d, J= 3.3 Hz), 4.02 (2H, t, J= 5.7 Hz, 5.7 Hz), 3.35 (2H, t, J= 3.5 Hz, 3.7 Hz), 3.30 (6H, t, J= 7.4 Hz, 8.0 Hz), 3.06 (6H, t, J= 7.5 Hz, 7.6 Hz), 2.17 (2H, p, J= 6.0 Hz, 8.5 Hz, 8.5 Hz, 6.0 Hz), 1.94 (3H, s). Figure 18 shows the mass result of M3. Both ^{1}H NMR analysis and mass analysis were also performed for the M1 and M2, but synthesis route of these monomer not involved in scope of thesis.

3.2. Synthesis and characterization of Polymers

Characterization of polymers were carried out with using ^{1}H NMR analysis, UV-VIS measurement and fluorescence measurement. After purification, polymers dissolved in D_2O and ^{1}H NMR analysis performed for PT1, PT2 and PT3. General behaviour of polymer in NMR that aromatic hydrogen peaks disappeared and band broadening of corresponding peaks in NMR spectrum.

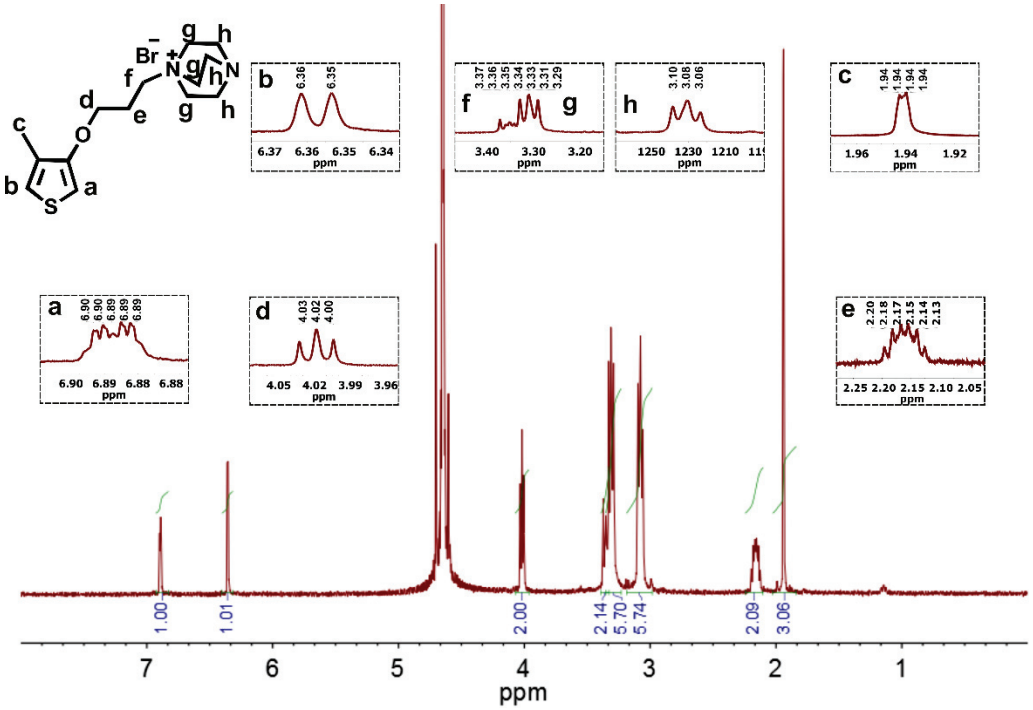

Figure 17. ^{1}H NMR spectrum of M3

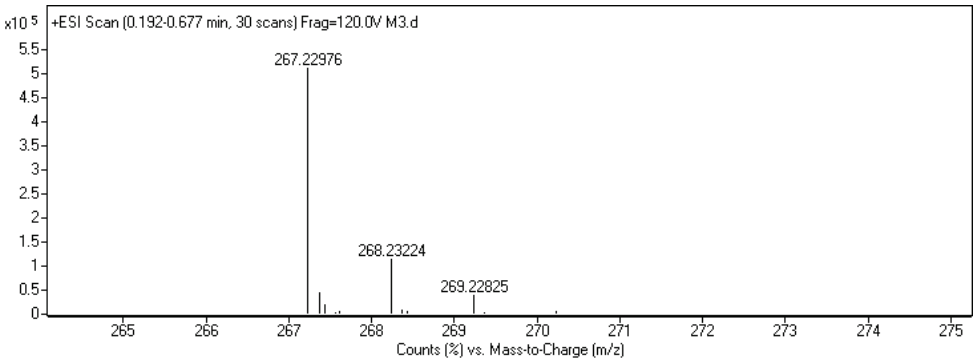

Figure 18. Mass result of M3

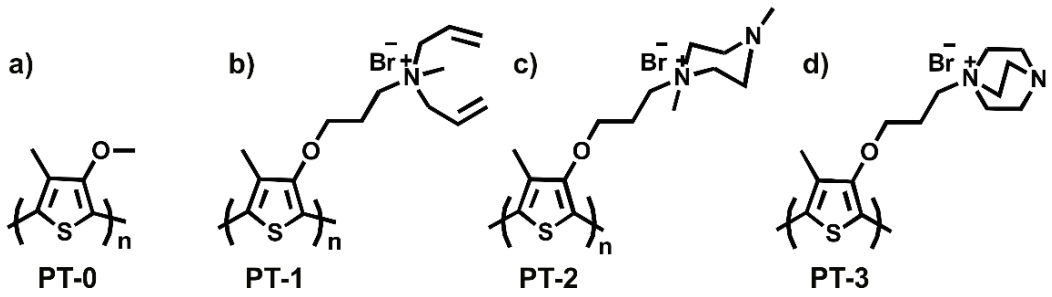

Figure 19. Synthesized polymers

Disappearances of aromatic hydrogen peaks resulted from the bonding of monomer units with each other then, 2' or 5' positioned H-C bonds break regarding octet rule. Band broadening resulted from the increasement of repeated monomer unit. Figure 20 shows the ^{1}H NMR stack of PT3 and M3. Red spectrum represents the M3 and teal blue spectrum represent the PT3. Both band broadening and disappearances of aromatic hydrogen peaks observed. Also, all responsible signals merely shifted to high field.

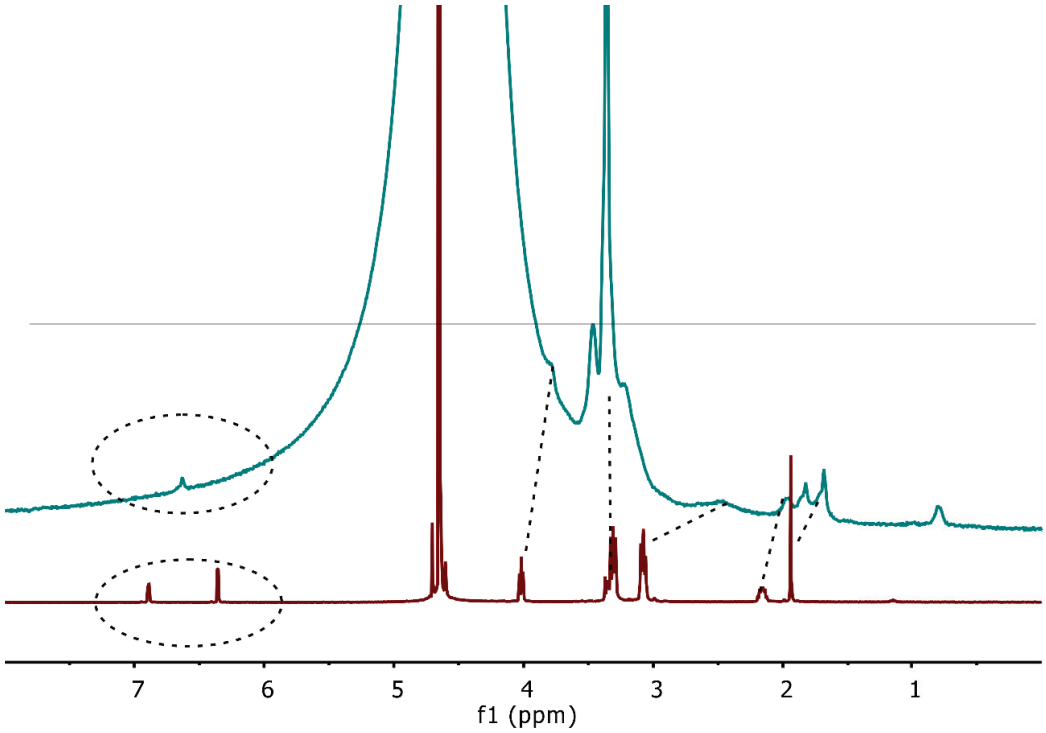

Figure 20. ^{1}H NMR stack of PT3 and M3

Figure 21 shows the NMR stack of PT1, PT2 and PT3. NMR stack indicates the band broadening, disappearances of aromatic hydrogen peaks and shifting of all

responsible signals to high field. Maroon spectrum represents the PT1, blue spectrum represents the PT2 and red spectrum represents the PT3.

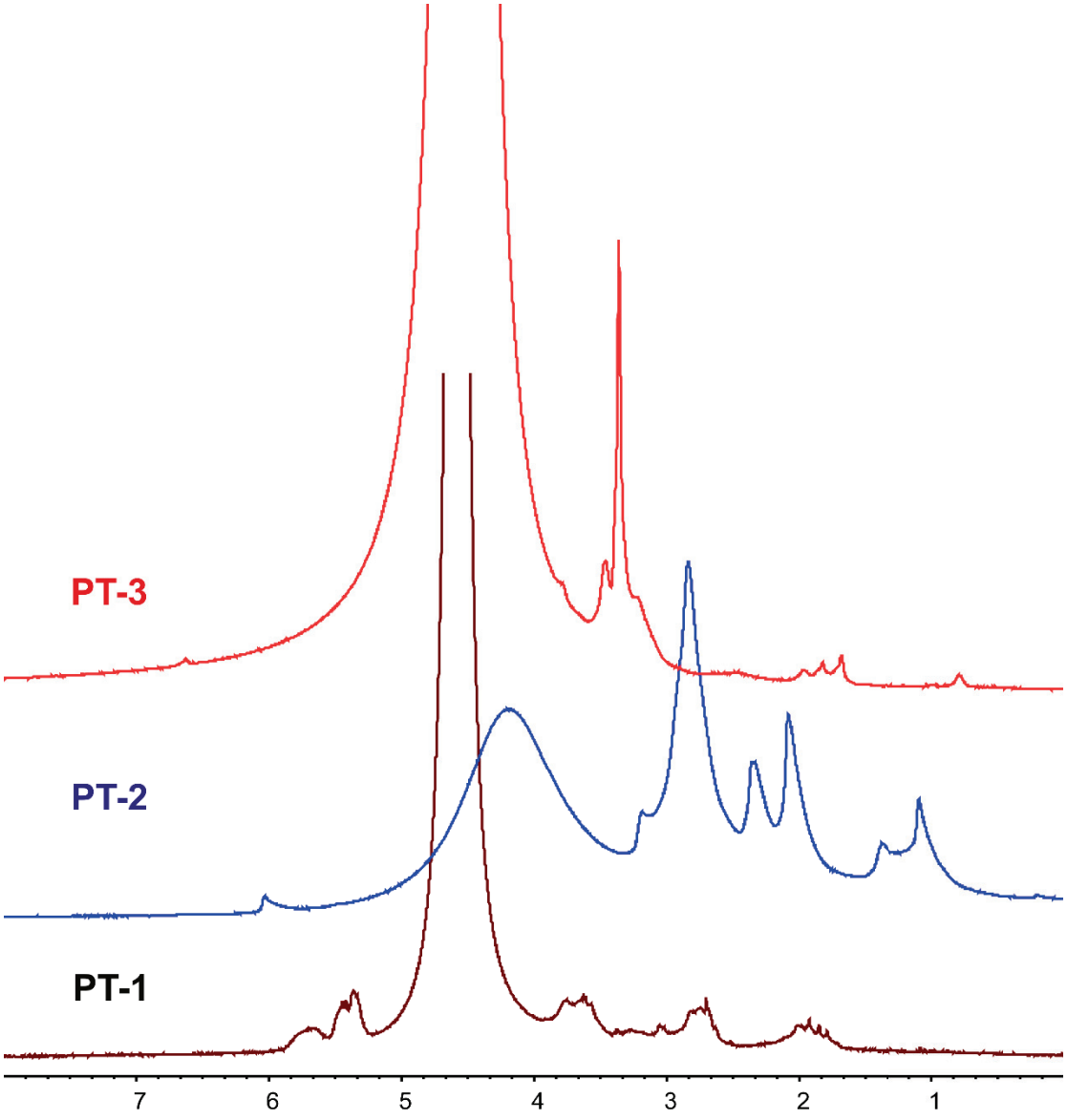

Figure 21. ^{1}H NMR stack of polymers

Figure 22 shows the UV-VIS measurement of polymers dissolved in water. Monocationic conjugated polythiophenes (PT1, PT2 and PT3) absorbance maximum close to each other with similar intensities. Absorbance maximum of PT1, PT2 and PT3; 401 nm, 387 nm and 397 nm respectively.

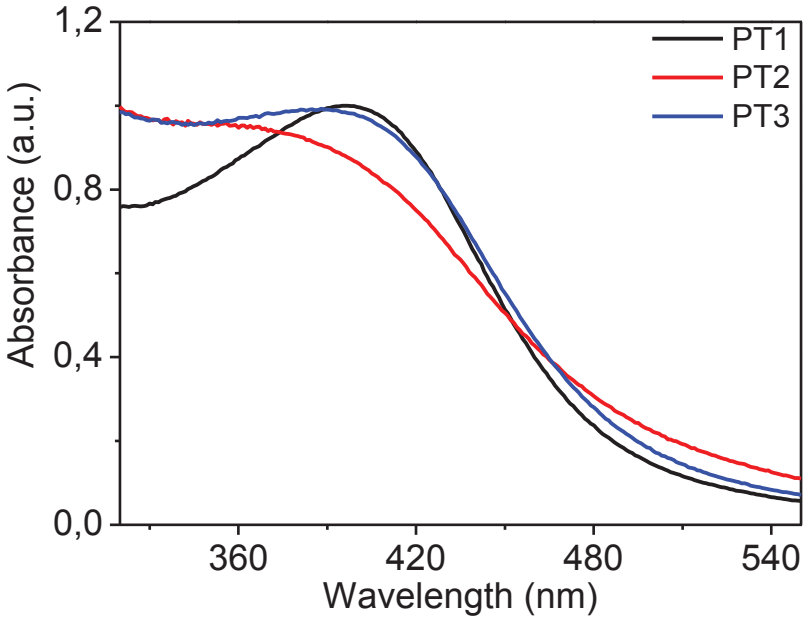

Figure 22. UV-VIS spectrum of PT1, PT2 and PT3

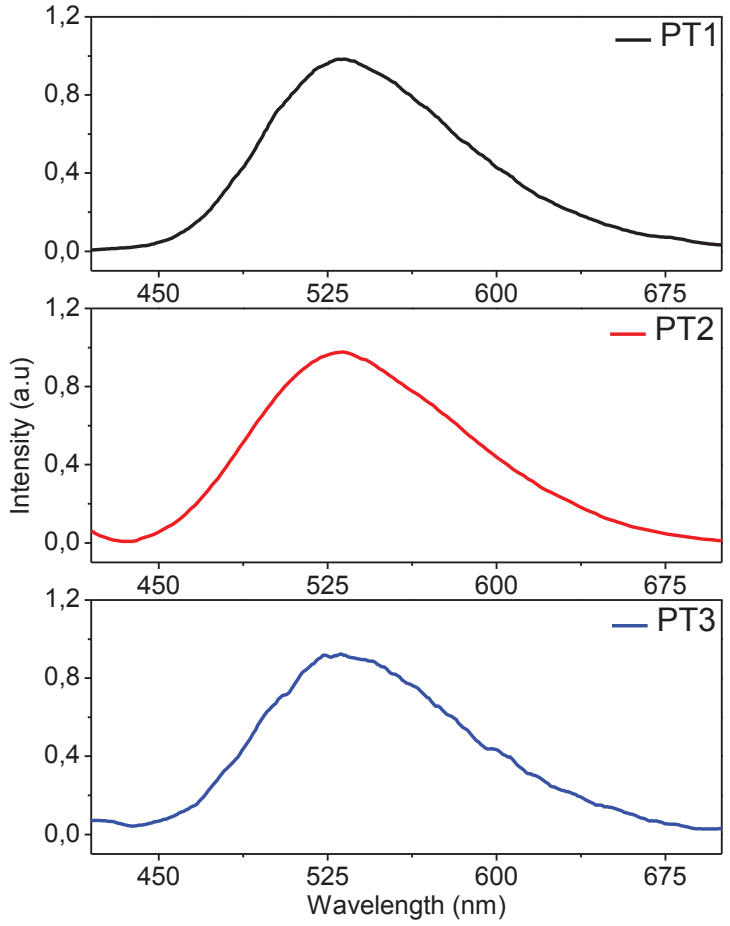

Figure 23. Fluorescence spectrum of PT1, PT2 and PT3

The corresponding wavelength of maximum emission for PT1, PT2 and PT3 at 533 nm, 532 nm and 535 nm respectively (Figure 23). All monocationic polymer-DNA interactions monitoring with fluorescence spectrophotometer.

3.3. Characterization of Homopurine and Homopyrimidine with Monocationic Conjugated Polythiophenes

Characterization of DNA samples carried out with using UV-VIS spectrophotometer. There are several interactions, during occurrence of polymer-DNA complex and these are; π-π, π-cation, H-bonding and electrostatic interactions. Ionic interaction is the most powerful interaction by considering polymer-DNA interactions. Conjugated polythiophenes dissolved in water that provide fast formation of polymer-DNA complex. Formation of polymer-DNA complexes are different for the different homopurine and homopyrimidine DNA samples. Also, formation polymer-DNA complexes are different with using different polymer. Differences of formation of complex effect the optical properties and with using this property both homopurine and homopyrimidine classified. Figure 24 shows the comparison of different polymer substituent group for the polymer-DNA interactions while Figure 24a show the PT1-PolyC (10) and Figure 24b shows the PT2-PolyC (10) titration curve for complexes. In both titration curve absorbance maximum of polymer nearly at 395 nm. The 395 nm peak decreases with addition of polyC (10) and new peaks at 505 nm 545 nm and 595 nm were observed. These new peaks correspond to formation of polymer-DNA complex. The maximum absorbance ratio of 395 nm/595 nm of PT1-PolyC (10) complex is 1,25 while PT2-PolyC (10) complex 395 nm/595 nm maximum absorbance ratio is 1,4. Final ssDNA concentration is 13,04 μM in 230 μl final volume for each case.

PT1-PolyG (10) and PT2-PolyG (10) interaction also examined to compare the effect of the polymer substituent group to a Polymer-DNA interaction. Figure 25a shows the PT1-PolyG (10) UV-VIS titration curve while Figure 25b shows the PT2-PolyG (10) UV-VIS titration curve. Only, a peak at 395 nm slightly decreased and there is no newly peaks occurred. Polymer-DNA interaction is not observed owing to formation of the guanine quartet or tertiary structure. There is no polymer conformation change on PT1 or PT2 titrated with PolyG (10). Final ssDNA concentration is 13,04 μM while the total volume is 230 μl. Also, further amount of ssDNA added into titration medium of PT2-

PolyG (10) and there are no new peaks observed with 23,07 µM final concentration of PolyG (10).

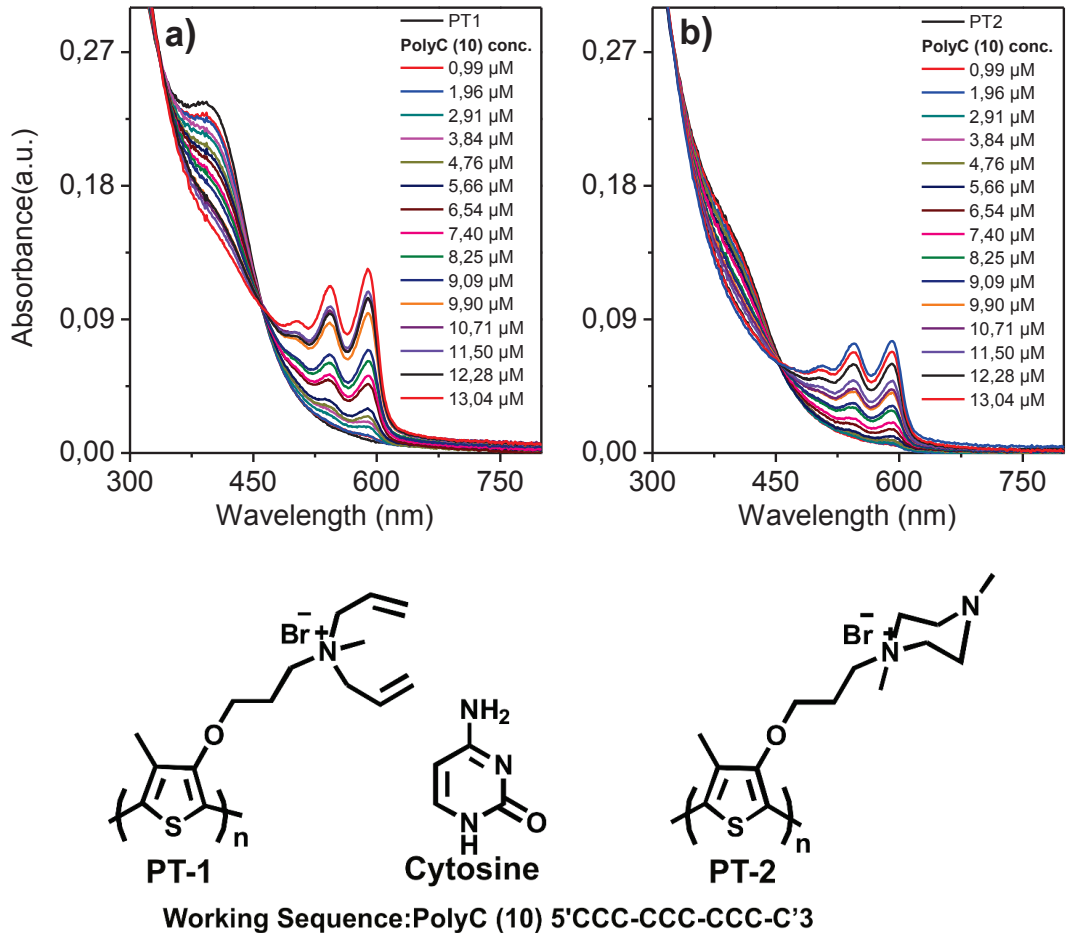

Figure 24. a) UV-VIS spectrum of PT3-PolyC (10) titration, b) UV-VIS spectrum of PT2-PolyC (10) titration

Figure 26a shows the UV-VIS titration curve of the PT1-PolyTh (10) complex. A peak at 395 nm slightly decreased for all 2 µl addition of ssDNA. There is no new peak observed until concentration of PolyTh (10) is 9,09 µM. Then, peaks at 545 nm and 595 nm gradually increased with the addition of continually ssDNA. The maximum absorbance ratio of 395 nm/595 nm of PT1-PolyTh (10) is 4,01. To observe the effect of concentration of PT1-PolyTh (10) complex, extra 10µl ssDNA added into medium. A peak at 505 nm emerge with addition of extra ssDNA. Figure 26b shows the UV-VIS titration curve of the PT1-PolyA (10) complex. In every ssDNA addition, a peak at 395 nm gradually decreased. The reason of decrease is dilution. PT1-PolyA (10) complex did not formed because of PolyA strong intramolecular secondary interactions. Conformation

of PT1 did not change twisted to planar during titration with PolyA (10) and no new peaks observed in PT1-PolyA (10) titration curve. Final concentration of polyTh (10) is 16,67 µM for PT1-PolyTh (10) titration and 13,04 µM of polyA (10) for PT1-PolyA (10) titration.

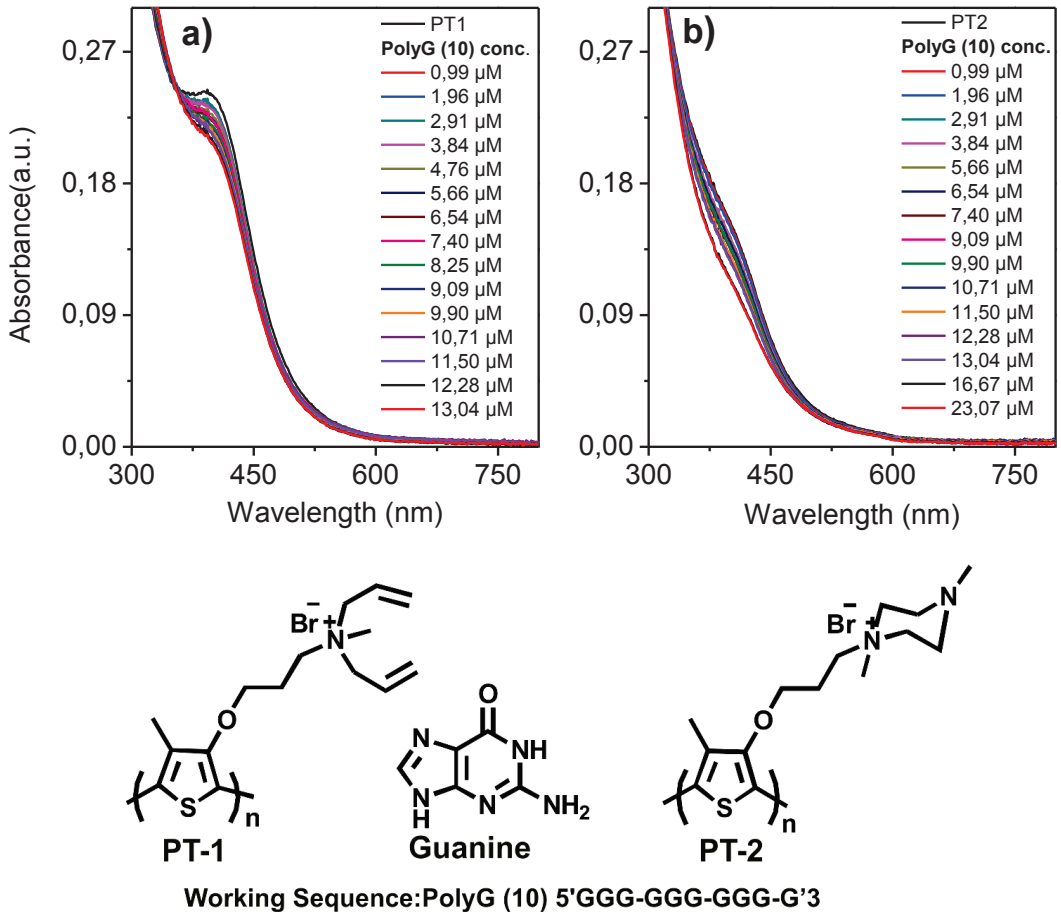

Figure 25. a) UV-VIS spectrum of PT1-PolyG (10) titration, b) UV-VIS spectrum of PT2-PolyG (10) titration

Table 3 shows the maximum absorbance ratio of 395 nm/595 nm of PT1-DNA complex titration curves. The 395 nm/595 nm ratio is low with PT1-homopyrimidine complexes. 1,25 and 4.01 for PT1-PolyC (10) complex and PT1-PolyTh (10) complex respectively. On the other hand, PT1-homopurines did not form complex and no spectral change observed during titrations. The 10mer long homopurine and homopyrimidine have a different spectrum in case of titration with PT1(Figure 27). Homopyrimidine yield a reddish colour, while homopurine yield a yellowish colour which is also PT1 colour (Figure 28).

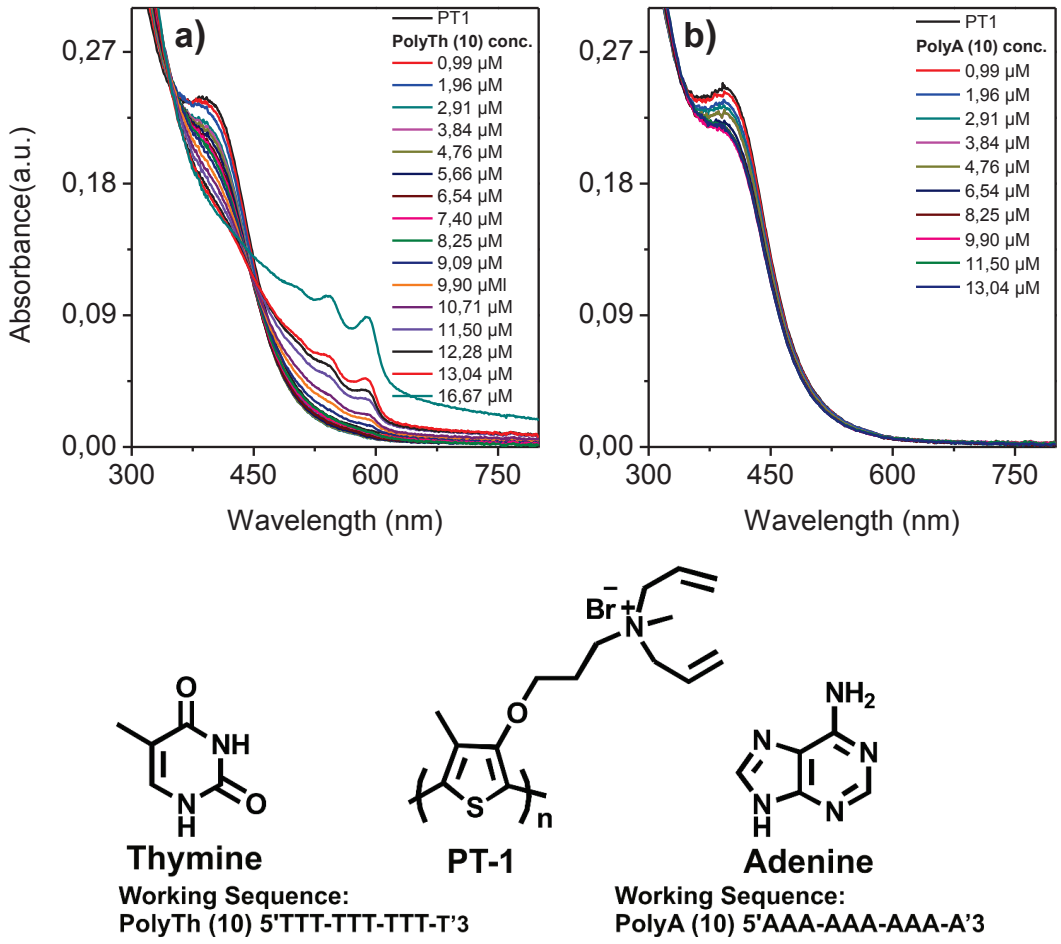

Figure 26. a) UV-VIS spectrum of PT1-PolyTh (10) titration, b) UV-VIS spectrum of PT1-PolyA (10) titration

Table 3. 395 nm/595 nm ratio of PT1-DNA complex in UV-VIS titration curves

Sequences	PolyC (10)	PolyTh (10)	PolyA (10)	PolyG (10)
Ratio	1,25	4,01	nan	nan
Sequences	PolyC (20)	PolyTh (20)	PolyA (20)	PolyG (20)
Ratio	0,84	1,44	9,00	28,60

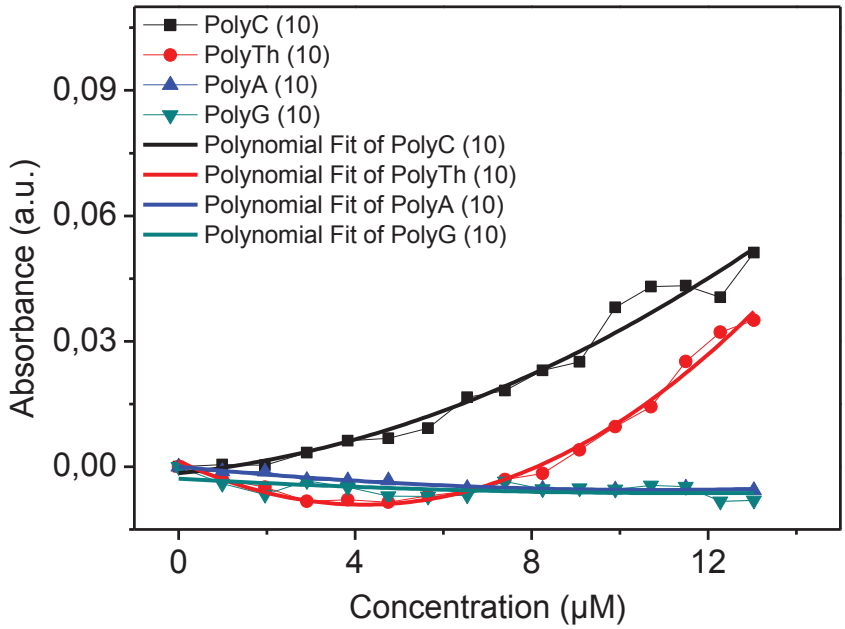

Figure 27. Intensity differences in absorbance maximum at 505 nm versus concentration of medium (10 bases long oligonucleotides)

Figure 29a shows the UV-VIS titration curve of the PT1-PolyC (20) complex. The spectrum resembles to PT1-PolyC (10) complex with different intensities of peaks at 395 nm, 505 nm, 545 nm and 595 nm. There are both macroscopic and spectral aggregation observed after concentration of ssDNA is 10,71 µM. PT1-PolyTh (20) complex UV-VIS titration curve shown in Figure 29b. General behaviour of 20 bases homopyrimidine is similar to 10 bases homopyrimidine. Red shift observed in both 10 and 20 bases homopyrimidine added into PT1 medium but maximum absorbance and maximum absorbance ratio of PT1-DNA complex is different. Also, PT1-PolyC (20) have sharp isosbestic point before aggregation nearly at 465 nm and after aggregation observed, isosbestic point shifted to a 455 nm. On the contrary PT1-PolyTh (20) have four different isosbestic point during titration and corresponding isosbestic point refers to different PT1-ssDNA complex formed during titration.

UV-VIS titration curve of the PT1-PolyA (20) shown in Figure 30a. A peak at 395 nm gradually decreased with addition of 100 µM of ssDNA. No new peaks and no isosbestic point observed until concentration of PolyA (20) is 9,09 µM. Then, intensity of peak at 505 nm slightly increased and isosbestic point form nearly at 435 nm to the end of titration. Formation of isosbestic point shows the new polymer-ssDNA complex occur

in titration medium. The number of interaction between polymer-ssDNA increased with the ssDNA chain length increased. However, polymer conformation not fully change twisted to planar during this interaction. PolyA (20) have a strong intramolecular interaction that stabilize the polymer as a twisted conformation with different dihedral angle compared to initial dihedral angle. At the same time polymer-ssDNA interaction formed and effect the UV-VIS region. UV-VIS titration curve of PT1-PolyG (20) shown in Figure 30b and no spectral change observed during titration.

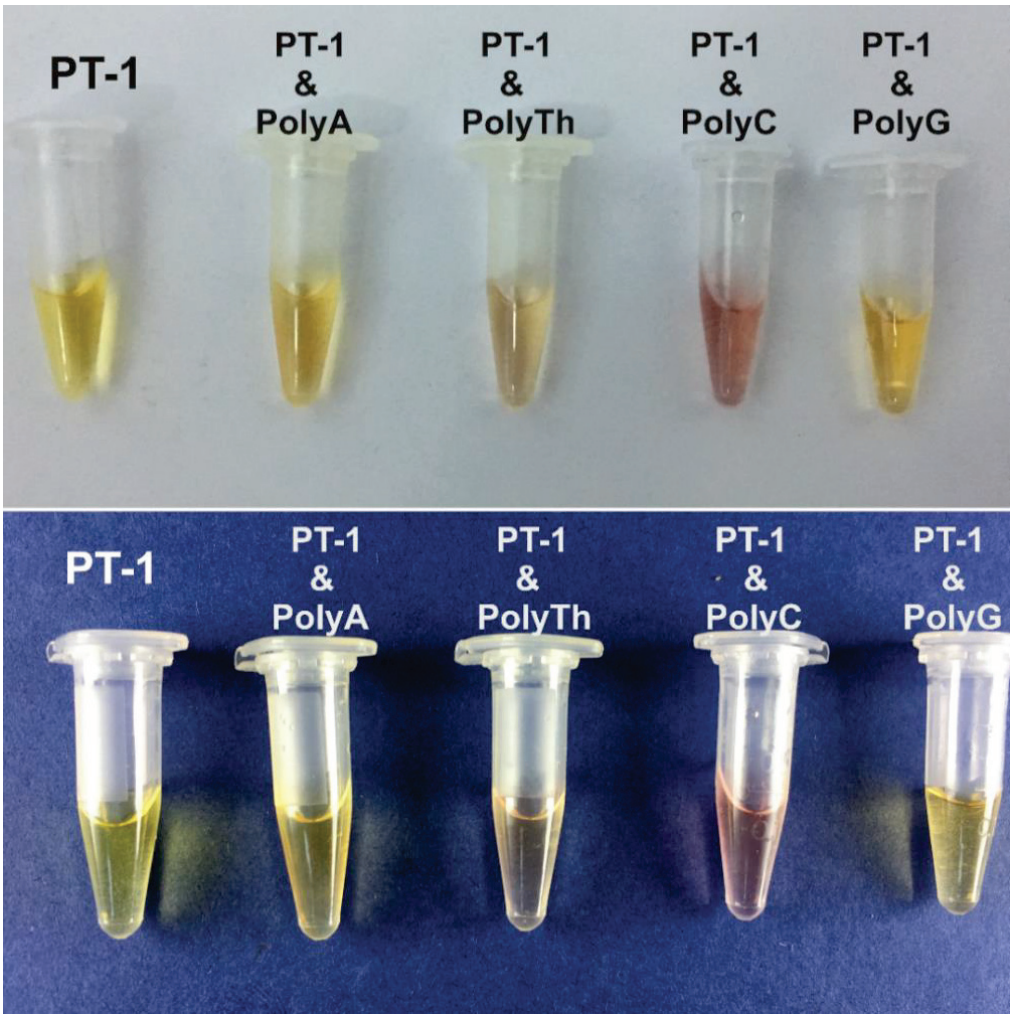

Figure 28. Image of PT1-ssDNA complex with different background

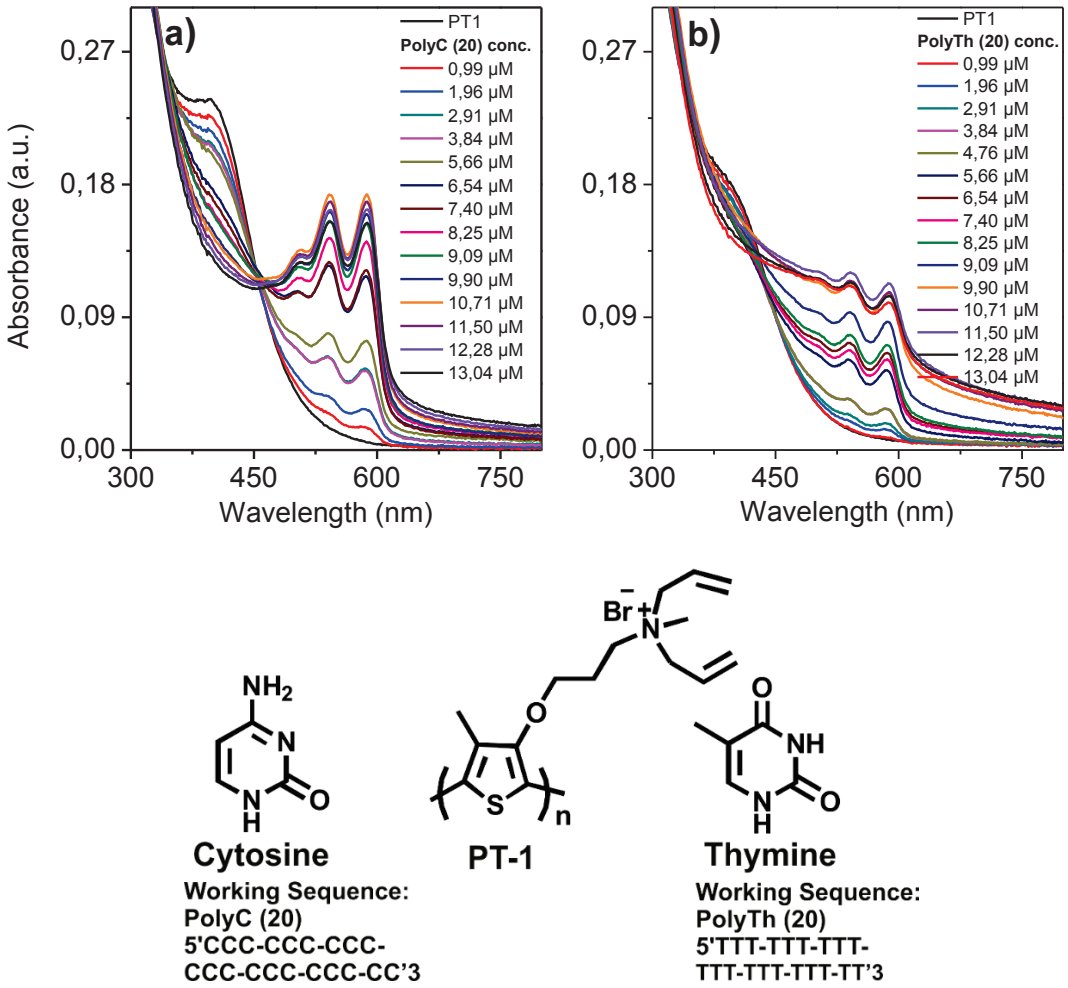

Figure 29. a) UV-VIS spectrum of PT1-PolyC (20) titration, b) UV-VIS spectrum of PT1-PolyTh (20) titration

20 bases long homopurine and homopyrimidine characterized with PT1. All types of homonucleotides have a different corresponding titration curves (Figure 31). In this work both 10 and 20 bases long homopurine and homopyrimidine have different behaviour while make the complex with PT1 shown in Figure 32.

In polymer-dsDNA interactions polymer conformation not change twisted to planar. Polymer surround the dsDNA complex and polymer-dsDNA make the triplex complex. On the contrary polymer-ssDNA make the duplex complex and random coiled polymer change conformation and became planar. Also, aggregation observed with Polymer-homopyrimidine. Graphical representation of polymer-ssDNA duplex complex and polymer-dsDNA triplex complex shown in Figure 33.

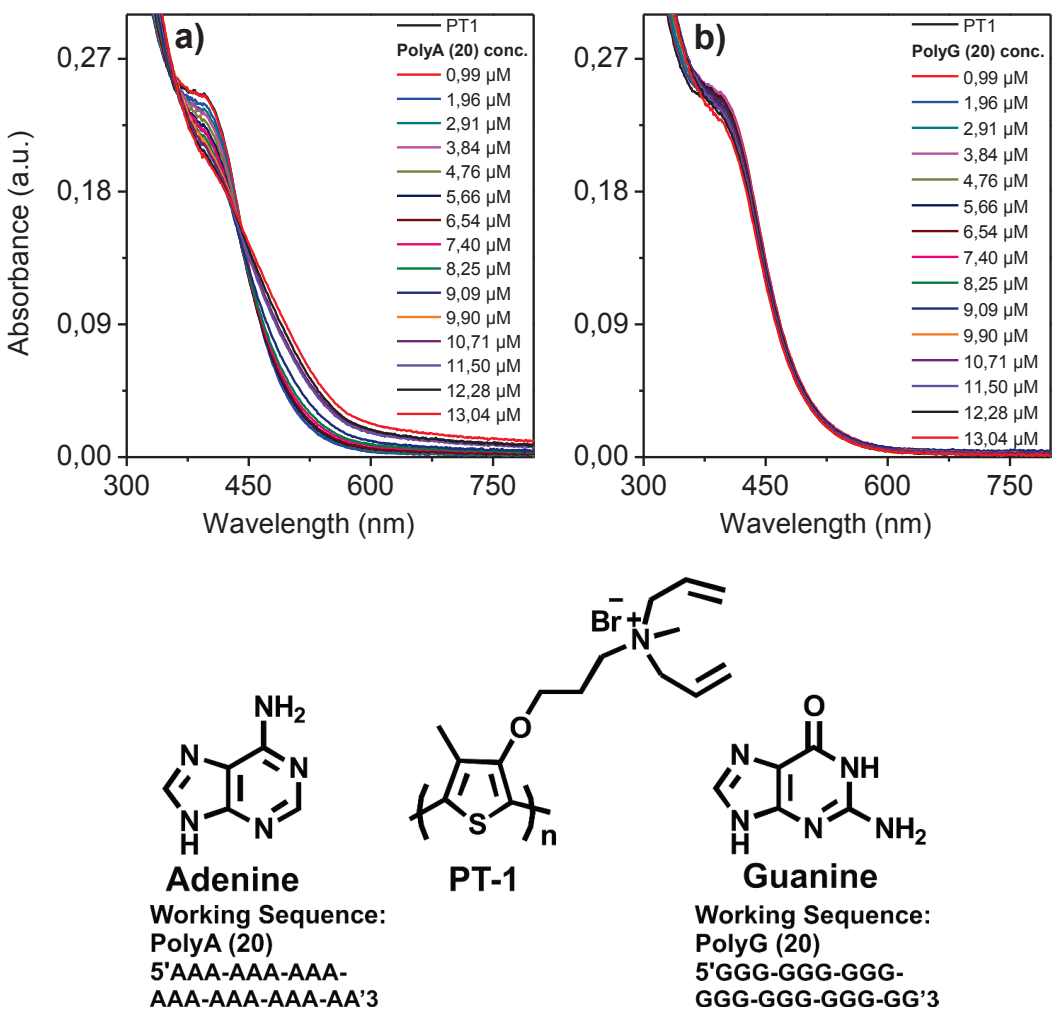

Figure 30. a) UV-VIS spectrum of PT1-PolyA (20) titration, b) UV-VIS spectrum of PT1-PolyG (20) titration

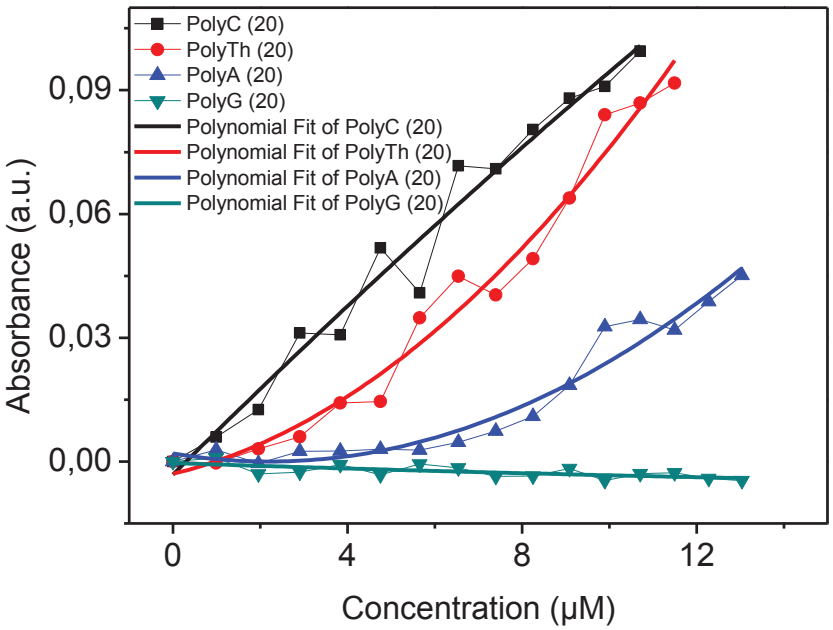

Figure 31. Intensity differences in absorbance maximum at 505 nm versus concentration of medium (20 bases long oligonucleotides)

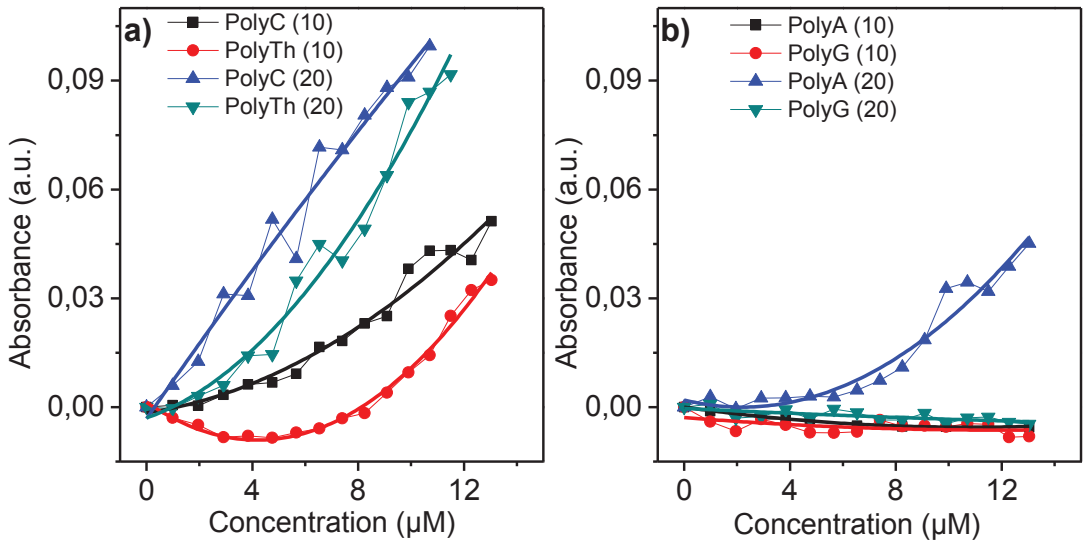

Figure 32. Intensity differences in absorbance maximum at 505 nm versus concentration of medium a) homopyrimidines, b) homopurines

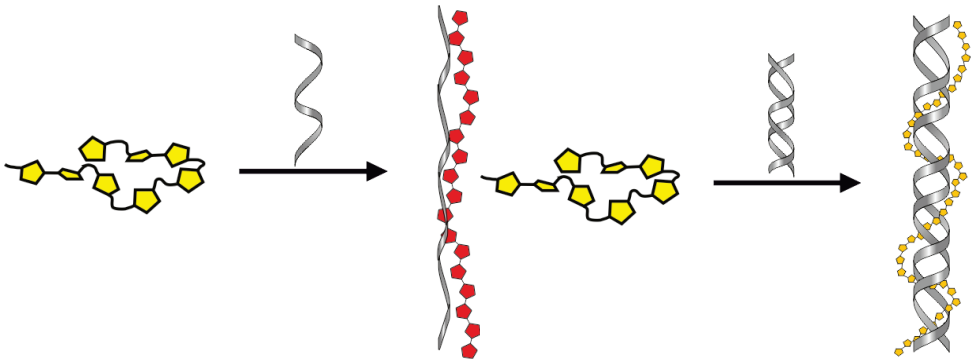

Figure 33. Polymer-ssDNA duplex complex and polymer-dsDNA triplex complex

Figure 34 shows the PT1-dsAT (10) UV-VIS titration curve. A peak at 395 nm slightly decrease with every addition of dsDNA. At the same time a peak at 505 nm gradually increased. The reason of 505 nm peaks increment is remaining ssDNA in the medium yield a duplex complex or polymer dihedral angle change during interacted with dsDNA. Isosbestic point of spectrum is 465 nm. The spectrum of PT1-PolyA (20) is resemble to PT1-dsAT (10) spectrum. The intensity ratio of PT1-PolyA (20)/ PT1-dsAT (10) peak at 505 nm is 1,51 and 30 nm differences observed while comparing isosbestic points of titration curves. This shows the PT1-dsAT (10) triplex complex successfully formed and have different environment compared to PT1-PolyA (20) duplex complex. In addition to this PT1-PolyA (10) duplex complex not formed and no spectral change observed and PT1-PolyTh (10) yield new peaks at 505 nm, 545 nm and 595 nm with four different isosbestic point. PT1-dsAT (20) titration curve shown in Figure 35 and a peak at 395 nm slightly decreased with addition of dsAT (20) while a peak at 505 nm gradually increased. The isosbestic point of titration curve is 449 nm and the intensity ratio of PT1-dsAT (20)/ PT1-PolyA (20) is 1,40 with a 14 nm shift of isosbestic point. PT1-dsAT (20)/ PT1-dsAT (10) is 2,11 with a 16 nm shift of isosbestic point. Furthermore, absence of peaks at 545 nm and 595 nm shows the triplex complex of polymer-dsDNA formed successfully. Three titration curves which PT1-PolyA (20), PT1-dsAT (10) and PT1-dsAT (20) resulted the different species formed during polymer-DNA interactions due to the occurrence of different isosbestic point and different absorbance maximum intensity.

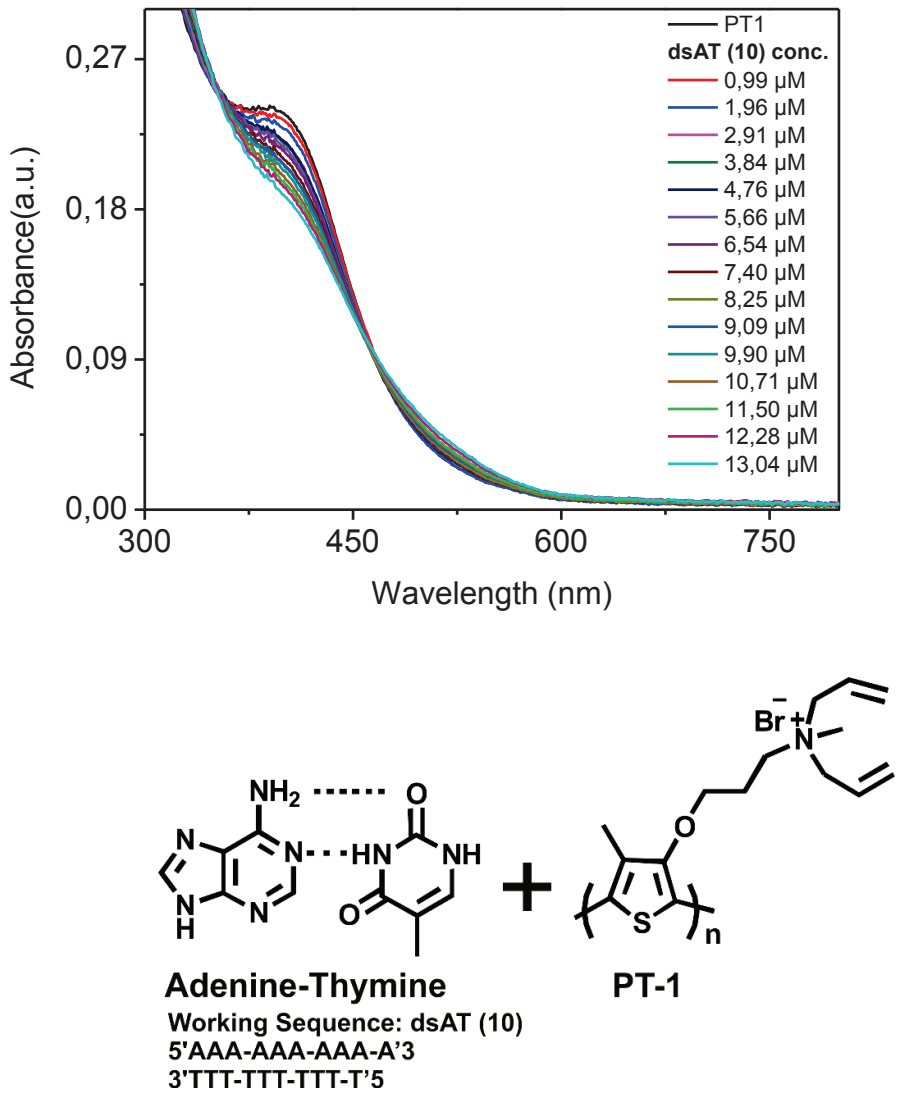

Figure 34. UV-VIS spectrum of PT1-dsAT (10) titration

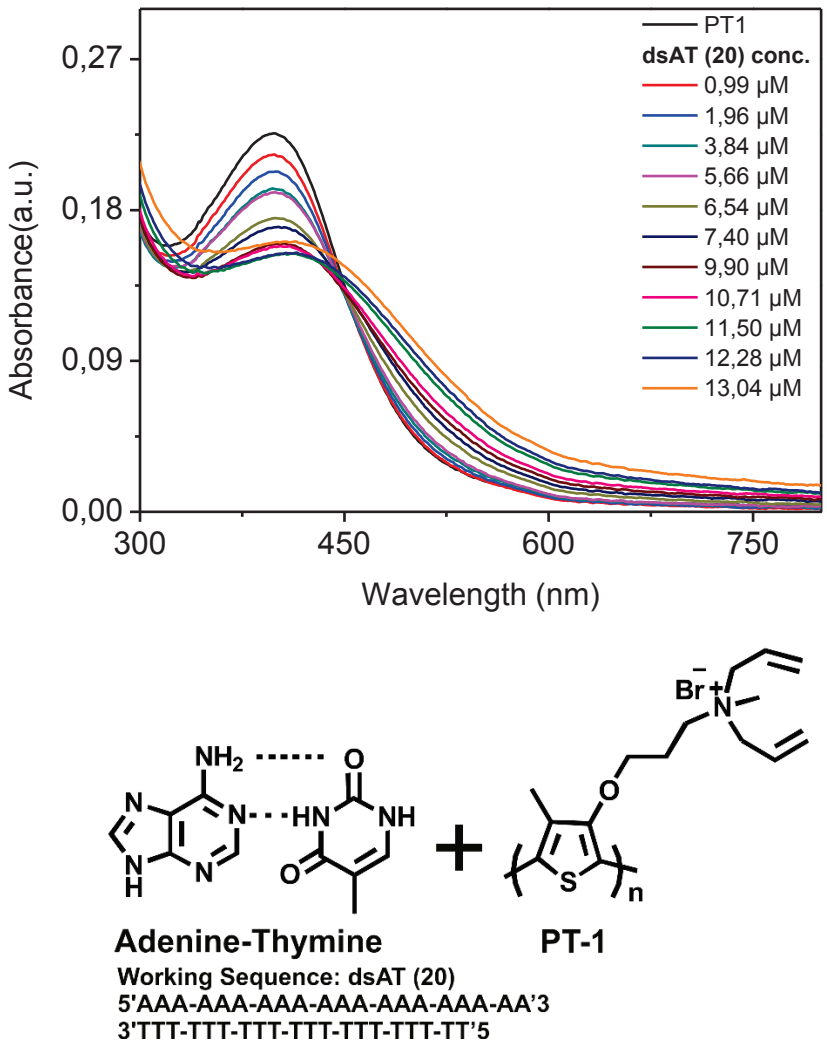

Figure 35. UV-VIS spectrum of PT1-dsAT (20) titration

To understand the fluorescence behaviour of the oligonucleotides of homopurine and homopyrimidine, titration experiments were performed for 10 bases long homonucleotides and monitored with fluorescence spectrophotometer. PT1-PolyC (10) titration curve shown in Figure 36a. Emission of PT1 observed at 533 nm. Quenching observed with addition of polyC (10) and emission maximum shifted to 548 nm. The maximum emission ratio of PT1/PT1-PolyC (10) is 3,2 with a 0 and 13,04 µM concentration of polyC (10) in medium. Figure 36b shows the titration curve of the PT1-PolyTh (10). Quenching observed with addition of polyTh (10) and emission maximum shifted from 533 nm to 554 nm. The maximum emission ratio of PT1/PT1-PolyTh (10) is 2,17 with a 0 and 13,04 µM concentration of polyTh (10) in medium.

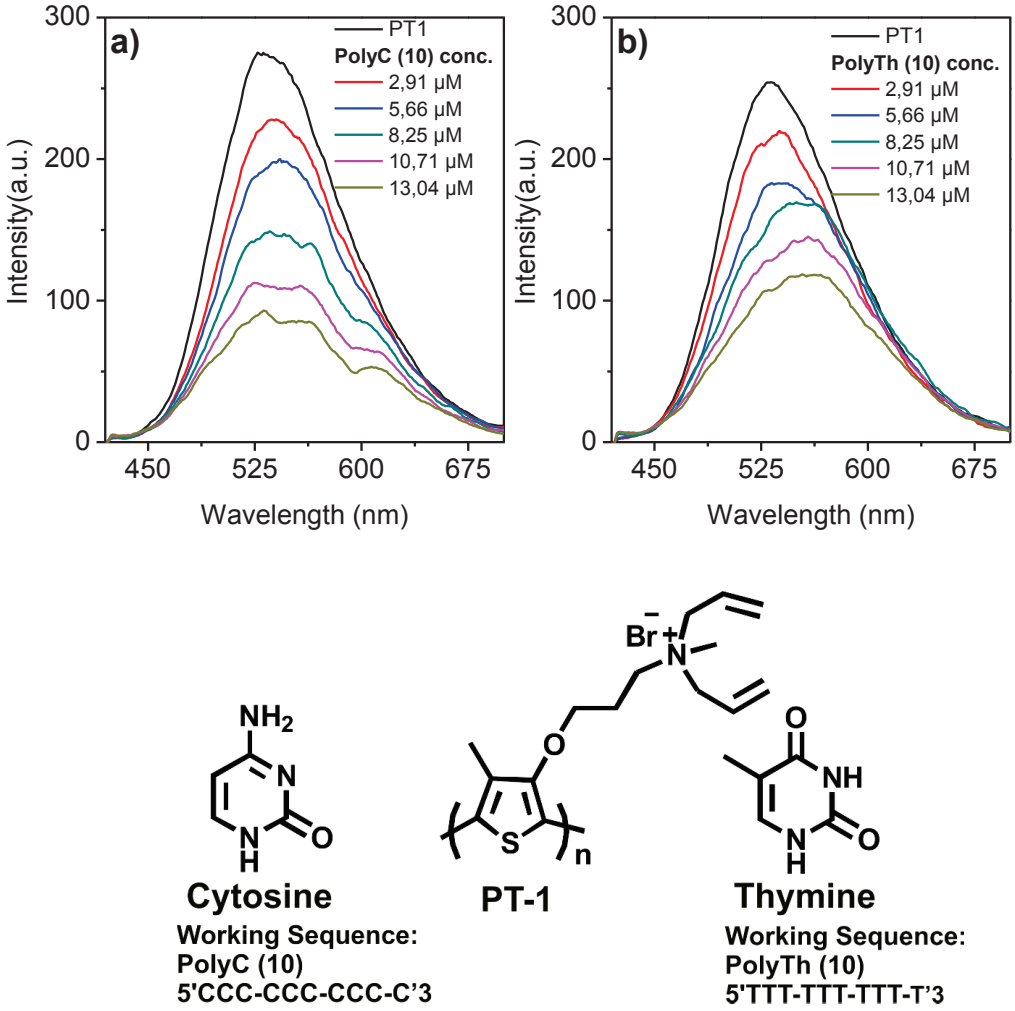

Figure 36. a) Fluorescence spectra of PT1-PolyC (10) titration b) Fluorescence spectra of PT1-PolyTh (10) titration

Titration curve of PT1-PolyA (10) shown in Figure 37a. Quenching observed with addition of polyA (10) and emission maximum shifted from 533 nm to 538 nm. The maximum emission ratio of PT1/PT1-PolyA (10) is 1,42 with a 0 and 13,04 µM concentration of polyA (10) in medium. Figure 37b shows the titration curve of the PT1-PolyG (10). The emission maximum decreased and shifted from 535 nm to 538 nm with addition of polyG (10). The emission ratio of PT1/PT1-PolyG (10) is 1,29 with a 0 and 13,04 µM concentration of polyG (10) in medium.

3.4. Characterization of Methylated and Unmethylated DNA

PT3 based spectrophotometer analysis were applied for the characterization of methylated and unmethylated DNA. PT3-ssDNA titration were performed and monitored with the UV-VIS spectrophotometer and target ssDNA were; PolyC (10), Methylated

sequence, Unmethylated sequence and Complementary-2. Working sequences methylated and unmethylated are the 20 bases long pair ssDNA at position +137 to +156 from gene $p16^{INK4A}$ which 1200 base pair long at cytogenetic position 9p21.3. Complementary-2 is the complementary sequences of after unmethylated sequences cytosine turn to uracil. Also, PolyC (10) focused in this characterization step owing to providing the ten unmethylated cytosine.

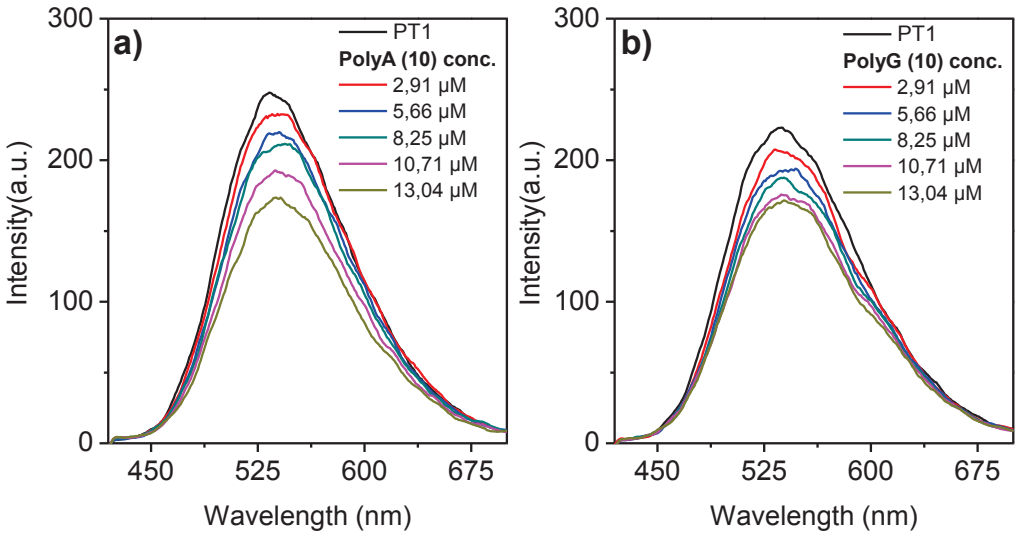

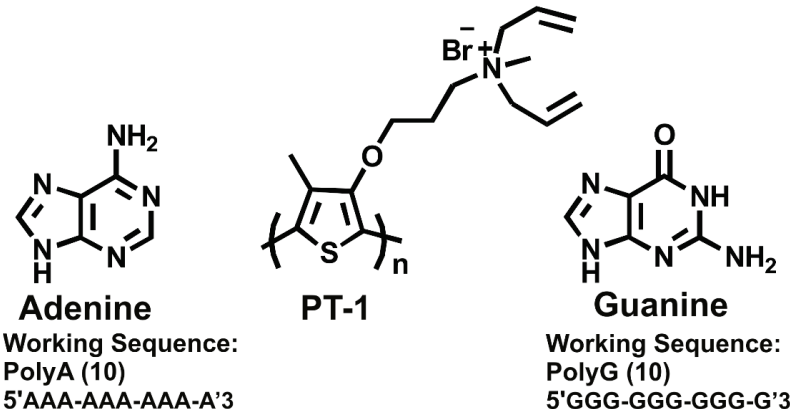

Figure 37. a) Fluorescence spectra of PT1-PolyA (10) titration b) Fluorescence spectra of PT1-PolyG (10) titration

PT3-ssDNA complexes and interaction focused to understand the behaviour of newly formed polymer-ssDNA complex to compare the before and after SBC. Figure 38 shows the titration curve of the PT3-Unmethylated sequence. A peak at 395 nm gradually decrease with the addition of the ssDNA and intensity of peak at 505 nm increase with the addition of ssDNA. Added amount of unmethylated sequence into medium has fast effect on polymer behaviour. Figure 38a shows the titration curve which corresponds the

multiple isosbestic point and formation of aggregates with respect to the further addition of ssDNA. On the contrary one isosbestic point observed at 433 nm with addition of 5,52 µg unmethylated sequence. This graph shows the further titration experiments should be performed with the final amount of unmethylated sequence is 5,52 µg which has dominantly one type of polymer-ssDNA complex.

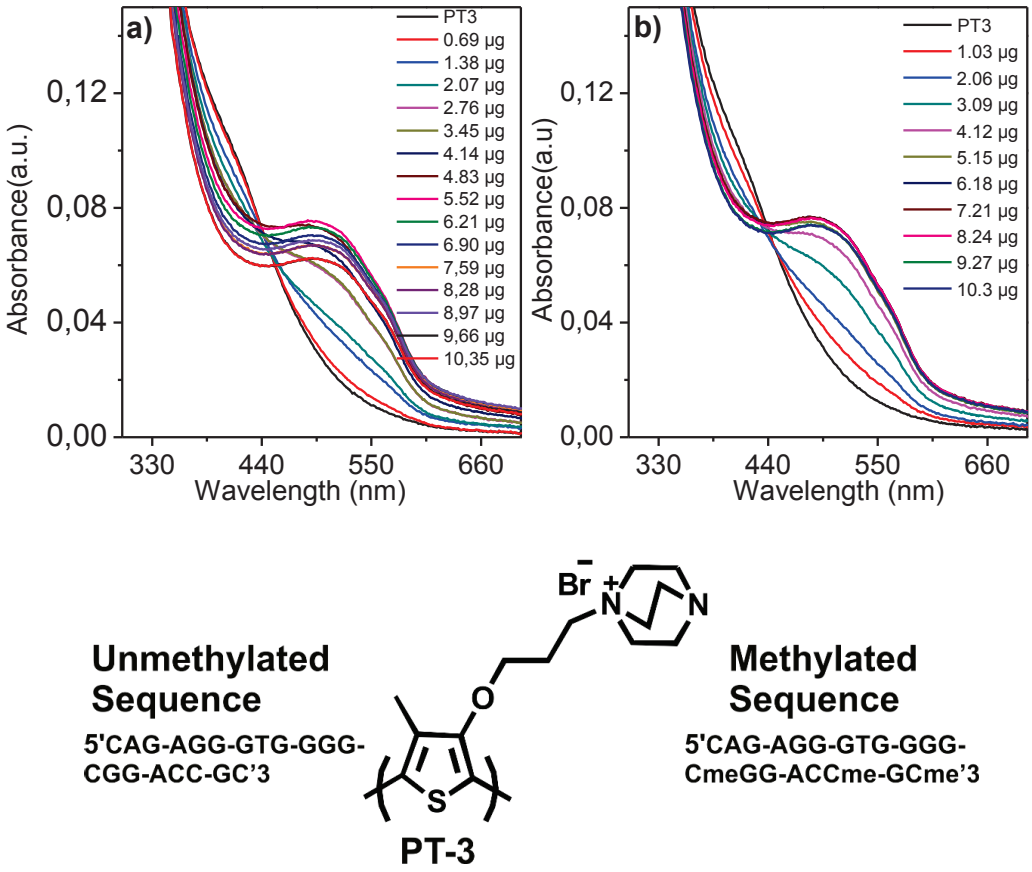

Figure 38. a) UV-VIS spectra of PT3-Unmethylated sequence titration b) UV-VIS spectra of PT3-Methylated sequence titration

Same titration process was performed with using PT3 and methylated sequence shown in Figure 38b. A peak at 395 nm decreased while a peak at 505 nm increased with addition of methylated sequence. Both aggregation and multiple isosbestic point observed during titration. However, one isosbestic point occurred at 430 nm until addition 8,24 µg methylated sequence. It shows the final amount of methylated sequence should be 7,21 µg for the further titration experiments.

These two titration curves; PT3-Unmethylated sequence and PT3-Methylated sequence have a similar behaviour. The observed isosbestic point nearly at the same wavelength which are at 433 nm and at 430 nm for the PT3-Unmethylated sequence and

PT3-Methylated sequence respectively. Corresponding absorbance maximum at 505 nm is the same for both titration curves which is 0,075 (a.u.). This similarity is significant while unmethylated sequence and methylated sequence have an identical sequence as bases. The only difference of these sequences is the methylated cytosine bases at positions 13, 18 and 20 (Table 1). Also, some spectral differences observed in UV-VIS titration curves. Absorbance maximum at 505 nm is 0,075 (a.u.) with addition of 5,52 µg unmethylated sequence while amount of methylated sequence is 7,21 µg to yield a 0,075 (a.u.) absorbance maximum at 505 nm. The reason of this amount difference is methyl groups at 5' position in cytosine structure, interrupt the interaction of polymer-ssDNA complex. PT3-Complemenlatary-2 titration curve has a different behaviour compared to methylated and unmethylated sequence (Figure 39). New peak occurred after addition of ssDNA at 525 nm. Corresponding absorbance maximum is 0,063 (a.u.) with addition of 4,2 µg complementary-2. The isosbestic point of curve observed at 448 nm before aggregation start. The fast increase of a peak at 525 nm resulted from the fast change in polymer conformation. Conformational change is fast with the polymer-homopyrimidine complex formation. In this scenario, evolution of titration curve resulted from the homopyrimidine content in complementary-2. The ratio of cytosine is 55% while the thymine ratio is 15% (70% homopyrimidine ratio) in complementary-2. PT3-PolyC (10) interaction already examined and monitored with UV-VIS spectrophotometer. In detection of DNA methylation section, working polymer is PT3 and titration experiment repeated with PT3. Maximum absorbance ratio of 395 nm/595 nm of PT3- PolyC (10) complex is 1,27. The behaviour of 2 different titration curves is similar with different intensities.

To understand the nature of sequences and behaviour of the polymer-DNA complex is crucial for the further DNA methylation detection. The comparison of homopyrimidine ratio in target sequences also give an idea about the required amount of ssDNA for the analysis and evolution of the UV-VIS spectra (Figure 41). Considering 20 base pairs target sequences for the DNA methylation detection from the $p16^{INK4A}$ gene, both unmethylated and methylated sequence cytosine ratio is 25% while the thymine ratio is 5% (30% homopyrimidine ratio). Homopyrimidine content effect the rate of the formation of polymer-ssDNA complex in heterosequence regarding UV-VIS titration curve of the unmethylated sequence, methylated sequence, complementary-2 with the PT3.

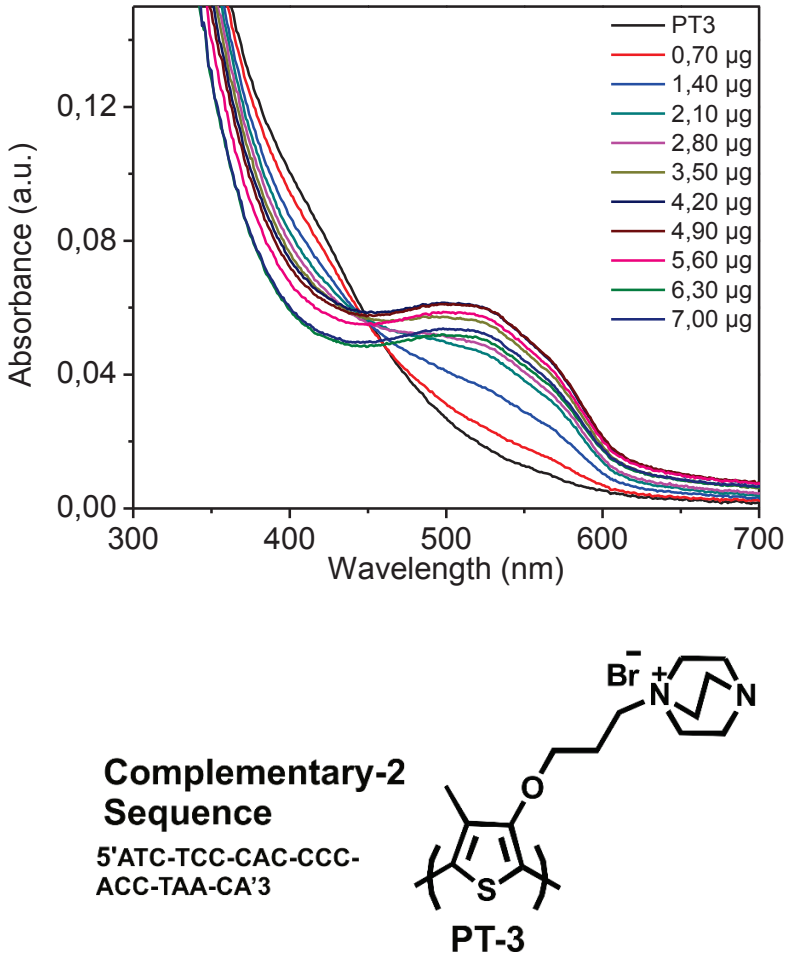

Figure 39. UV-VIS spectra of PT3- Complementary-2 titration

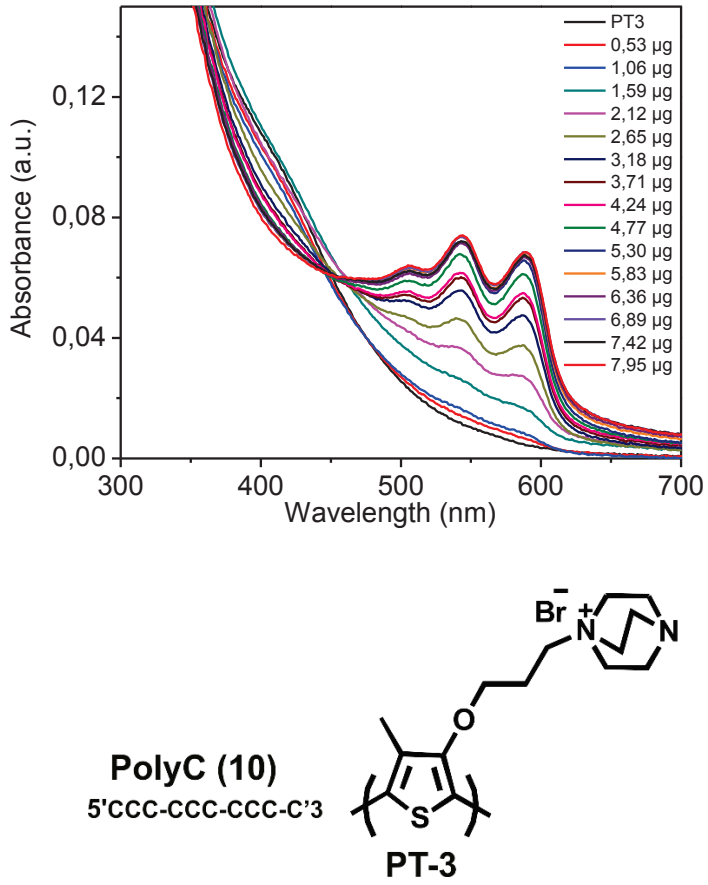

Figure 40. UV-VIS spectra of PT3- PolyC (10) titration

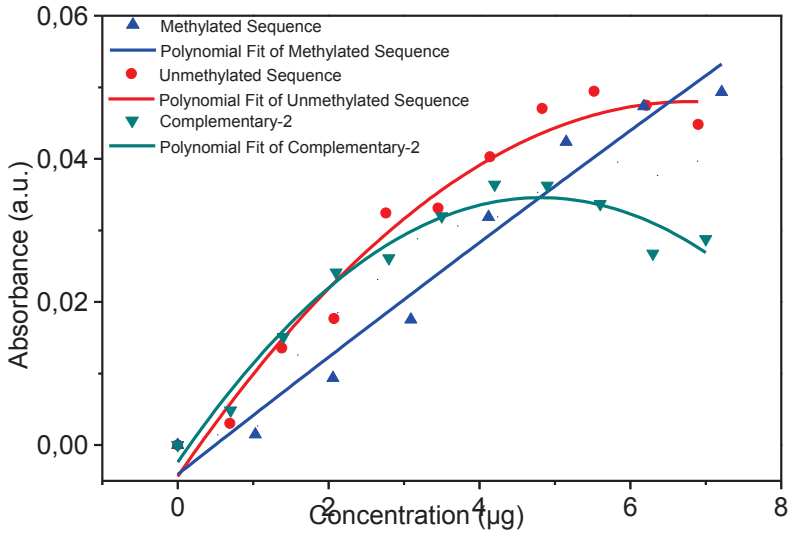

Figure 41. Intensity differences in absorbance maximum at 505 nm versus amount of adding oligonucleotides (µg) in a medium

3.5. Detection of DNA Methylation of p16^{INK4A} gene by Polythiophene

The conformational change in polythiophene backbone with addition of DNA samples monitoring with UV-VIS and fluorescence spectrophotometer and methylated and unmethylated sequence can be detected by the proposed assay shown in Figure 42.

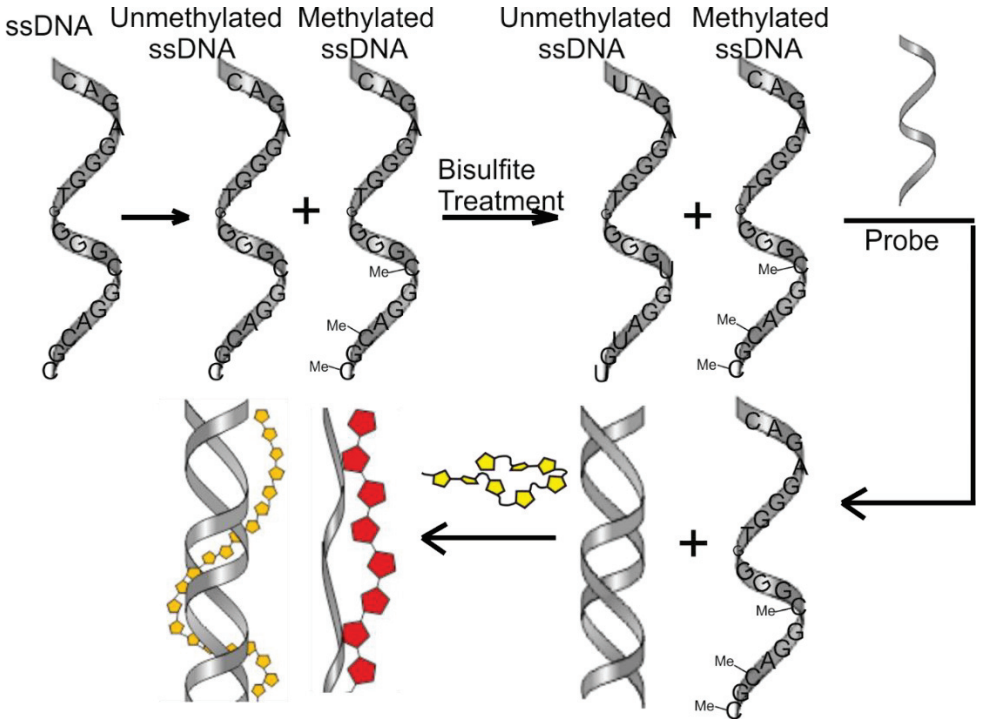

Figure 42. Detection mechanism of DNA methylation of p16INK4A gene by polythiophene based optical sensor

For the detection of DNA methylation of p16^{INK4A} gene, PolyC (10) used as reference sequence. All SBC protocols applied to the PolyC (10) and converted to PolyU (10). The aim of this step is also ensuring the SBC efficiency. 100 µM DNA samples were used in every step of DNA characterization. However, in detection of DNA methylation section the molarity of DNA samples smaller or equal to 10 µM. This molarity difference originated from the SBC protocols. Reference titration curves are required to understand the accomplishment of SBC. Figure 43a shows the titration curve of the PT3-PolyC (10) complex and the molarity of added polyC (10) into a PT3 medium is 10 µM. A peak at 405 nm gradually decreased with addition of ssDNA. At the same time, the peaks at 545 nm and 585 nm slightly occurred. This result shows the PT3 is suitable for the low concentrated DNA samples. PT3-PolyA (10) titration curve in low concentration shown in Figure 43b. Decrease of polymer absorbance maximum observed during titration while there is no spectral change in longer wavelength.

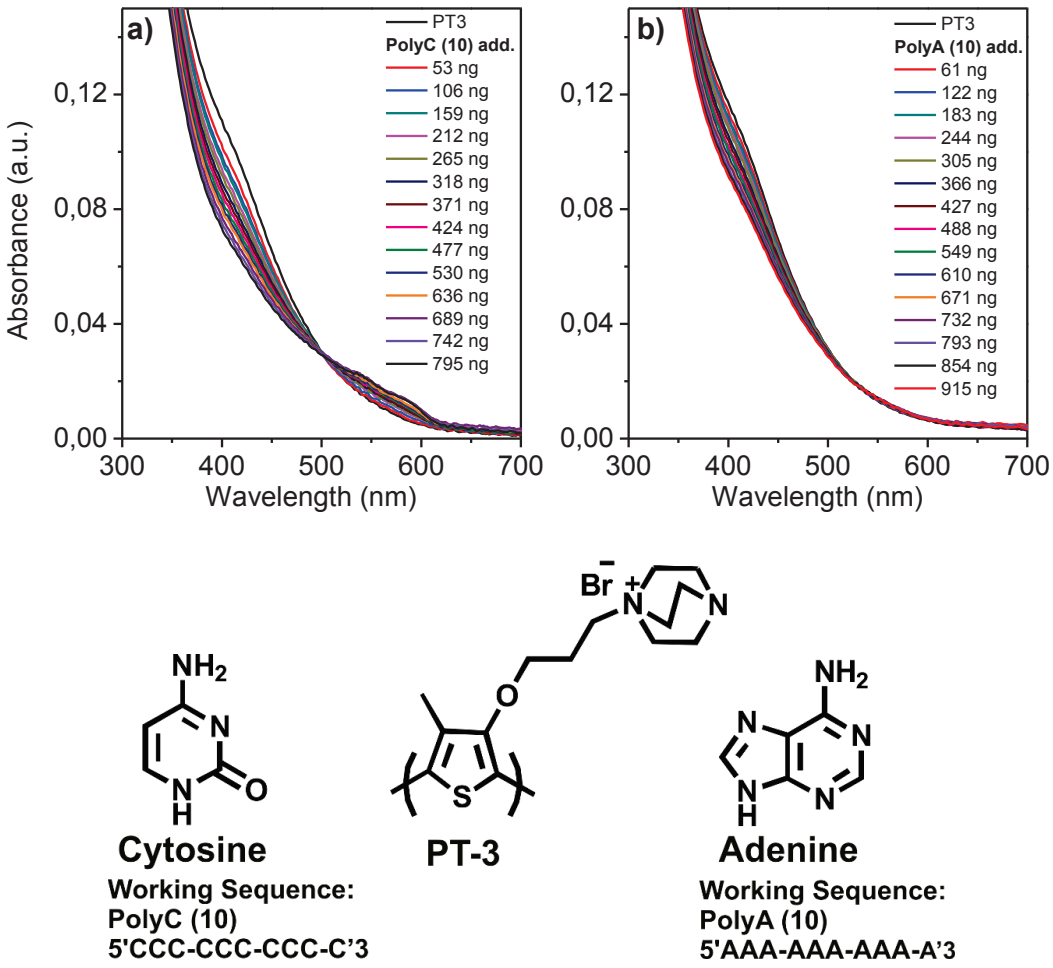

Figure 43. a) UV-VIS spectra of PT3-PolyC (10) titration b) UV-VIS spectra of PT3-PolyA (10) titration

Polymer-ssDNA titration curves are required to compare the before and after SBC to demonstrate the all cytosine units in polyC (10) chain converted to uracil successfully. Figure 44a shows the titration curve of PT3-PolyU (10). The intensity of polymer band slightly decreased with addition of ssDNA while there is no spectral change in longer wavelength. However, formation of isosbestic point shows the 2-different species in a medium which are PT3 and PT3-PolyU (10) complex. PT3-dsAU titration curve shown in Figure 44b. A peak at 405 nm gradually decrease while the intensity of a range between 505 nm to 595 nm is slightly increased with addition of dsDNA. Also, a peak at 405 nm intensity difference is 0,026 (a.u.) while the intensity changes on PT3-PolyU (10) is 0,016 (a.u.). Isosbestic point observed at 485 nm. Comparison of isosbestic points of both before and after SBC polymer-DNA titration curves also give the information about the accomplishment of SBC. The isosbestic points of titration curves;

505 nm, 520 nm, 515 nm and 485 nm for the PT3-PolyC (10), PT3-PolyA (10), PT3-PolyU (10) and PT3-dsAU respectively.

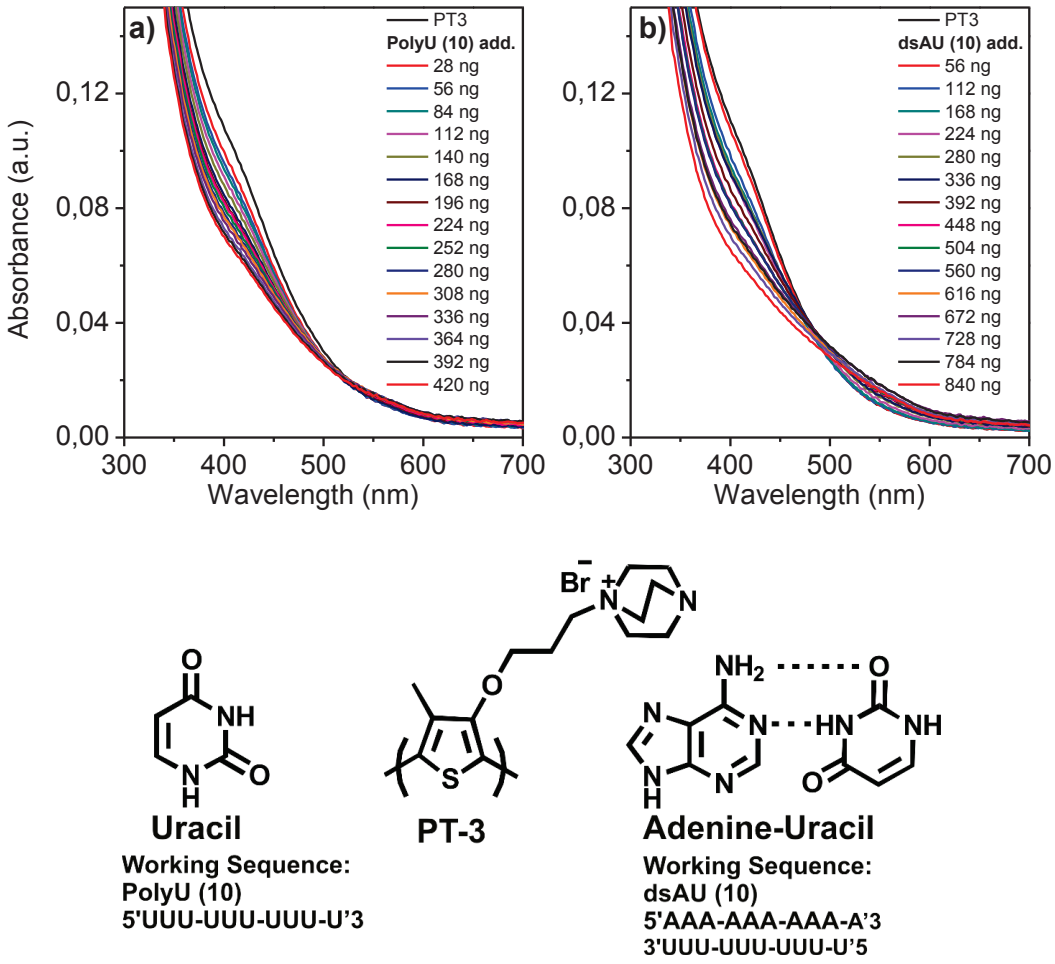

Figure 44. a) UV-VIS spectra of PT3- PolyU (10) titration after SBC b) UV-VIS spectra of PT3- dsAU (10) titration after SBC

The final UV-VIS spectra of PT3-PolyC (10), PT3-PolyA (10), PT3-PolyU (10) and PT3-dsAU complexes shown in Figure 45. This graph shows the all species have a different spectral behaviour. Optimization of SBC reaction and titration experiments have been done successfully and target sequences from the $p16^{INK4A}$ prepared and converted with respect to these reference experiments. Both low concentrated unmethylated and methylated sequences reference titration curves are required to comparison. PT3-Unmethylated titration curve before SBC shown in Figure 46a. A peak at 405 nm slightly decreased while a peak at 545 nm gradually increased with the addition of unmethylated sequence.

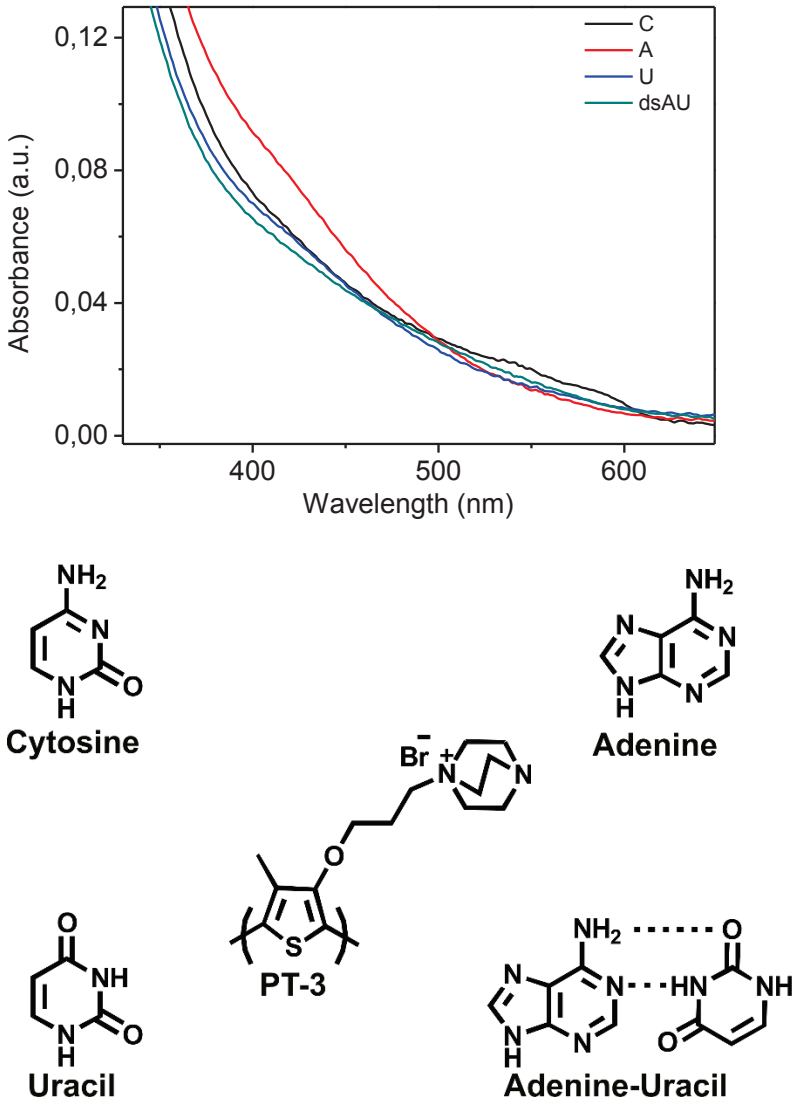

Figure 45. Final UV-VIS spectra with different DNA species

Formation of isosbestic point observed at 505 nm during titration. Corresponding intensity change in both polymer absorbance maximum and longer wavelength with addition of unmethylated sequence is merely observed owing to low concentrated DNA samples to compared with 100 µM DNA samples. Figure 46b shows the titration curve of PT3-Unmethylated sequence after SBC. A peak at 405 nm slightly decreased while a peak at 545 nm gradually increased with the addition of unmethylated sequence. Formation of isosbestic point observed at 485 nm. PT3-Methylated sequence titration curves before and after SBC shown in Figure 47. A peak at 405 gradually decreased while the intensity of a range between 520 nm to 595 nm slightly increased with addition of methylated sequence in both UV-VIS spectra a and b. Also, formation

of isosbestic points of 2 titration curves observed at 517 nm and 519 nm for the PT3-Methylated sequence before SBC and PT3-Methylated sequence after SBC respectively.

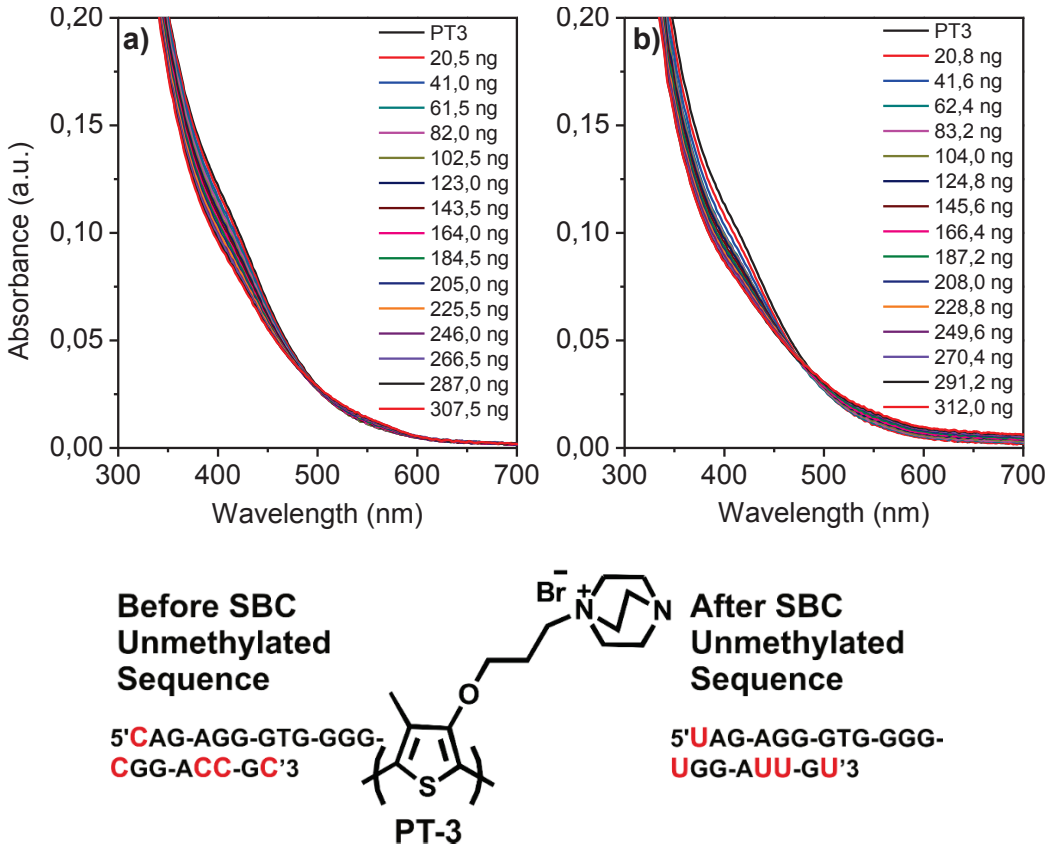

Figure 46. UV-VIS spectra of PT3-Unmethylated sequence titration a) before SBC b) after SBC

. The base content change in unmethylated sequence resulted 15 nm isosbestic point shift while the base content change in methylated sequence resulted 2 nm isosbestic shift. PT3-dsDNA (unmethylated/complementary-2) titration curve after SBC shown in Figure 48. SBC applied on unmethylated sequence while the complementary-2 sequence remains unchanged. A peak at 405 nm slightly decreased while the no spectral change observed in longer wavelength region with addition of dsDNA. Also, isosbestic point of titration curve observed at 525 nm which represent the 2-different medium; PT3 and PT3-dsDNA complex. The main difference between polymer-ssDNA and polymer-dsDNA is the new intensities in longer wavelength region. In polymer-ssDNA slightly increment of new peak observed at 545 nm in PT3-Unmethylated sequence titration curve and intensity of a range between 520 nm to 595 nm slightly increased in PT3-Methylated sequence titration curve.

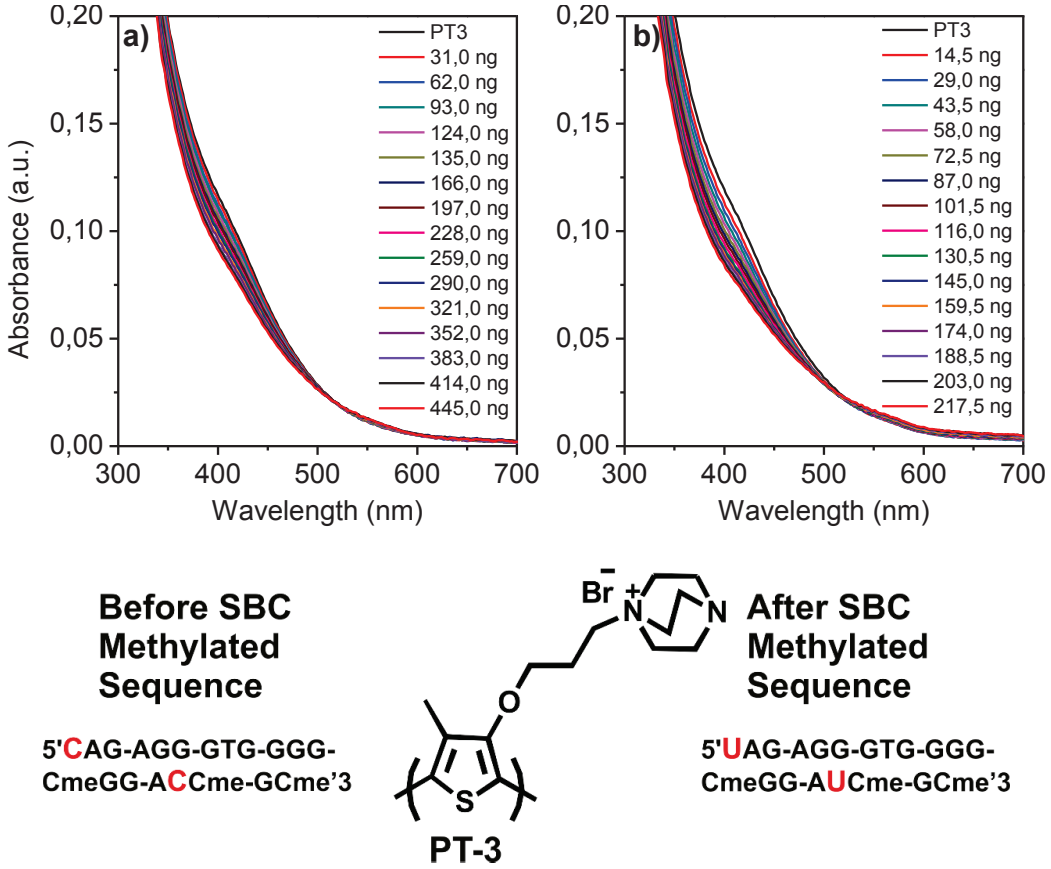

Figure 47. UV-VIS spectra of PT3-Methylated sequence titration a) before SBC b) after SBC

These UV-VIS titration curves prove the Polymer-ssDNA and Polymer-dsDNA titration curves yield an essential spectral change in UV-VIS region. The fast time analyse desired for the clinical use that is why fluorescence characterization and detection of DNA methylation with fluorescence spectrophotometer required. To detect the DNA methylation titration experiments were performed for the unmethylated sequence, methylated sequence and dsUnmethylated-Complementary-2 with monitoring fluorescence spectrophotometer. PT3-Unmethylated sequence titration curve shown in Figure 49. Quenching observed with addition of unmethylated sequence and emission maximum shifted from 535 nm to 542 nm. The intensity of maximum emission ratio of PT3/PT3-Unmethylated sequence is 2,13 with a 0 and 312 ng ssDNA in a medium. Figure 50 shows the titration curve of the PT3-Methylated sequence. Quenching observed with addition of methylated sequence and emission maximum shifted from 535 nm to 539 nm. The intensity of emission maximum ratio of PT3/PT3-Methylated sequence is 1,53 with a 0 to 217 ng ssDNA in a medium. PT3-dsDNA(Unmethylated-Complementary-2) titration curve shown in Figure 51. The emission maximum shifted from 535 nm to 537

nm and quenching observed with addition of dsDNA in a medium. The intensity of maximum emission ratio of PT3-PT3-dsDNA(Unmethylated-Complementary-2) is 1,42 with a 0 and 332 ng dsDNA in a medium. The maximum emission ratio is high with the PT3-ssDNA complex and low with PT3-dsDNA complex. The final amount of ssDNA and dsDNA are different for all medium. To make better comparison, similar or nearly amount of DNA required.

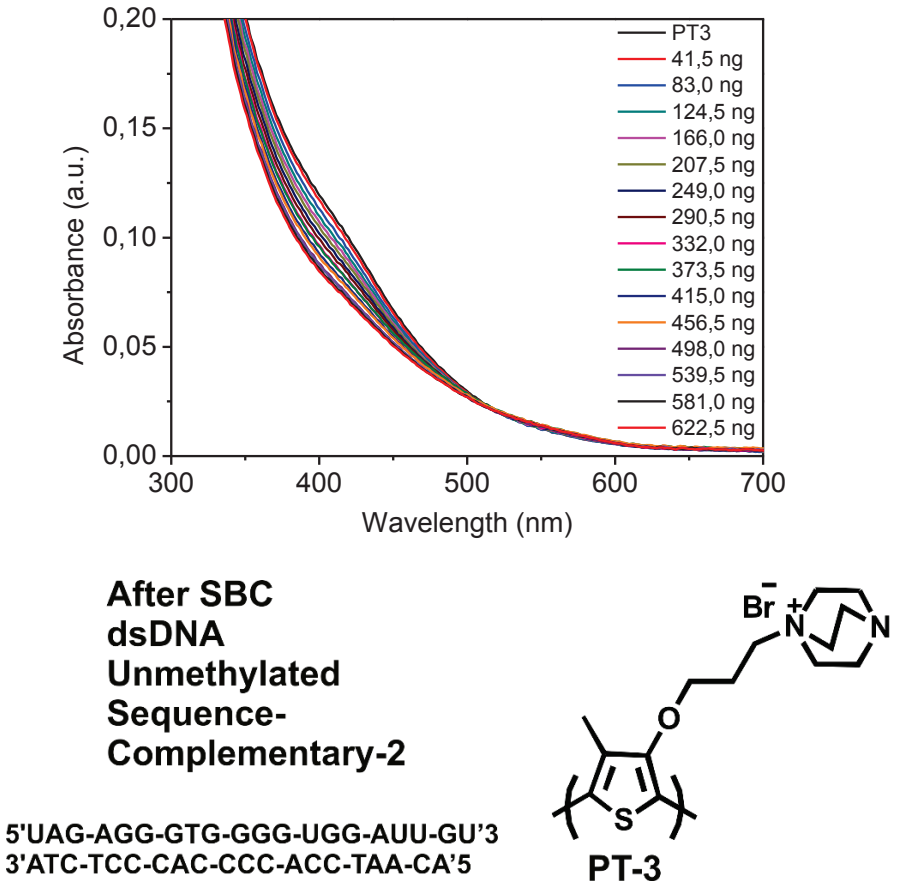

Figure 48. UV-VIS spectra of PT3-dsDNA(unmethylated/complementary-2) titration after SBC

Figure 52 shows the nearly similar amount of DNA used in titration experiments which the amount of unmethylated sequence, methylated sequence and dsDNA (Unmethylated sequence-Complementart-2) are 249,6 ng, 217,5 ng and 249,0 ng respectively. The emission maximum of PT3-Unmethylated sequence shifted from 535 nm to 539 nm to compare the PT3 emission maximum. PT3-Methylated sequence has the same shift from 535 to 539 nm. On the other hand, PT3-dsDNA complex corresponds the 2 nm shift which from 535 nm to 537 nm.

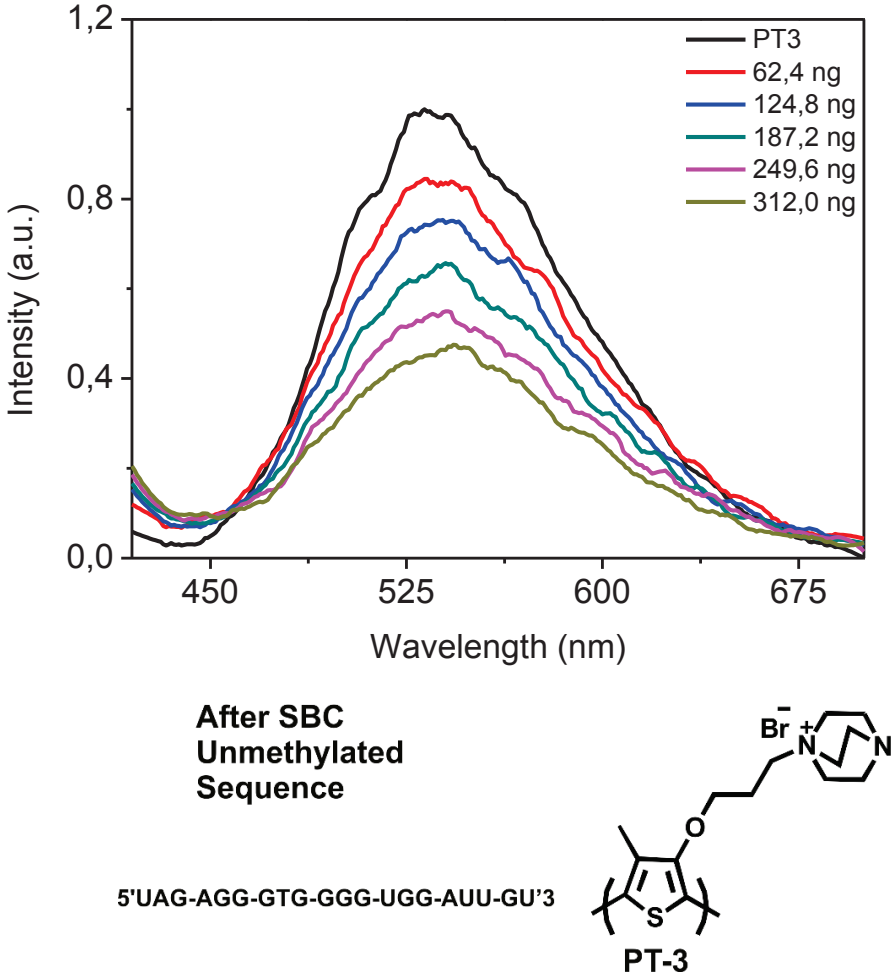

Figure 49. Fluorescence spectra of PT3-Unmethylated sequence titration after SBC

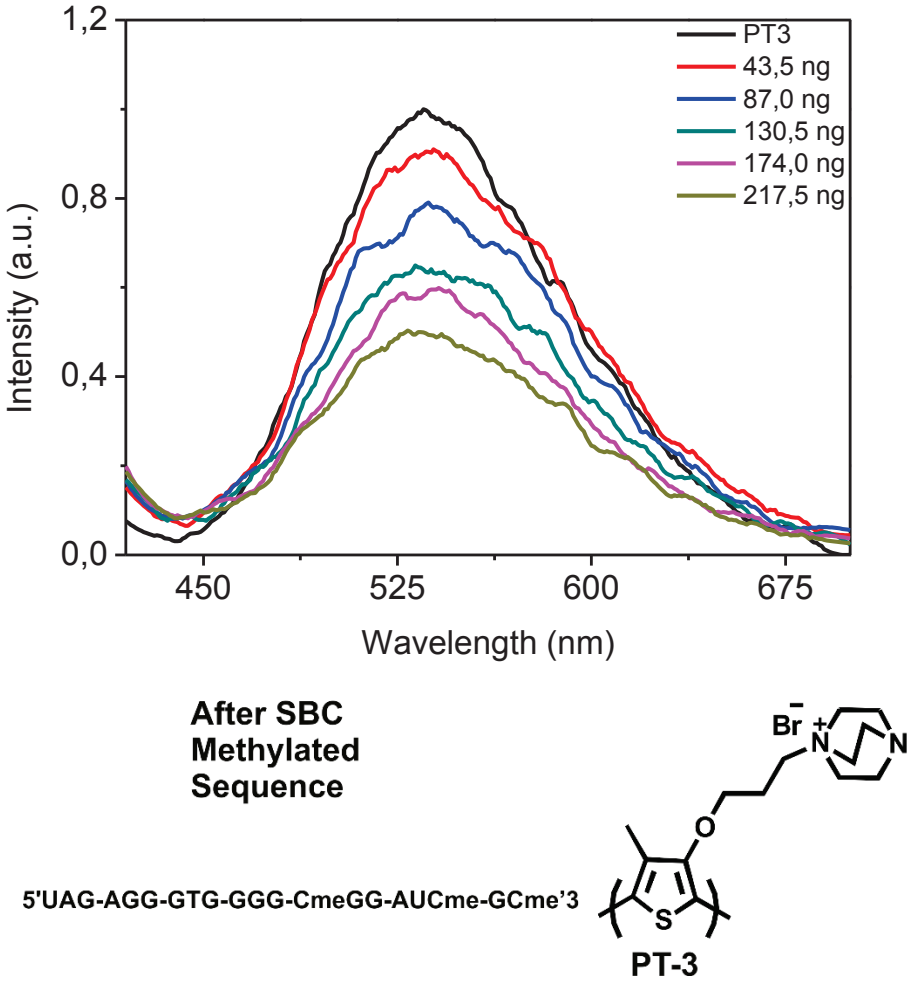

Figure 50. Fluorescence spectra of PT3-Methylated sequence titration after SBC

The intensity of emission maximum ratio of PT3/PT3-dsDNA is 1,17 with a 0 and 249,0 ng of dsDNA in a medium. The ratio is 1,65 for PT3/PT3-Unmethylated sequence with 0 and 249,6 ng of ssDNA in a medium while the ratio is 1,77 for PT3/PT3-Methylated sequence with 0 and 217,5 ng in a medium. Furthermore, under the curve area of corresponding spectra are calculated for PT3-Unmethylated sequence, PT3-Methylated sequence, PT3-dsDNA and PT3. The graph plotted I_o/I with respect to the different polymer-DNA complex where the I_o is the under the curve are of PT3 and I is the under the curve are a corresponding PT3-DNA complex (Figure 53). The general behaviour of ssDNA is I_o/I distributed from 1,6 to 1,7 while the behaviour of the dsDNA is I_o/I is equal to 1,16. The intensity of emission maximum ratio and under the curve area ratio have nearly same result but under the curve area calculation consider the all point of

spectra and better method for comparison in detection of DNA methylation. This result proved the low amount of ssDNA and dsDNA can classify with a fluorescence spectrophotometry and methylated and unmethylated sequences detected via cationic polythiophene-DNA complex behaviour. All titration experiments in detection of DNA methylation of $p16^{INK4A}$ gene by Polythiophene part were performed with addition of 1µl sample including range between 14 ng to 40 ng into the medium. To achieve the fast detection, different addition volume is tried, and titration experiments were performed with addition of 1µl, 5 µl and 15 µl sample into a medium with a same final amount of sample. This experiment carried out with PT3 and unmethylated sequence. The titration curves show the addition of 1µl and 5µl sample into the medium, yield a nearly same spectrum while the final amount of added sample is same (Figure 54).

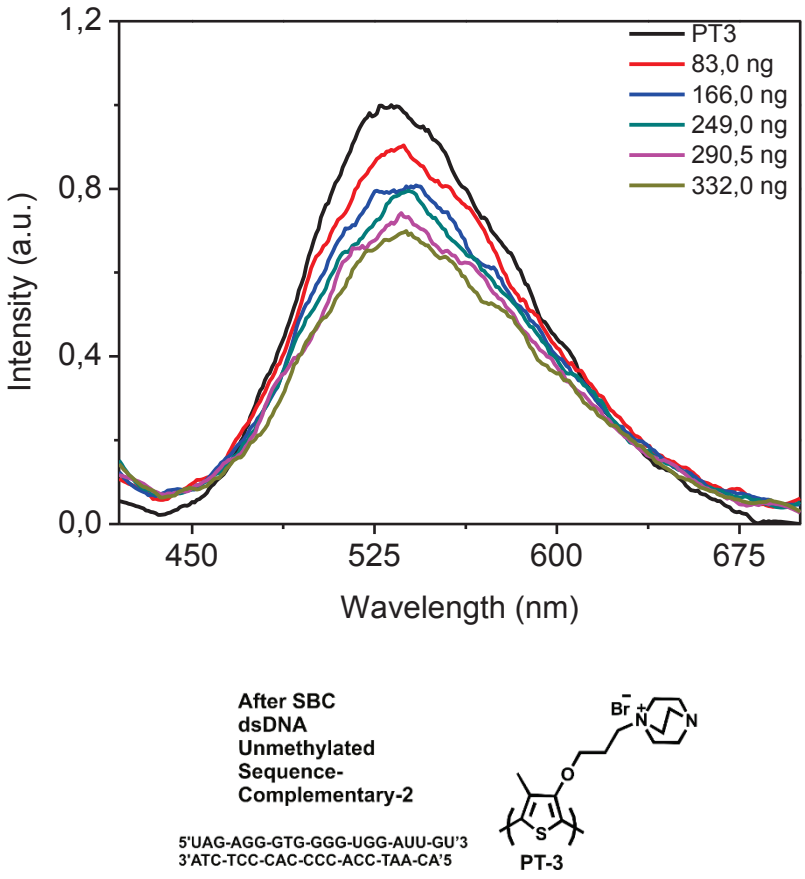

Figure 51. Fluorescence spectra of PT3-dsDNA (Unmethylated-sequence/ Complementary-2) titration after SBC

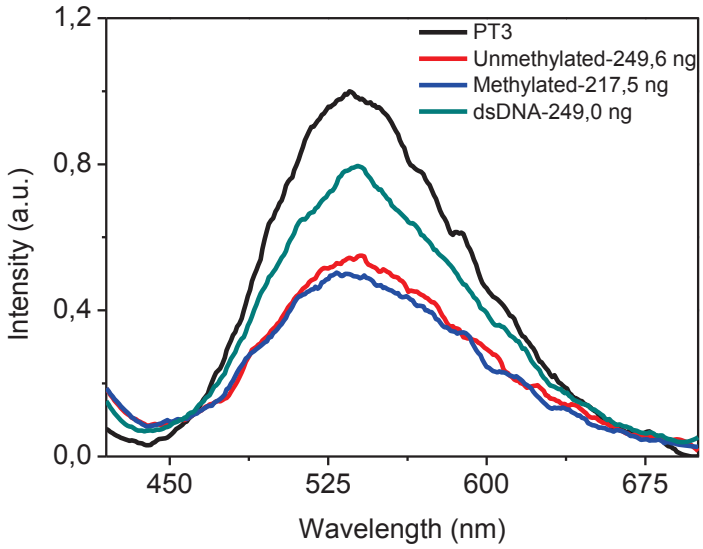

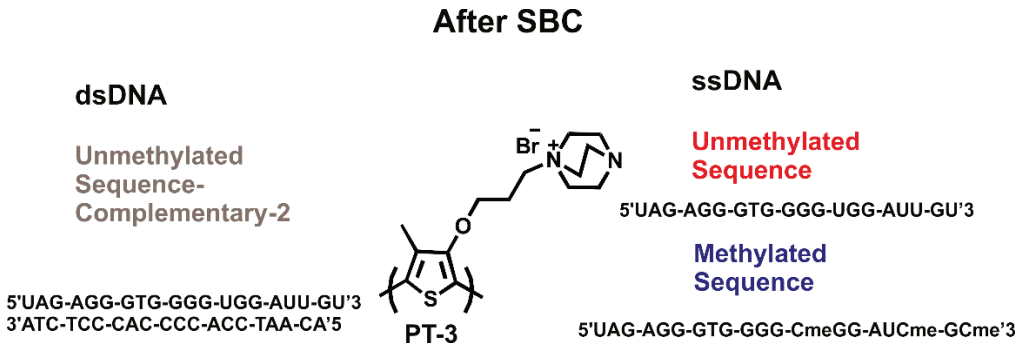

Figure 52. Fluorometric comparison of Polymer-DNA complex spectra

Titration experiments of PT3 with addition of ssDNA and dsDNA were performed to achieve the general behaviour of the ssDNA and dsDNA in under the curve area ratio for the detection of DNA methylation. Figure 55a shows the 3 different trials of both PT3-ssDNA (Unmethylated sequence) and PT3-dsDNA (Unmethylated sequence-Complementary-2) titration curves. The working scale is 700 ng for each trial of unmethylated sequence and dsDNA (Unmethylated sequence-Complementary-2). The area under the curve ratio of PT3/PT3-ssDNA trials are 1,60, 1,61 and 1,70 while the ratio of PT3/PT3-dsDNA trials are 1,39, 1,37 and 1,12 shown in Figure 56. Previous calculations show the ratio of PT3-ssDNA higher than 1,6 and ratio of PT3-dsDNA is 1,17 (Figure 53). These ratios show the PT3-ssDNA complexes and PT3-dsDNA have the different behaviour and the population of behaviour has been accomplished with the different titration trials. The region of ssDNA higher than 1.60 in I_o/I ratio while the dsDNA lower than the 1,40 in I_o/I ratio.

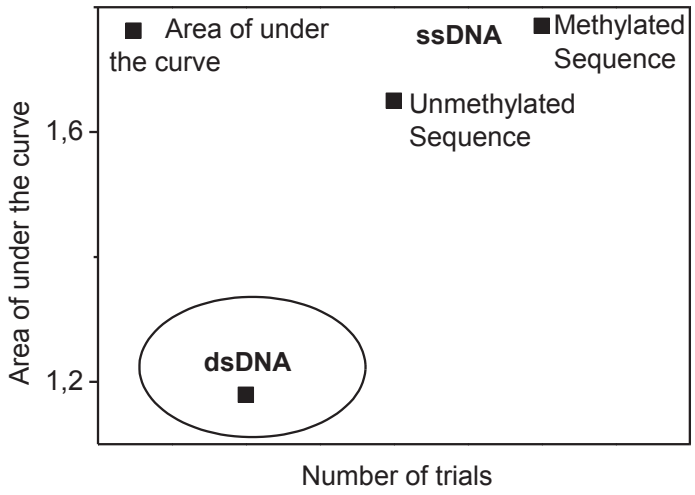

Figure 53. Comparison of under the curve area of Unmethylated, methylated and dsDNA sequences

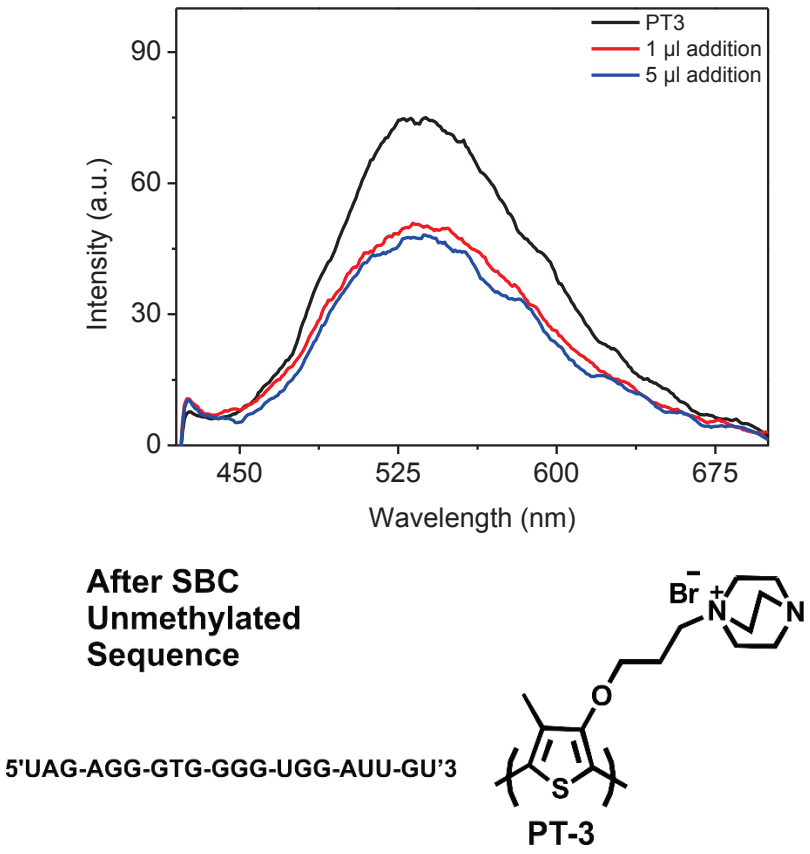

Figure 54. Comparison of different addition amount of Unmethylated sequence into a polymer medium (final DNA content same)

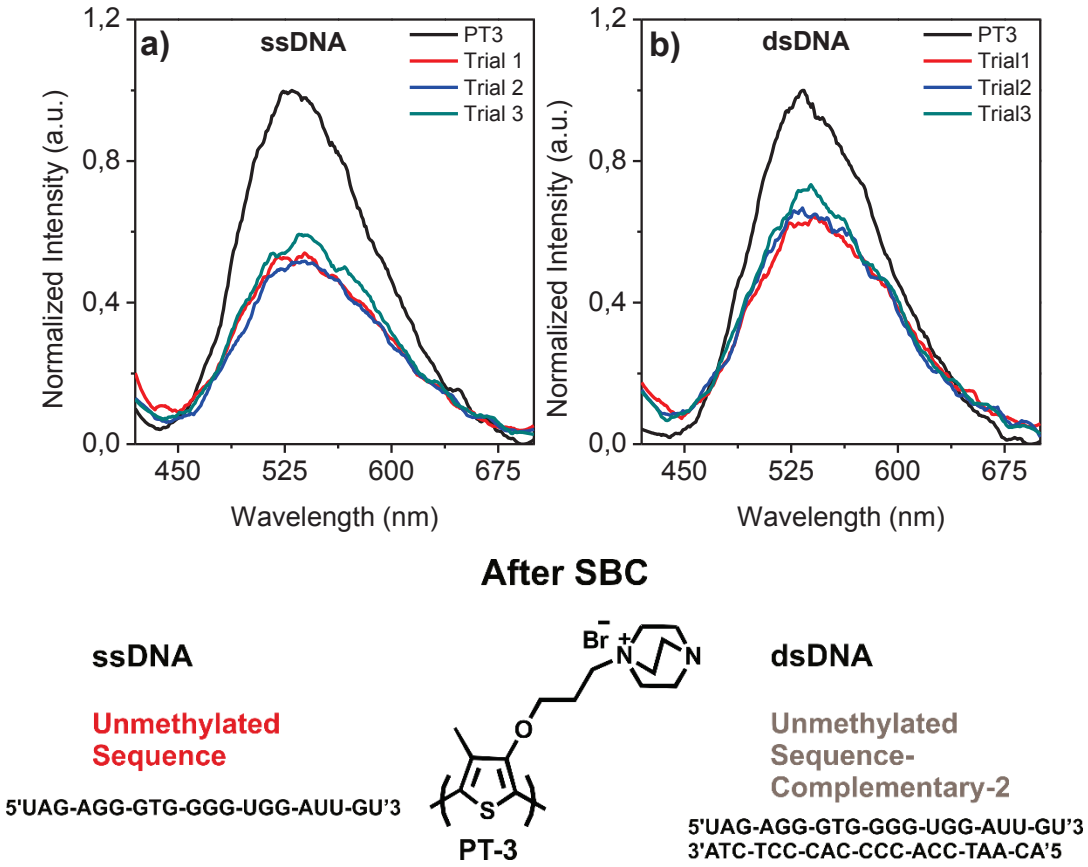

Figure 55. Fluorescence spectra of a) PT3-ssDNA b) PT3-dsDNA with 3 different trials

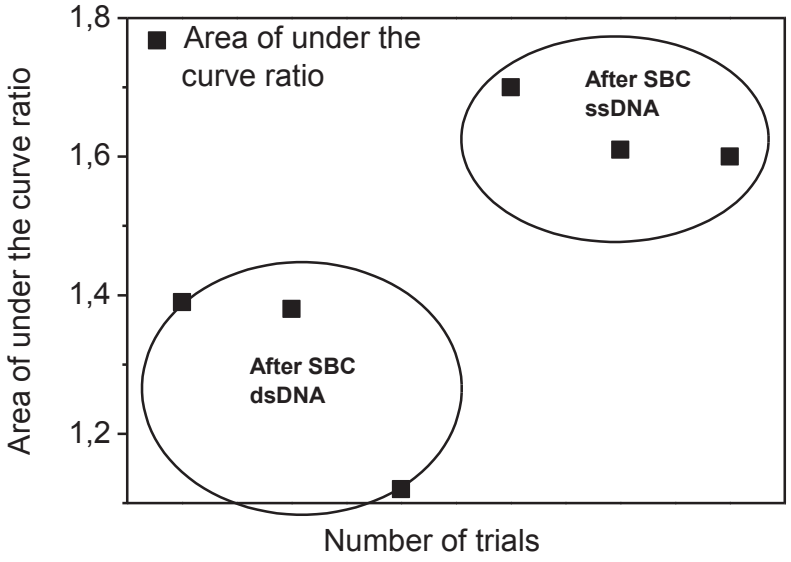

Figure 56. Comparison of under the curve area ratio

3.6. Investigation of Dihedral Angle change on Polythiophene backbone with Computational Methods

Computational calculation performed for PC1, PC1 oligomers, M3 and M3 oligomers to understand the how change of dihedral angle and coupling type affect the optoelectronic properties of polythiophene. Computational UV-VIS spectra of oligomers compared with experimental PT0 and PT3.

The ground state geometries and electronic structure of PC1 molecule were obtained at B3LYP/631-G level of the theory via G09 software package in gas phase. The method validation for excited state calculations was performed by comparing computational UV-VIS spectra with experimental ones. Different combinations of DFT functionals (B3LYP, CAM-B3LYP, MPW1PW91, PBEPBE) and basis sets (631-G, 631-G (d,p), 6311-G(d,p) and CC-PVDZ/+(d,p)) for the ground and excited states calculations were used in method validation. Computational UV-VIS spectra obtained at PBEPBE/631-G level of theory in gas phase. Conformational analysis was done through SPARTAN'10 program suite.

Calculation of polythiophene chain started with the optimization of monomer. First step of the optimization of monomer is to determine the possible conformations of monomer. Each conformation optimized with same methods and compared as an energetically. Energetically most favorable monomer conformation used as a model for the further coupling. In every step of elongation of oligomer, conformation analysis, optimization of conformations and comparison of conformations energies carried out. Furthermore, in every step of elongation of oligomer, computational UV-VIS spectra compared with the experimental ones. PC1 have only one conformation in the space and shown in Figure 57. There are 3 possible coupling types for the PC1 monomer and these are HH, TT, HT. Three possible coupling types arranged with model monomer (Figure 57) possible conformations optimized and their energies were compared. Energetically favorable conformation of dimer coupled as TT and dihedral angle is 56^{o} shown in Figure 58. Investigation of dihedral angle change started with the dimer. The structure of dimer distorted with the change of the dihedral angle and in every distortion step excited state calculation performed to obtain corresponding UV-VIS spectrum for the related dihedral angle. The values of dihedral angle, corresponding λ_{max} and relative energies shown in Table 4. Red shift observed in UV-VIS spectra with the planarization of the dimer. λ_{max}

equal to 333 nm with the 56° dihedral angle while λ_{max} equal to 350 nm with the 180° dihedral angle (planar) shown in Figure 59.

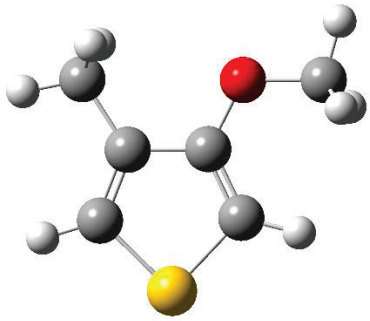

Figure 57. 3-methoxy-4-methylthiophene

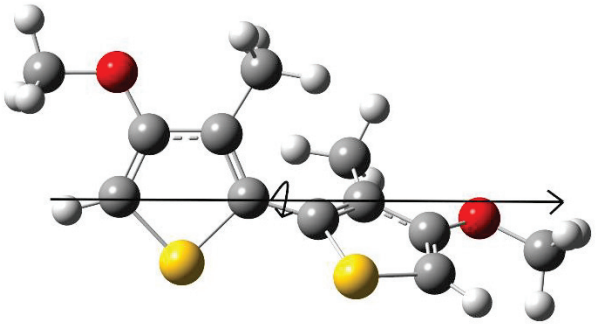

Figure 58. Energetically stable conformation of dimer

Arrangement of the trimer performed with addition of energetically favorable monomer to the energetically favorable dimer. There are two possible coupling types is available for this arrangement. The reason of this, monomer units coupled as a TT during dimer formation and HT or HH coupling occurs for the addition of the monomer units to the dimer. Energetically favorable conformation of trimer (Figure 60) coupled as TT-HT and dihedral angles (θ1, θ2) are 55°-52°. The values of dihedral angle, corresponding λ_{max} and relative energies shown in Table 5. Stable conformation of trimer has λ_{max} at 392 nm and planar conformation of trimer has λ_{max} at 429 nm (Figure 61). In the dihedral angle investigation of trimer two different method experienced, these are distortion of structure with the change of dihedral angles. First method is the change of dihedral angle θ1 from 55 ° to 180 °. Then, θ1 remain constant as 180 ° and dihedral angle θ2 changed from 52 °

to 180°. In every step of the dihedral angle change, single point energy calculation performed and plotted (Figure 62a).

Table 4. Dihedral angle change of dimer with related λ_{max} and relative energies

Dihedral Angle(°)	λ_{max} (nm)	Relative Energy (kj/mol)
56(Stable)	**333**	0
70	**329**	1,64834197
80	**328**	2,971783
90	**327**	3,73772594
100	**327**	4,192944289
110	**329**	4,911002669
120	**334**	7,24915533
130	**340**	12,71342944
140	**346**	21,76447761
150	**351**	33,42381667
160	**352**	44,39276748
170	**351**	49,87111293
180	**350**	47,09092067

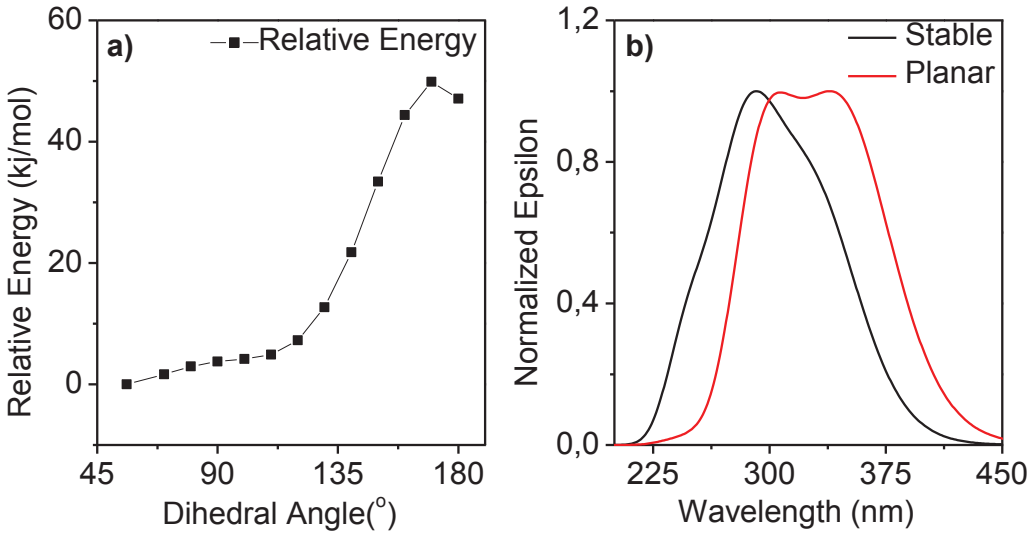

Figure 59. a) Graph of Table 4 b) UV-VIS spectrum of the stable and planar conformation of dimer

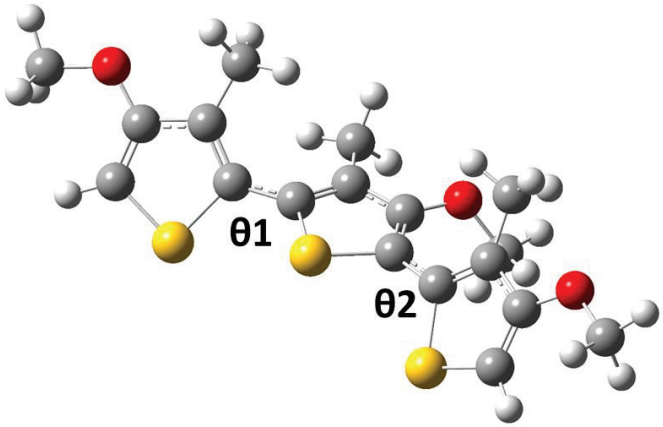

Figure 60. Stable conformation of trimer

Table 5. Dihedral angle change of trimer with related λ_{max} and relative energies

Dihedral Angle(°)	**λ_{max} (nm)**	**Relative Energy (kj/mol)**	**Dihedral Angle**	**λ_{max} (nm)**	**Relative Energy (kj/mol)**
55-52	**392**	0	180-60	**400**	48,6943184
70-52	**386**	2,18911722	180-70	**394**	51,3061796
80-52	**384**	3,84396981	180-80	**390**	54,2085772
90-52	**383**	4,68630752	180-90	**391**	58,3531119
100-52	**383**	5,16927477	180-100	**397**	66,5774951
110-52	**384**	5,73745762	180-110	**408**	82,6656572
120-52	**387**	8,00207703	180-120	**423**	111,142033
130-52	**394**	13,2313125	180-130	**439**	154,124201
140-52	**402**	22,1010084	180-140	**448**	207,323081
150-52	**407**	33,5895487	180-150	**444**	254,389718
160-52	**410**	44,2774665	180-160	**435**	267,884894
170-52	**410**	49,5559517	180-170	**430**	235,081424
180-52	**409**	46,7560438	180-180	**429**	178,287553

Second method is the change of dihedral angle θ1 and θ2 from 55 ° to 180 ° and 52 ° to 180 ° independently. In every step of the dihedral angle change, single point energy calculation performed and plotted (Figure 62b). These graphs show the planarization of θ1 is favorable. Planarization of θ2 required nearly 220 kj/mol energy while the θ1 is

180º. On the contrary, approximately 507 kj/mol energy required to planarize to θ2 while θ1 is 55 º.

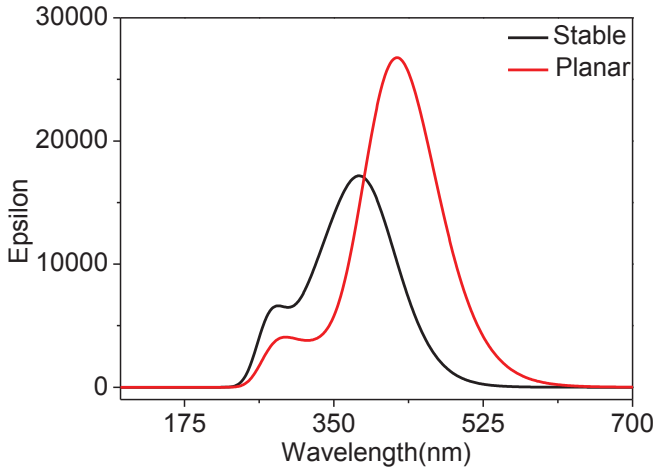

Figure 61. UV-VIS spectrum of the stable and planar conformation of trimer

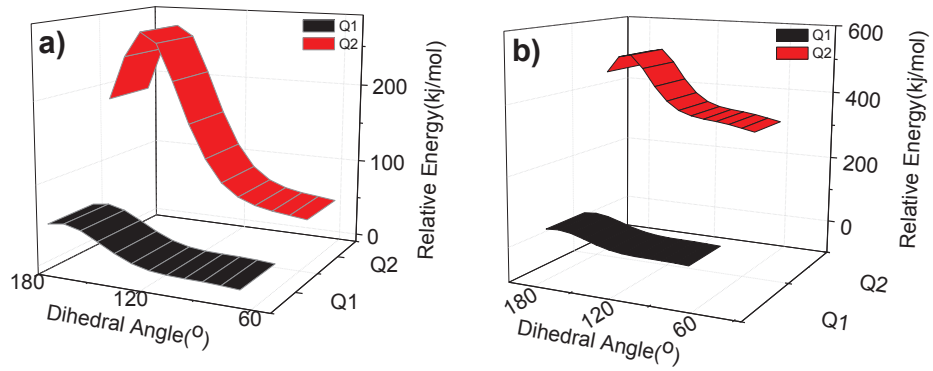

Figure 62. Dihedral change of trimer with two different angle (θ1 and θ2) a) dependently, b) independently

Arrangement of tetramer performed with the addition of model monomer to the energetically favorable conformation of trimer and all conformation calculation protocol carried out. In formation of tetramer four possible coupling type exist and these are HT-TT-HT, HH-TT-HT, TT-HT-HT and TT-HT-HH. Energetically favorable conformation of tetramer coupled as TT-HT-HT and dihedral angles (θ1, θ2, θ3) are 54º -49º -161º shown in Figure 63. The values of dihedral angle, corresponding λ_{max} and relative

energies shown in Table 6. Relative energy curves of the different conformations shown in Figure 64a and UV-VIS spectra of the stable and planar conformation of tetramer shown in Figure 64b.

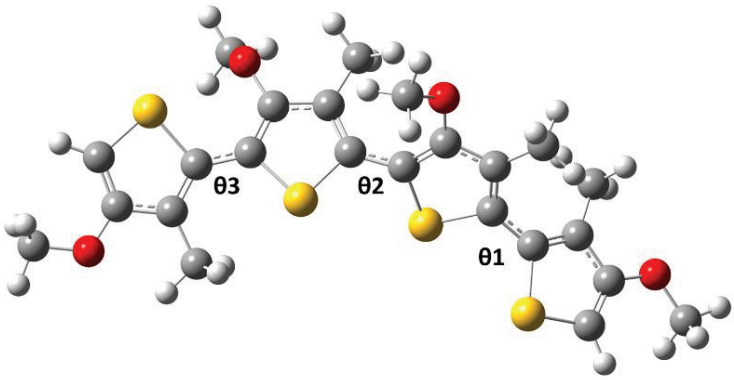

Figure 63. Stable conformation of tetramer

Table 6. Dihedral angle change of tetramer with related λ_{max} and relative energies

Dihedral Angle(°)	**λ_{max} (nm)**	**Relative Energy(kj/mol)**	**Dihedral Angle(°)**	**λ_{max} (nm)**	**Relative Energy(kj/mol)**
161-49--54	**458**	0	180-180--54	**477**	142,0187268
180-49--54	**458**	5,386487951	180-180--60	**473**	142,5535165
180-60--54	**451**	7,052209076	180-180--75	**461**	145,3323961
180-75--54	**439**	11,02738888	180-180--90	**452**	147,2509026
180-90--54	**432**	15,08408269	180-180--105	**456**	410,4267808
180-105--54	**435**	25,31014026	180-180--120	**470**	150,901969
180-120--54	**451**	52,05734237	180-180--135	**485**	160,5277894
180-135--54	**471**	106,0346613	180-180--150	**497**	176,9882907
180-150--54	**481**	174,6576725	180-180--165	**501**	429,0805997
180-165--54	**479**	197,4345252	180-180--180	**501**	187,9482894

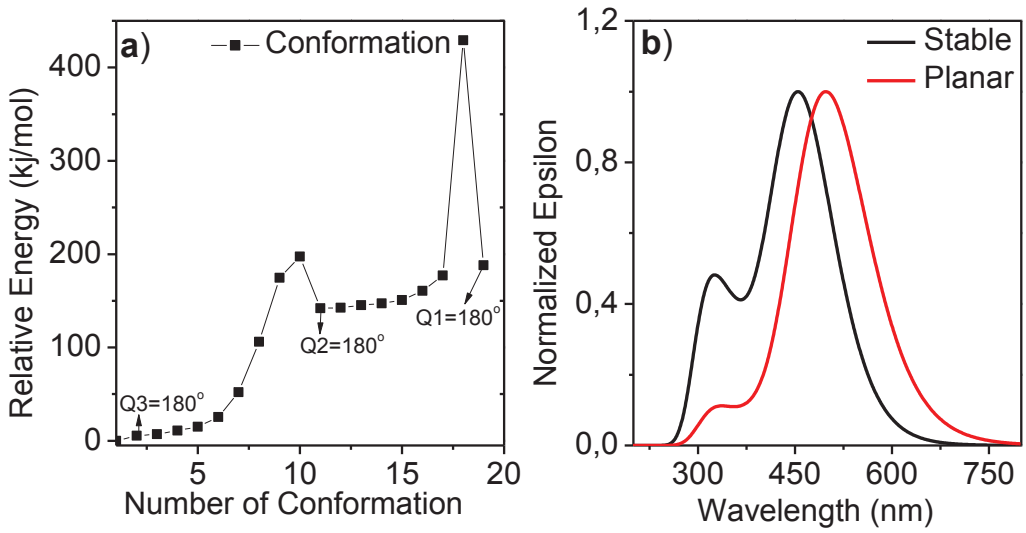

Figure 64. a) Graph of Table 6, b) UV-VIS spectrum of the stable and planar conformation of tetramer

Arrangement of pentamer performed with the addition of model monomer to the energetically favorable conformation of tetramer and all conformation calculation protocol carried out. There are 4 possible coupling types exist for arrangement of pentamer and these are HT-TT-HT-HT, HH-TT-HT-HT, TT-HT-HT-HT and TT-HT-HT-HH. Energetically favorable conformation of pentamer coupled as TT-HT-HT-HT and dihedral angles (θ1, θ2, θ3, θ4) are 55° -48° -165° -160° shown in Figure 65. Table 7 shows the values of dihedral angle, corresponding λ_{max} and relative energies and also plotted in Figure 66a. UV-VIS spectra of the stable and planar conformation of pentamer shown in Figure 66b.

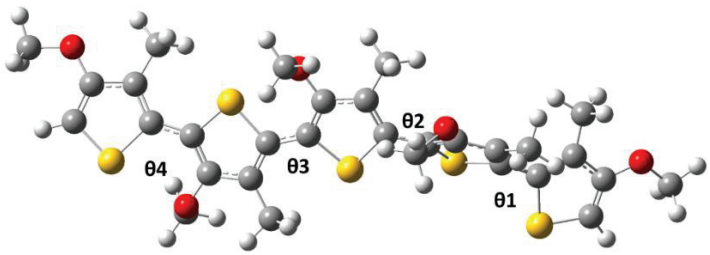

Figure 65. Stable conformation of pentamer

Table 7. Dihedral angle change of pentamer with related λ_{max} and relative energies

Dihedral Angle(°)	λ_{max} (nm)	Relative Energy (kj/mol)	Dihedral Angle(°)	λ_{max} (nm)	Relative Energy (kj/mol)
160-165-48-55	**529**	0	180-180-165-55	**543**	152,1191137
180-165-48-55	**529**	5,252180159	180-180-180-55	**542**	92,98354598
180-180-48-55	**528**	8,445087967	180-180-180-75	**528**	102,7722106
180-180-60-55	**518**	16,18553258	180-180-180-90	**523**	107,0272684
180-180-75-55	**503**	28,88932735	180-180-180-105	**526**	105,7404496
180-180-90-55	**487**	42,55892535	180-180-180-120	**537**	102,5077955
180-180-105-55	**483**	56,4833301	180-180-180-135	**551**	104,6167376
180-180-120-55	**503**	75,03374039	180-180-180-150	**562**	115,6607705
180-180-135-55	**524**	117,267686	180-180-180-165	**567**	127,9785223
180-180-150-55	**538**	162,4327233	180-180-180-180	**557**	126,4017184

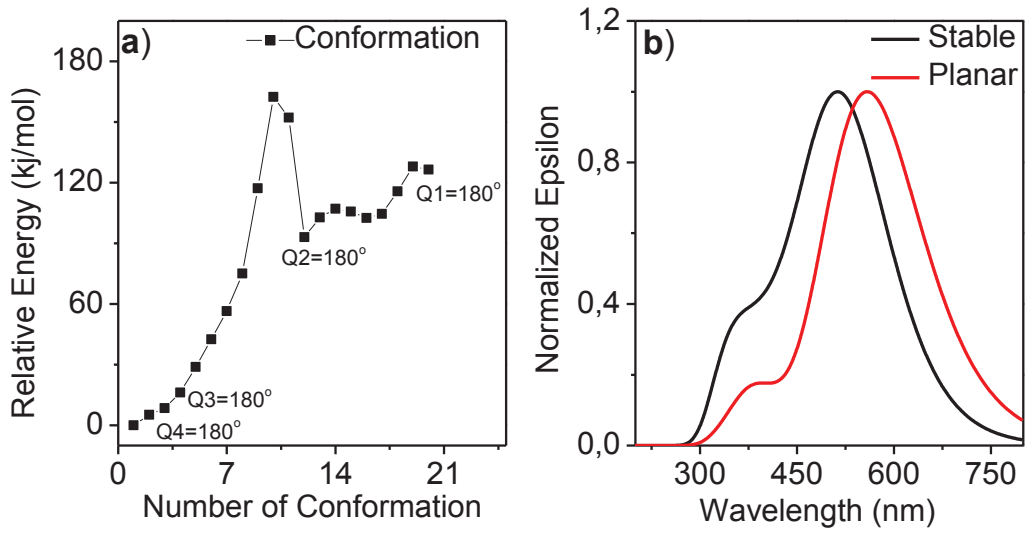

Figure 66. a) Graph of Table 7, b) UV-VIS spectrum of the stable and planar conformation of pentamer

Arrangement of hexamer had the same path with previous oligomers. There are four possible coupling types through the nature of the addition of monomer to the pentamer. Energetically favorable conformation of hexamer coupled as TT-HT-HT-HT-HT and dihedral angles (θ1, θ2, θ3, θ4, θ5) are 55°-49°-160°-164°-47° shown in Figure 67. Table 8 shows the values of dihedral angle, corresponding λ_{max} and relative energies and also plotted in Figure 68a. UV-VIS spectra of the stable and planar conformation of hexamer shown in Figure 68b.

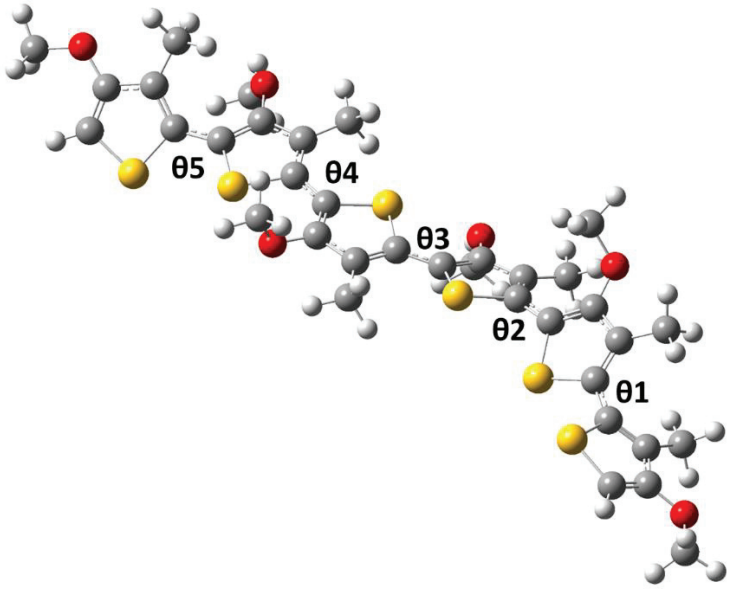

Figure 67. Stable conformation of hexamer

Table 8. Dihedral angle change of hexamer with λ_{max} and relative energies

Dihedral Angle(°)	**λ_{max} (nm)**	**Relative Energy (kj/mol)**	**Dihedral Angle(°)**	**λ_{max} (nm)**	**Relative Energy (kj/mol)**
47-164-160-49-55	**556nm**	0	180-180-180-105-55	**538nm**	87,42604925
60-164-160-49--55	**544nm**	7,824505119	180-180-180-120-55	**560nm**	104,7901091
75-164-160-49--55	**531nm**	19,18096908	180-180-180-135-55	**582nm**	149,7350191
90-164-160-49-55	**525nm**	26,83086883	180-180-180-150-55	**597nm**	208,8395301
105-164-160-49-55	**533nm**	32,36854493	180-180-180-165-55	**602nm**	220,7607641
120-164-160-49-55	**548nm**	46,81256541	180-180-180-180-55	**603nm**	162,0344991
135-164-160-49-55	**563nm**	75,35853632	180-180-180-180-75	**592nm**	170,3668064
150-164-160-49-55	**573nm**	94,4034387	180-180-180-180-90	**586nm**	174,1420209
165-164-160-49-55	**578nm**	77,01050113	180-180-180-180-105	**588nm**	173,8238406
180-164-160-49-55	**580nm**	39,06093724	180-180-180-180-120	**596nm**	172,7846091
180-180-160-49-55	**580nm**	42,79131248	180-180-180-180-135	**608nm**	176,6414689
180-180-180-49-55	**578nm**	47,91459286	180-180-180-180-150	**619nm**	188,4603969
180-180-180-60-55	**566nm**	55,47108621	180-180-180-180-165	**624nm**	200,267065
180-180-180-75-55	**547nm**	68,84536983	180-180-180-180-180	**624nm**	197,636827
180-180-180-90-55	**531nm**	80,83430902			

The most significant behaviour of oligomers observed in relative energy curves through the change of dihedral angle. As shown in Figure 68a, occurrence of energy barrier was observed before the corresponding dihedral angle planarized. The peak of the energy barrier observed between 150º and 165 º. However, planarization of dihedral angles that equal or close to 160 º there were no observable energy barrier. Two dihedral angles of energetically favorable conformation of hexamer is equal or close to 160º (θ3 and θ4).

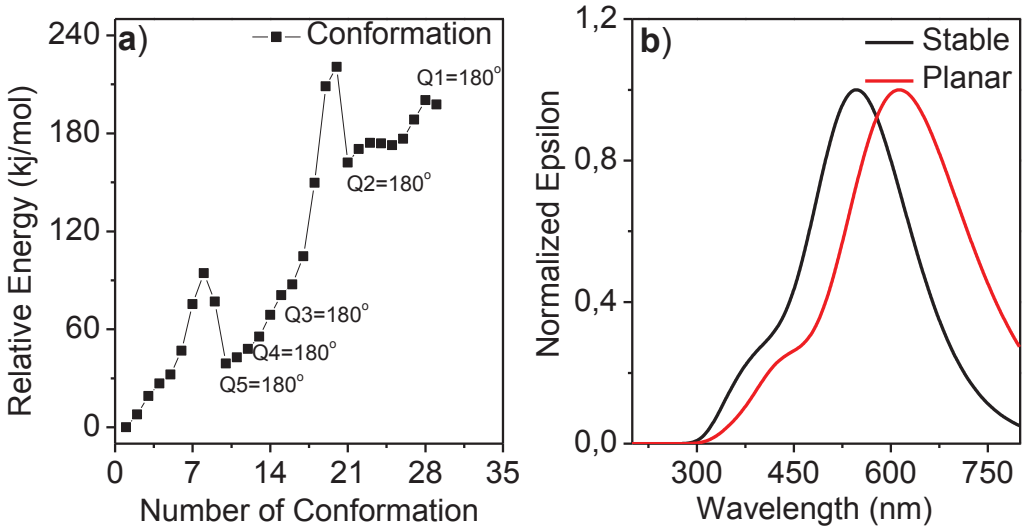

Figure 68. a) Graph of Table 8, b) UV-VIS spectrum of the stable and planar conformation of hexamer

Further discussion in hexamer structure is the order of the planarization. Clearly, which dihedral angle planarized (reach 180º) first in the five dihedral angles of hexamer structure. For this reason, every dihedral angle planarized independently and single point energy calculation carried out. More specifically, θ1 equal to 180º while the other dihedral angles (θ2, θ3, θ4 and θ5) remain same as stable conformation of hexamer (Table 9). Then, θ2 equal to 180º while the other dihedral angles (θ1, θ3, θ4 and θ5) remain same as stable conformation of hexamer and continued for θ3, θ4 and θ5(Figure 69a). The graph shows the planarization of θ4 energetically favorable than other dihedral angles (θ1, θ2, θ3 and θ5). In this scenario, θ4 planarized first (equal to 180º). Next step is the defining the secondly planarized dihedral angle. For this reason, same single point energy calculation carried out for the remaining twisted dihedral angles (θ1, θ2, θ3 and θ5) shown in Figure 69b. The graph shows the planarization of θ3 energetically favorable than other

dihedral angles (θ1, θ4 and θ5). Then, remaining dihedral angles (θ1, θ2 and θ5) planarized and single point energy calculation performed. Figure 69c shows the planarization of θ1 energetically favorable than other dihedral angles (θ2 and θ5). These calculation steps show the planarization of hexamer structure have an order. First planarization state of hexamer structure occurs in θ4, second planarization occurs in θ3, third planarization occurs in θ1 and goes on. Dihedral angles of hexamer (θ1, θ2, θ3, θ4, θ5) are 55º-49º-160º-164º-47º and 1st,2nd, 3rd, 4th and 5th planarization of hexamer ordered as θ4, θ3, θ1, θ5 and θ2 respectively.

Table 9. Order of the planarized dihedral angle

Dihedral Name	Dihedral Angle(º)	After 1st Planarization	After 2nd Planarization	After 3rd Planarization
θ1	55	55	55	**180**
θ2	49	49	49	49
θ3	160	160	**180**	**180**
θ4	164	**180**	**180**	**180**
θ5	47	47	47	47

Further oligomer calculation performed to compare experimental and computational UV-VIS spectra. Figure 70 shows UV-VIS spectra of the stable and planar conformation of heptamer and octamer. Evolution of oligomerization in UV-VIS region shown in Figure 71. Red shift observed with the elongation of oligomer as expected. The intensity of absorbance maximum of octamer 16 times greater than the monomer. This could be show the why the oligo/polythiophenes are fluorescence active while the monomer is fluorescently inactive.

The comparison of experimental and computational UV-VIS spectra carried out with hexamer, heptamer and octamer (Figure 72). The experimental spectrum has absorbance maximum at 391 nm with a 595 nm shoulder. In computational spectra the intensities of corresponding peaks are different than experimental one. Intensity differences of peaks originated from the electron transition states.

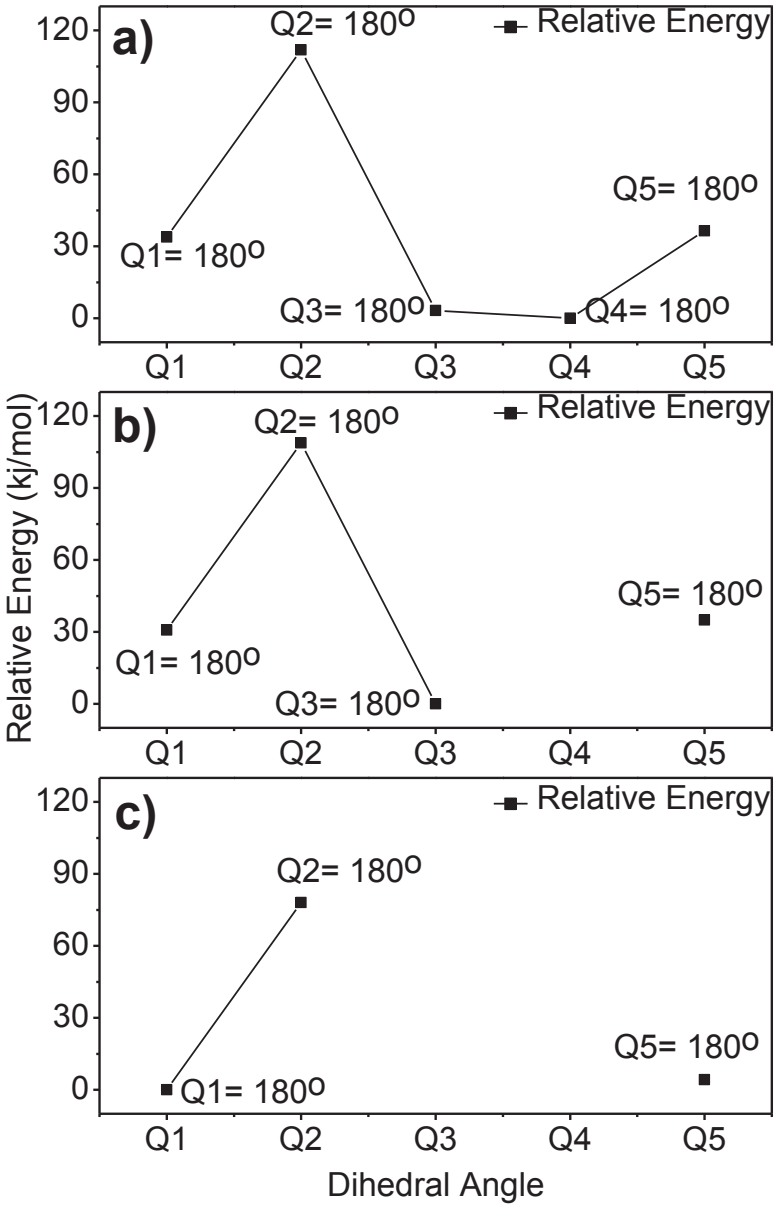

Figure 69. Relative energy versus different dihedral planarization, a) First planarization relative energy comparison, b) planarization relative energy comparison, c) planarization relative energy comparison

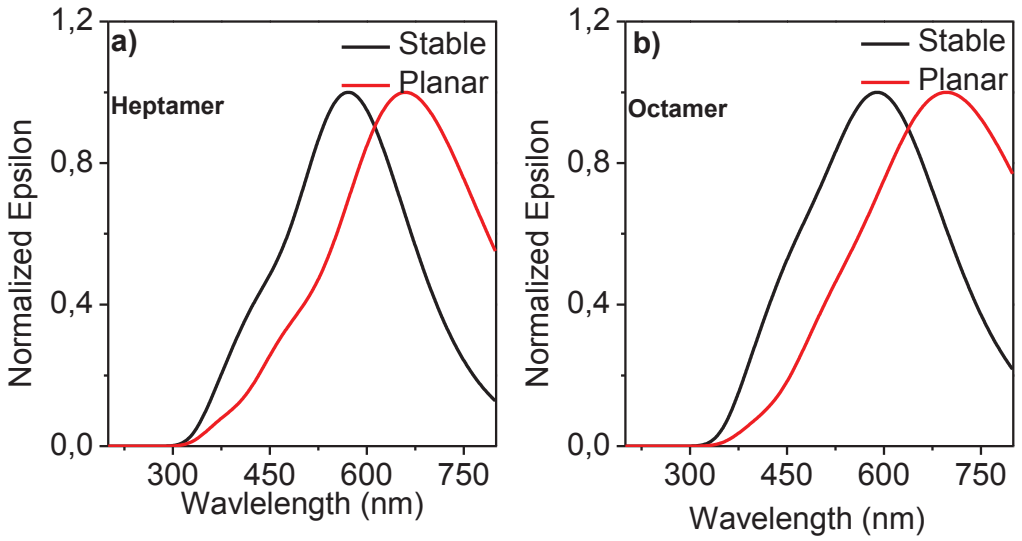

Figure 70. UV-VIS spectra of the stable and planar conformation of a) heptamer, b) octamer

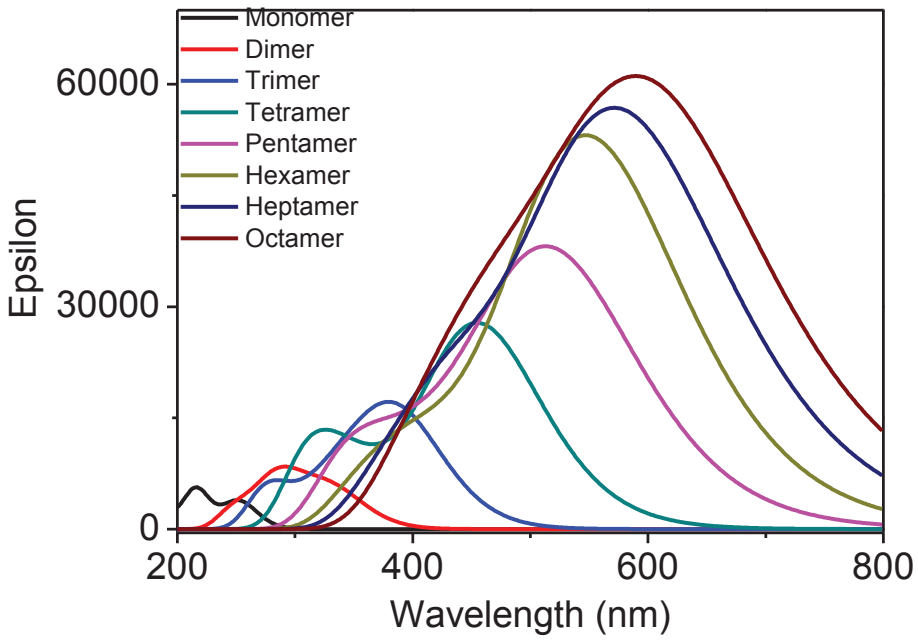

Figure 71. UV-VIS spectra of oligomers

A peak at 595 nm in experimental spectrum has a shoulder behaviour while the corresponding computational longer wavelength peaks have HOMO to LUMO transition. The longer wavelength peaks at 547, 571 and 591 nm for hexamer, heptamer and octamer respectively. Heptamer is more appropriate as a model of polythiophene than hexamer

and octamer considering experimental absorbance maximum at 391 nm with a 595 nm shoulder.

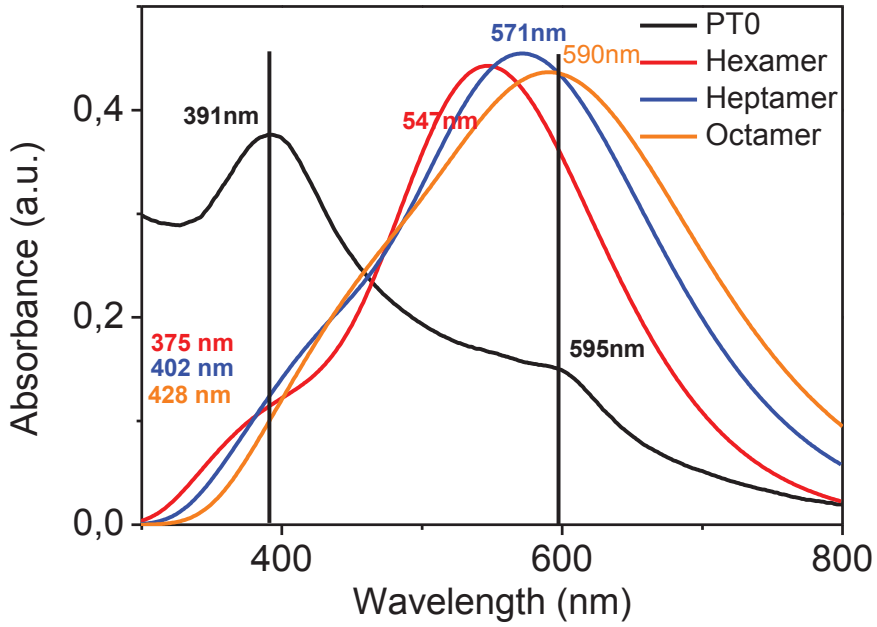

Figure 72. Merged UV-VIS spectra of experimental polythiophene and computational oligomers

Polymeric behaviour of oligomers increases with the linearization of plot (energy/n versus n). Figure 73 shows the sharp increment from monomer to tetramer. Then, addition of new monomer unit from tetramer to octamer decreased the rate of increment and plot linearized. Therefore hexamer, heptamer or octamer can used as model for the polymer behaviour. Generally, tetramer or hexamer used as a model in the literature [62] but we decided to heptamer which corresponding UV-VIS region behaviour similar to experimental one. Every step of elongation of oligomers with the corresponding dihedral angle and coupling type shown in Figure 74. Addition of monomer unit to the oligomer chain affects the value of dihedral angle not nature. The change of dihedral angle values range is +/- 8^{o} during elongation of oligomer chain and this proves the accuracy of longer oligomers dihedral angles reinforced with the previous oligomer dihedral angles.

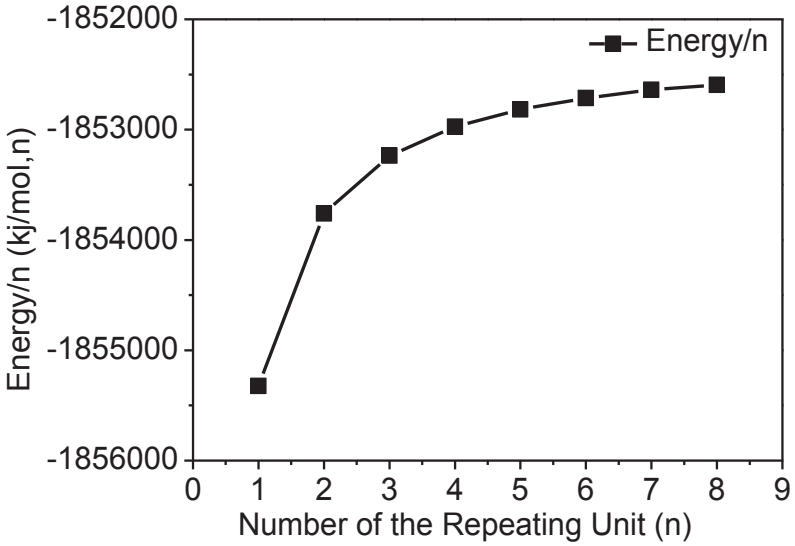

Figure 73. Energy distribution with increasing number of repeating unit

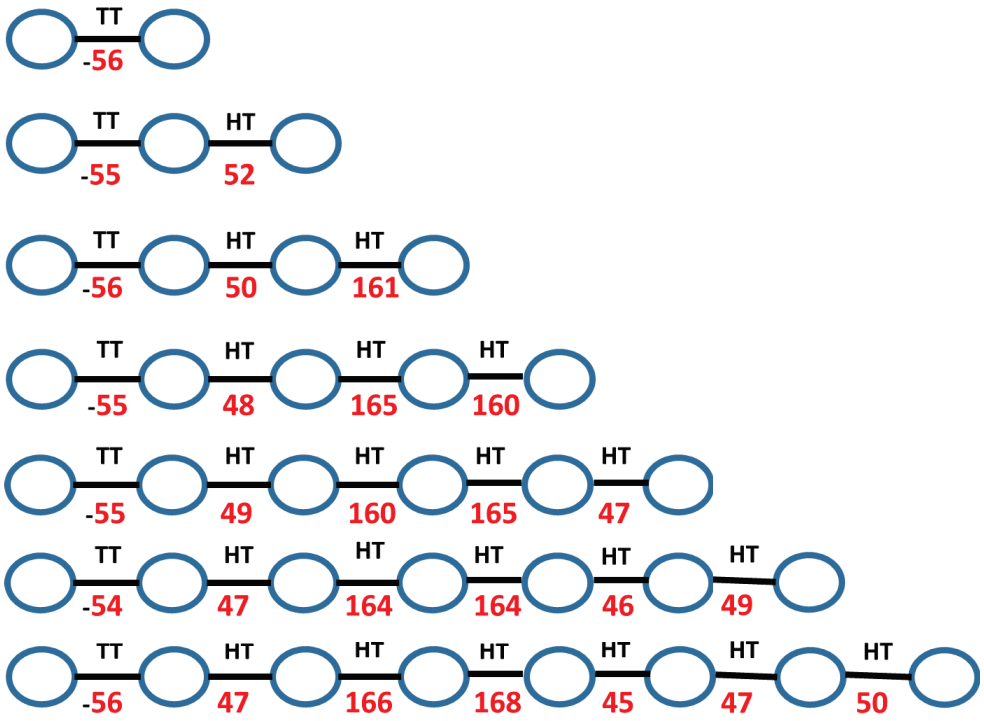

Figure 74. Representation of thiophene oligomers starting from monomer and related dihedral angle

The ground state geometries and electronic structure of PC1 monomer, dimer and trimer molecules were obtained at semi-empirical method (PDDG). These calculation

steps performed to obtain the bond, angle and dihedral angle average error between DFT and semi-empirical method. The average percentage errors shown in Table 10. Resultant percentage error is acceptable for the further M3 and M3 based oligomers semi-empirical calculation.

Table 10. DFT and Semi-empirical(PDDG) method comparison

	Bond Av. Error%	**Angle Av. Error%**	**Dihedral Av. Error%**
Monomer	1,771655	1,236562	0,086032
Dimer	1,770988	1,340654	1,395901
Trimer	1,88	0,517989	3,224729

Semi-empirical method PDDG used to obtain the M3 and M3 based oligomer ground state geometries and electronic structure considering DFT and semi-empirical(PDDG) method comparison. Same calculation steps were performed in M3 and M3 based oligomer as a PC1 and PC1 based oligomers calculation. The only difference is the optimization method. In every step of elongation of oligomers chain, conformation analysis, optimization of conformations and comparison of conformations energies were performed. Excited state works have been done through the TD-DFT/PBEPBE/631-G level of theory. The comparison of computational spectra with the experimental spectra crucial to understand the optical properties of cationic polythiophene(PT3). Energetically favorable conformation of M3 is shown in Figure 75. Excited state calculation was performed to obtain three main conformational state of structure which are, stable, planar and coiled conformation. These conformations yield an optical potential range of the cationic polythiophene in UV-VIS region. UV-VIS spectra of stable, planar and coiled conformations of dimer and trimer shown in Figure 76 while tetramer and pentamer shown in Figure 77. The general behaviour of the backbone explained as twisted conformation has a shorter absorbance maximum while the planar conformation of the backbone yields a higher absorbance maximum. In this work, coiled conformation calculated as a most twisted conformation, and all dihedral angles equal to 90^{o}. Corresponding absorbance maximum shifted to the longer wavelength with elongation of oligomers monomer to pentamer. In addition to this, differences between stable and planar conformation absorbance maximums increased such as 36 nm red shift observed with planarization of dimer while the 76 nm, 147 nm and 170 nm red shift observed for trimer, tetramer and pentamer respectively. The coupling type is TT, TT-HT and TT-HT-

HT for dimer, trimer and tetramer, respectively. These coupling types are the same with PC1 oligomers. Most significant coupling differences observed in pentamer that energetically favorable conformation coupled as a HT-TT-HT-TT. Coupling type difference originated from the different substituent group even substituent bounded to thiophene unit from the same methoxy group.

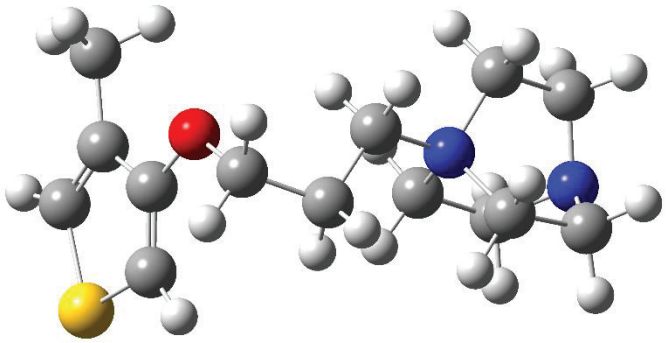

Figure 75. Stable conformation of 1-(3-((4-methylthiophen-3-yl) oxy) propyl)-1,4-diazabicyclo [2.2.2] octan-1-ium

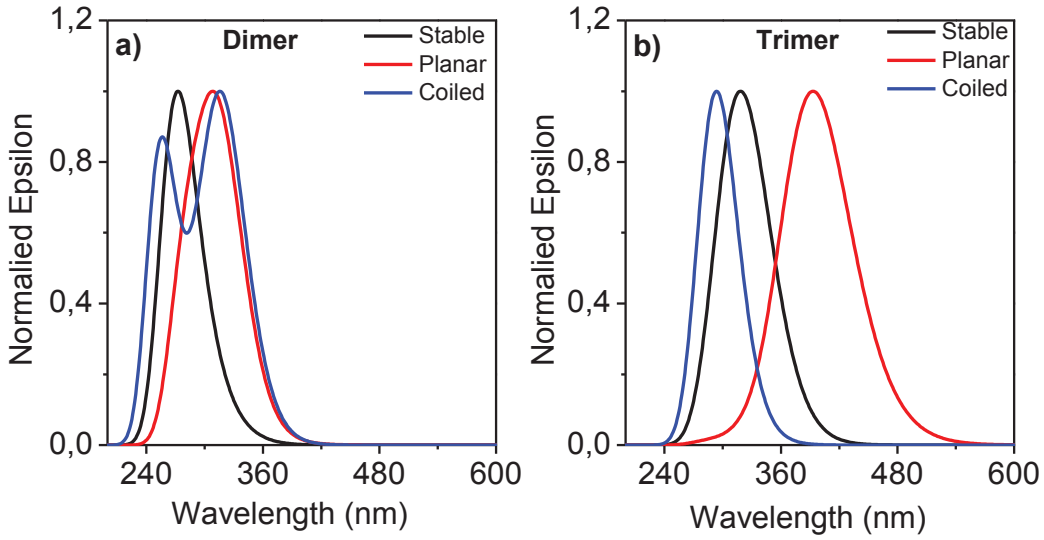

Figure 76. UV-VIS spectra of stable, planar, coiled conformation of a) dimer and, b) trimer

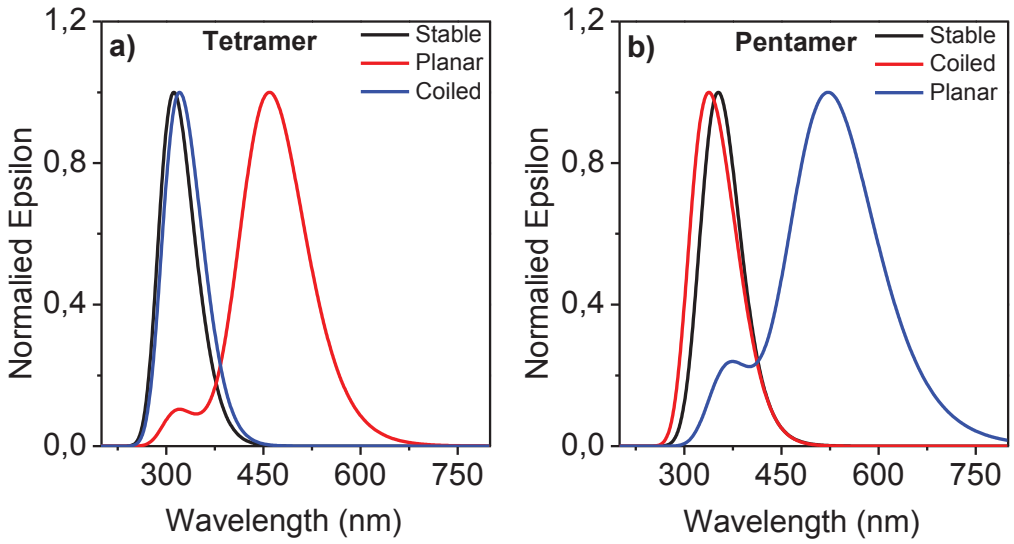

Figure 77. UV-VIS spectra of stable, planar, coiled conformation of a) tetramer and, b) pentamer

DFT calculation performed for the all possible conformation of pentamer to clarify the coupling type differences that resulted from semi-empirical method errors or not. Figure 78 shows the relative energy curves of possible conformation of pentamer with DFT (black) and Semi-empirical method (PDDG) (red). Conformation 17 energetically favorable in both calculation method. Furthermore, distribution of relative energies has a same path with DFT and PDDG method with a two disruption of path. This comparison shows the PDDG is an accurate, fast and inexpensive method determining the energetically favorable conformations of oligomers.

UV-VIS spectra of stable, planar and coiled conformations of hexamer and heptamer shown in Figure 79. Hexamer coupled as HT-HT-TT-HT-HT while heptamer coupled as HT-HT-HT-TT-HT-HT. Differences between stable and planar conformation absorbance maximums increased, 209 nm and 213 nm red shift observed with planarization of hexamer and heptamer respectively. Dihedral angle, coupling type and corresponding absorbance maximum of oligomers shown in Table 11 from monomer to heptamer. Experimental spectrum of PT3 compared with computational spectra of hexamer and heptamer shown in Figure 80. Absorbance maximum of heptamer has better fit with the experimental one than the absorbance maximum of hexamer. The absorbance maximum differences of experimental one and heptamer is 14 nm while the hexamer has 51 nm differences. For this reason, M3 based heptamer is appropriate model for the PT3.

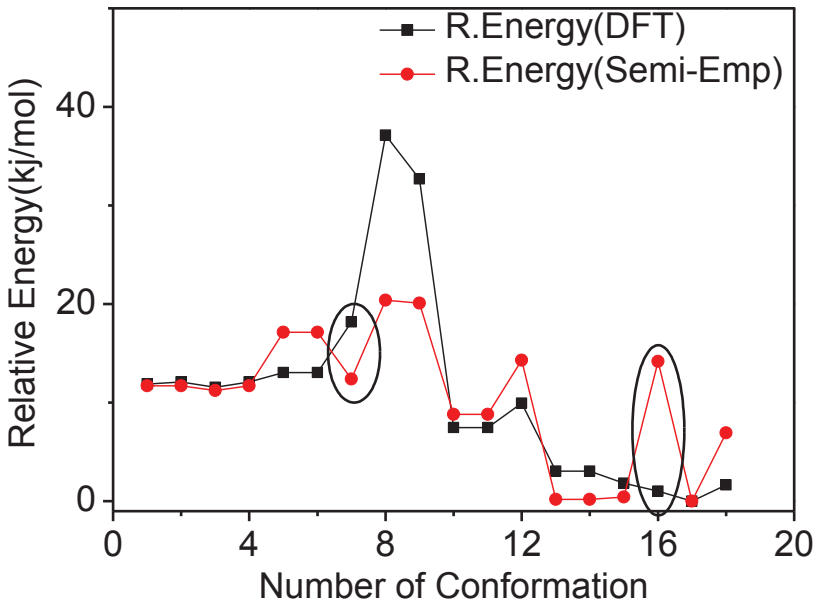

Figure 78. Relative Energy comparison of possible conformation of pentamer between DFT and Semi-Empirical(PDDG) methods

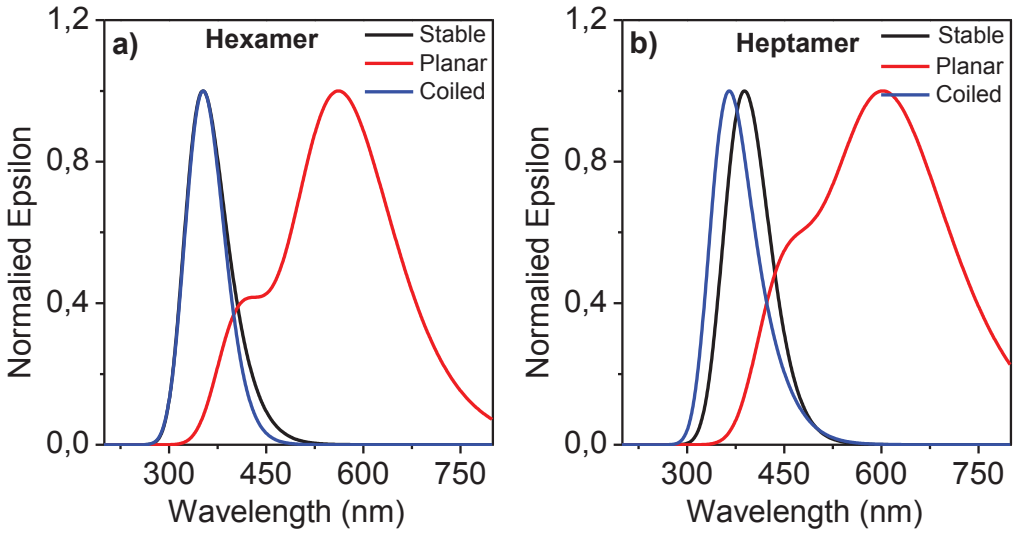

Figure 79. UV-VIS spectra of stable, planar, coiled conformation of a) hexamer and, b) heptamer

Table 11. Dihedral angle, coupling type and corresponding absorbance maximum of oligomers starting from monomer

Name	**λ_{max} (nm)**	**Dihedral Angle(°)**	**Coupling Type**
Monomer	**239**	-	-
Dimer	**272**	104	TT
Trimer	**318**	110-115	TT-HT
Tetramer	**312**	101-89-111	TT-HT-HT
Pentamer	**352**	53-53-89-110	HT-TT-HT-HT
Hexamer	**352**	109-105-55-99-102	HT-HT-TT-HT-HT
Heptamer	**389**	109-101-104-56-101-110	HT-HT-HT-TT-HT-HT

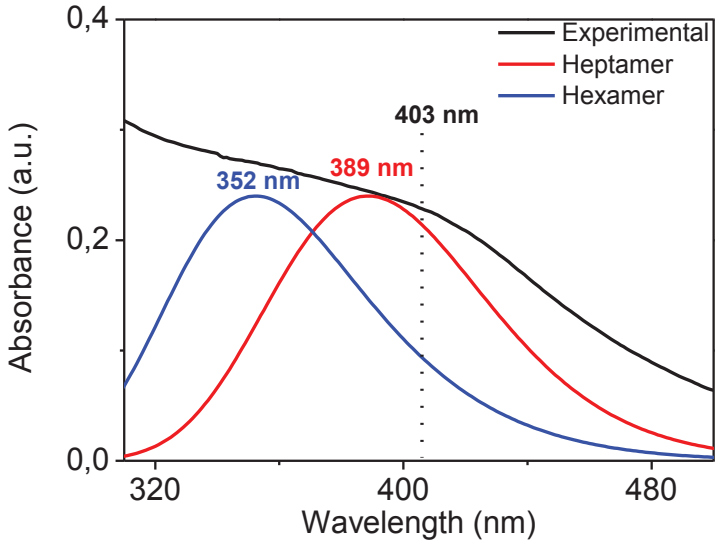

Figure 80. Comparison of Experimental and Computational UV-VIS Spectra

Figure 81 shows the model heptamer structure of PT0 and PT3. Dihedral angles and coupling types of oligomer chains are totally different. In the contrary, dihedral angle of TT coupling is similar in both structure which 54° for PT0 and 56° for PT3. The nature of TT coupling distorted the different polymer chain with a nearly same dihedral angle. The TT coupling is defect in the HT coupled polymer chains that number, position of defect and distortion of polymer chain have an influenced on the optical properties of polythiophene. HT content is 86% for both oligomer chain and HT content will increase with the elongation of the chains. The most significant result is, heptamer has the best fit with the experimental spectra for both structure.

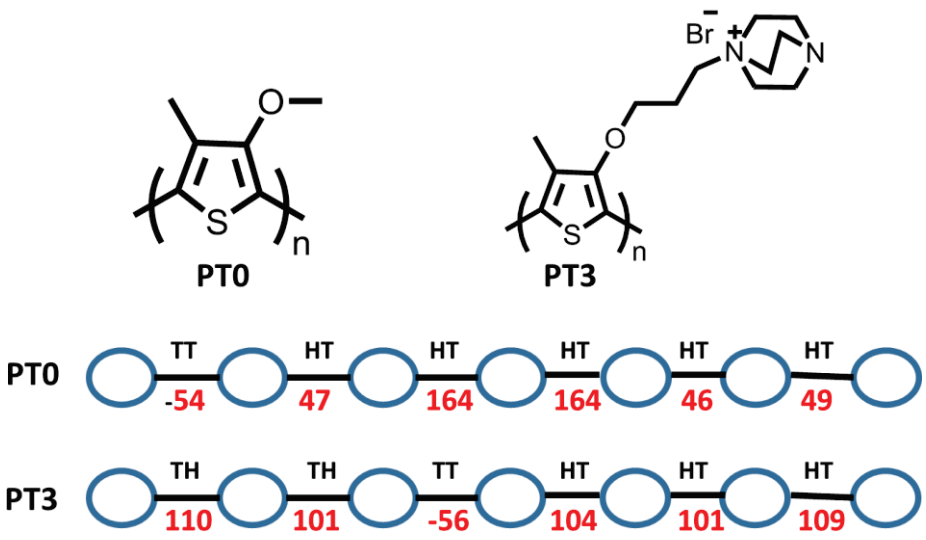

Figure 81. Comparison of coupling type and dihedral angle differences between PT0 and PT3

CHAPTER 4

CONLUSION

The goal of this work, developed the new detection method for DNA methylation via polythiophene. In order to do that water soluble polythiophene synthesized and detection of DNA methylation is achieved.

First of all, poly(1-(3-((4-methylthiophen-3-yl) oxy) propyl)-1,4-diazabicyclo [2.2.2] octan-1-ium bromide) (PT3) synthesized and characterized by ^{1}H NMR analysis, UV-VIS and fluorescence spectrophotometer and used for the detection of DNA methylation. Furthermore, poly(N-allyl-N-methyl-N-(3-((4-methylthiophen-3-yl) oxy) propyl) prop-2-en-1-aminium bromide) (PT1), used in characterization of homopurines and homopyrimidines while the poly(1,4-dimethyl-1-(3-((4-methylthiophen-3-yl) oxy) propyl) piperazin-1-ium bromide) (PT2) used as a control in experiments. Moreover, conformational change of polythiophene investigated with computational methods. The most significant results are the; firstly, occurrence of energy barrier was observed between 150^{o} and 165^{o} before corresponding dihedral angle planarized, secondly, heptamer has the best fit with the experimental spectra for PT0 and PT3.

Characterization of homopurines and homopyrimidines is crucial to understand the nature of polymer-DNA complexes. 395 nm/595 nm ratio of PT1-DNA complex in UV-VIS titration curves proved the different behaviour of homosequences observed which the ratio of polyC (10) is 1,25, polyC (20) is 0,84, polyTh (10) is 4,01, polyTh (20) is 1,44, polyA (20) is 9,0. In addition to this, polyG (10), polyG (20) and polyA (10) did not form complex with PT1 and no spectral change observed during titrations. Also, the intensity ratio of PT1-dsAT (20)/ PT1-dsAT (10) is 2,11 with a 16 nm shift of isosbestic point. Fluorescence spectra of 10 bases long homosequences shows that unique quencher behaviour with cationic polythiophene.

Characterization of unmethylated and methylated sequences were performed with using PT3. Increment of homopyrimidine ratio in heterosequences corresponds the aggregation. Complementary-2 homopyrimidine ratio is 70% and aggregation observed with higher than 4,2 µg sample addition while the 5,52 µg sample addition required to

aggregation in unmethylated sequence which homopyrimidine ratio is 30%. Methylated sequence homopyrimidine ratio is also 30% but aggregation observed with higher than 7,21 μg sample addition. This sample requirement differences originated from the methyl group at 5' position of cytosine even unmethylated and methylated sequence consequence spectra are similar. SBC protocols applied to polyC (10) and control experiments were performed and showed the PT3-PolyC (10), PT3-PolyA (10), PT3-PolyU (10) and PT3-dsAU complexes have a different spectral behaviour.

Detection of DNA methylation have been accomplished by the proposal assay. Before and after SBC PT1-DNA titration curves shows the base content change in unmethylated sequence resulted the 15 nm isosbestic point shift while the isosbestic point shift in methylated sequence is 2 nm in UV-VIS region. Polymer absorbance maximum is decreased with the addition of dsDNA(Unmethylated/complementary-2) while there is no spectral change in longer wavelength. In the contrary, intensity change is observed in both polymer absorbance maximum and longer wavelength with addition of ssDNA (unmethylated and methylated sequence). Furthermore, same titration experiments repeated monitoring with fluorescence spectrophotometer to achieve fast time and sensitive analysis. The ratio of I_o/I is equal to 1,16 for dsDNA and the ratio of I_o/I is 1,65 for unmethylated sequence while the I_o/I ratio equal to 1,77 for methylated sequence. The amount of ssDNA used in calculation of I_o/I ratio are 249,6 ng, 217,5 ng and 249,0 ng for unmethylated sequence, methylated sequence and dsDNA (Unmethylated sequence-Complementart-2) respectively. The titration experiments of ssDNA and dsDNA repeated three times with a nearly 700 ng DNA samples. These titration experiments proved the general behaviour of ssDNA is higher than the 1,60 I_o/I ratios while the behaviour of dsDNA lower than 1,40 I_o/I ratio.

In conclusion, new PCR free water soluble polythiophene based methodology has been developed to detect DNA methylation. This methodology used in detection of methylation in multiple tumor suppressor $p16^{INK4A}$ gene that including several types of cancer biomarker sequence. This methodology is usable for further investigation of different tumor suppressor genes such as *BRCA1*, p53 and *PTEN*.

REFERENCES

1. C. K. Chiang; C. B. Fincher; Jr. Y. W. Park; Heeger, A. J.; H. Shirakawa; E. J. Louis; S. C. Gau; MacDiarmid, A. G., Electrical Conductivity in Doped Polyacetylene. *PHYSICAL REVIEW I,ETTERS* **1977,** *39* (17), 1098−1101.

2. Diaz, A. F.; Kanazawa, K. K.; Gardini, G. P. J., Electrochemical Polymerization of Pyrrole. *J.C.S. CHEM. COMM* **1979,** *0* (14), 636-636.

3. A. Vassar; J. Roncali; Gamier, F., Preparation and electroactivity of poly(thiophene) electrodes modified by electrodeposition of palladium particles. *J. ElectroanaL Chem,* **1988,** *255* (17), 53-69.

4. G. TOURILLON; GARNIER, F., NEW ELECTROCHEMICALLY GENERATED ORGANIC CONDUCTING POLYMERS. *J. Electroanal. Chem* **1982,** *135* (1), 173-178.

5. Bates, N.; Cross, M.; Lines, R.; Walton, D., Flexible and heat-processable conductive films of polypyrrole. *Journal of the Chemical Society, Chemical Communications* **1985,** (13), 871-872.

6. Delamar, M.; Lacaze, P. C.; Dumousseau, J. Y.; Dubois, J. E., Electrochemical oxidation of benzene and biphenyl in liquid sulfur dioxide: formation of conductive deposits. *Electrochimica Acta* **1982,** *27* (1), 61-65.

7. Rault-Berthelot, J.; Simonet, J., The anodic oxidation of fluorene and some of its derivatives: Conditions for the formation of a new conducting polymer. *Journal of Electroanalytical Chemistry and Interfacial Electrochemistry* **1985,** *182* (1), 187-192.

8. Friend, R. H.; Gymer, R. W.; Holmes, A. B.; Burroughes, J. H.; Marks, R. N.; Taliani, C.; Bradley, D. D. C.; Santos, D. A. D.; Brédas, J. L.; Lögdlund, M.; Salaneck, W. R., Electroluminescence in conjugated polymers. *Nature* **1999,** *397*, 121.

9. Ashraf, R. S.; Meager, I.; Nikolka, M.; Kirkus, M.; Planells, M.; Schroeder, B. C.; Holliday, S.; Hurhangee, M.; Nielsen, C. B.; Sirringhaus, H.; McCulloch, I., Chalcogenophene Comonomer Comparison in Small Band Gap Diketopyrrolopyrrole-Based Conjugated Polymers for High-Performing Field-Effect Transistors and Organic Solar Cells. *Journal of the American Chemical Society* **2015,** *137* (3), 1314-1321.

10. Nielsen, C. B.; Ashraf, R. S.; Treat, N. D.; Schroeder, B. C.; Donaghey, J. E.; White, A. J. P.; Stingelin, N.; McCulloch, I., 2,1,3-Benzothiadiazole-5,6-Dicarboxylic Imide – A Versatile Building Block for Additive- and Annealing-Free Processing of Organic Solar Cells with Efficiencies Exceeding 8%. *Advanced Materials* **2014,** *27* (5), 948-953.

11. Liu, X.; Wang, H.-Q.; Li, Y.; Gui, Z.; Ming, S.; Usman, K.; Zhang, W.; Fang, J., Regular Organic Solar Cells with Efficiency over 10% and Promoted Stability by Ligand- and Thermal Annealing-Free Al-Doped ZnO Cathode

Interlayer. *Advanced science (Weinheim, Baden-Wurttemberg, Germany)* **2017,** *4* (8), 1700053-1700053.

12. Chai, R.; Xing, C.; Qi, J.; Fan, Y.; Yuan, H.; Niu, R.; Zhan, Y.; Xu, J., Water-Soluble Conjugated Polymers for the Detection and Inhibition of Protein Aggregation. *Advanced Functional Materials* **2016,** *26* (48), 9026-9031.

13. Wang, H.-J.; Chen, C.-P.; Jeng, R.-J. Polythiophenes Comprising Conjugated Pendants for Polymer Solar Cells: A Review *Materials (Basel)* [Online], 2014, p. 2411-2439. PubMed. (accessed 2014/03//).

14. Pesant, S.; Boulanger, P.; Côté, M.; Ernzerhof, M., Ab initio study of ladder-type polymers: Polythiophene and polypyrrole. *Chemical Physics Letters* **2008,** *450* (4), 329-334.

15. Xu, Y.; Berger, P. R., High electric-field effects on short-channel polythiophene polymer field-effect transistors. *Journal of Applied Physics* **2004,** *95* (3), 1497-1501.

16. Kaloni, T. P.; Gangopadhyay, S.; Singh, N.; Jones, B.; Schwingenschlögl, U., Electronic properties of Mn-decorated silicene on hexagonal boron nitride. *Physical Review B* **2013,** *88* (23), 235418.

17. Kaloni, T. P.; Schreckenbach, G.; Freund, M. S.; Schwingenschlögl, U., Current developments in silicene and germanene. *physica status solidi (RRL) – Rapid Research Letters* **2016,** *10* (2), 133-142.

18. Radhakrishnan, S.; Ananthakrishnan, S. J.; Somanathan, N., Structure-property relationships of electroluminescent polythiophenes: role of nitrogen-based heterocycles as side chains. *Bulletin of Materials Science* **2011,** *34* (4), 713.

19. Zade, S. S.; Bendikov, M., Theoretical Study of Long Oligothiophene Polycations as a Model for Doped Polythiophene. *The Journal of Physical Chemistry C* **2007,** *111* (28), 10662-10672.

20. Joule, J. A., Thiophenes. *Springer International Publishing* **2015,** *39* (39), 1-239.

21. Zamoshchik, N.; Salzner, U.; Bendikov, M., Nature of Charge Carriers in Long Doped Oligothiophenes: The Effect of Counterions. *The Journal of Physical Chemistry C* **2008,** *112* (22), 8408-8418.

22. Patra, A.; Wijsboom, Y. H.; Leitus, G.; Bendikov, M., Tuning the Band Gap of Low-Band-Gap Polyselenophenes and Polythiophenes: The Effect of the Heteroatom. *Chemistry of Materials* **2011,** *23* (3), 896-906.

23. Rittmeyer, S. P.; Groß, A., Structural and electronic properties of oligo- and polythiophenes modified by substituents. *Beilstein journal of nanotechnology* **2012,** *3*, 909-919.

24. Salzner, U., Does the Donor−Acceptor Concept Work for Designing Synthetic Metals? 1. Theoretical Investigation of Poly(3-cyano-3‘-hydroxybithiophene). *The Journal of Physical Chemistry B* **2002,** *106* (36), 9214-9220.

25. Zamoshchik, N.; Bendikov, M., Doped Conductive Polymers: Modeling of Polythiophene with Explicitly Used Counterions. *Advanced Functional Materials* **2008,** *18* (21), 3377-3385.

26. Hutchison, G. R.; Zhao, Y.-J.; Delley, B.; Freeman, A. J.; Ratner, M. A.; Marks, T. J., Electronic structure of conducting polymers: Limitations of oligomer extrapolation approximations and effects of heteroatoms. *Physical Review B* **2003,** *68* (3), 035204.

27. Roncali, J., Conjugated poly(thiophenes): synthesis, functionalization, and applications. *Chemical Reviews* **1992,** *92* (4), 711-738.

28. Yamamoto, T.; Sanechika, K.; Yamamoto, A., Preparation of thermostable and electric-conducting poly(2,5-thienylene). *Journal of Polymer Science: Polymer Letters Edition* **1980,** *18* (1), 9-12.

29. Lin, J. W. P.; Dudek, L. P., Synthesis and properties of poly(2,5-thienylene). *Journal of Polymer Science: Polymer Chemistry Edition* **1980,** *18* (9), 2869-2873.

30. Takahata, H.; Suzuki, T.; Maruyama, M.; Moriyama, K.; Mozumi, M.; Takamatsu, T.; Yamazaki, T., Iodine-induced iminothiolactonization of γ,δ-unsaturated secondary thio-amides. new entry to 2-acetoamidothiophenes. *Tetrahedron* **1988,** *44* (15), 4777-4786.

31. Ei-ichi Negishi; Fen-Tair Luo; Roger Frisbee; Matsushita, H., A Regiospecific Synthesis of Carbosubstituted Heteroaromatic Derivatives via Pd-Catalyzed Cross Coupling. *Heterocycles* **1982,** *18* (1), 117-122.

32. Tamao, K.; Sumitani, K.; Kumada, M., Selective carbon-carbon bond formation by cross-coupling of Grignard reagents with organic halides. Catalysis by nickel-phosphine complexes. *Journal of the American Chemical Society* **1972,** *94* (12), 4374-4376.

33. Carsten, B.; He, F.; Son, H. J.; Xu, T.; Yu, L., Stille Polycondensation for Synthesis of Functional Materials. *Chemical Reviews* **2011,** *111* (3), 1493-1528.

34. Chen, T. A.; Rieke, R. D., The first regioregular head-to-tail poly(3-hexylthiophene-2,5-diyl) and a regiorandom isopolymer: nickel versus palladium catalysis of 2(5)-bromo-5(2)-(bromozincio)-3-hexylthiophene polymerization. *Journal of the American Chemical Society* **1992,** *114* (25), 10087-10088.

35. McCullogh, R. D.; Williams, S. P.; Tristam-Nagle, S.; Jayaraman, M.; Ewbank, P. C.; Miller, L., The first synthesis and new properties of regioregular, head-to-tail coupled polythiophenes. *Synthetic Metals* **1995,** *69* (1), 279-282.

36. Katsumi, Y.; Shigenori, H.; Ryu-ichi, S., Preparation and Properties of Conducting Heterocyclic Polymer Films by Chemical Method. *Japanese Journal of Applied Physics* **1984,** *23* (12A), L899.

37. Andersson, M. R.; Selse, D.; Berggren, M.; Jaervinen, H.; Hjertberg, T.; Inganaes, O.; Wennerstroem, O.; Oesterholm, J. E., Regioselective polymerization of 3-(4-octylphenyl)thiophene with FeCl3. *Macromolecules* **1994,** *27* (22), 6503-6506.

38. Osaka, I.; McCullough, R. D., Advances in Molecular Design and Synthesis of Regioregular Polythiophenes. *Accounts of Chemical Research* **2008,** *41* (9), 1202-1214.

39. Wang, Q.; Takita, R.; Kikuzaki, Y.; Ozawa, F., Palladium-Catalyzed Dehydrohalogenative Polycondensation of 2-Bromo-3-hexylthiophene: An Efficient Approach to Head-to-Tail Poly(3-hexylthiophene). *Journal of the American Chemical Society* **2010,** *132* (33), 11420-11421.

40. Berrouard, P.; Najari, A.; Pron, A.; Gendron, D.; Morin, P.-O.; Pouliot, J.-R.; Veilleux, J.; Leclerc, M., Synthesis of 5-Alkyl[3,4-c]thienopyrrole-4,6-dione-Based Polymers by Direct Heteroarylation. *Angewandte Chemie International Edition* **2011,** *51* (9), 2068-2071.

41. Bura, T.; Morin, P.-O.; Leclerc, M., En Route to Defect-Free Polythiophene Derivatives by Direct Heteroarylation Polymerization. *Macromolecules* **2015,** *48* (16), 5614-5620.

42. Bura, T.; Beaupré, S.; Ibraikulov, O. A.; Légaré, M.-A.; Quinn, J.; Lévêque, P.; Heiser, T.; Li, Y.; Leclerc, N.; Leclerc, M., New Fluorinated Dithienyldiketopyrrolopyrrole Monomers and Polymers for Organic Electronics. *Macromolecules* **2017,** *50* (18), 7080-7090.

43. Rudenko, A. E.; Wiley, C. A.; Tannaci, J. F.; Thompson, B. C., Optimization of direct arylation polymerization conditions for the synthesis of poly(3-hexylthiophene). *Journal of Polymer Science Part A: Polymer Chemistry* **2013,** *51* (12), 2660-2668.

44. Gobalasingham, N. S.; Noh, S.; Thompson, B. C., Palladium-catalyzed oxidative direct arylation polymerization (Oxi-DArP) of an ester-functionalized thiophene. *Polymer Chemistry* **2016,** *7* (8), 1623-1631.

45. http://www.chem.cmu.edu/groups/mccullough/research/rr-poly3alkylthiophene/index.html.

46. Perepichka, I. F.; Perepichka, D. F.; Meng, H.; Wudl, F., Light-Emitting Polythiophenes. *Advanced Materials* **2005,** *17* (19), 2281-2305.

47. Casanovas, J.; Zanuy, D.; Alemán, C., Structural and electronic effects induced by carboxylic acid substitution in isomeric 2,2′-bithiophenes and oligothiophenes: A computational study. *Polymer* **2005,** *46* (22), 9452-9460.

48. Casanovas, J.; Aradilla, D.; Poater, J.; Solà, M.; Estrany, F.; Alemán, C., Properties of poly(3-halidethiophene)s. *Physical Chemistry Chemical Physics* **2012,** *14* (28), 10050-10062.

49. Li, C.; Shi, G., Polythiophene-Based Optical Sensors for Small Molecules. *ACS Applied Materials & Interfaces* **2013,** *5* (11), 4503-4510.

50. Rajwar, D.; Ammanath, G.; Cheema, J. A.; Palaniappan, A.; Yildiz, U. H.; Liedberg, B., Tailoring Conformation-Induced Chromism of Polythiophene Copolymers for Nucleic Acid Assay at Resource Limited Settings. *ACS Applied Materials & Interfaces* **2016,** *8* (13), 8349-8357.

51. Li, C.; Numata, M.; Takeuchi, M.; Shinkai, S., A Sensitive Colorimetric and Fluorescent Probe Based on a Polythiophene Derivative for the Detection of ATP. *Angewandte Chemie* **2005,** *117* (39), 6529-6532.

52. McQuade, D. T.; Pullen, A. E.; Swager, T. M., Conjugated Polymer-Based Chemical Sensors. *Chemical Reviews* **2000,** *100* (7), 2537-2574.

53. Leclerc, M., Optical and Electrochemical Transducers Based on Functionalized Conjugated Polymers. *Advanced Materials* **1999,** *11* (18), 1491-1498.

54. Faïd, K.; Leclerc, M., Responsive Supramolecular Polythiophene Assemblies. *Journal of the American Chemical Society* **1998,** *120* (21), 5274-5278.

55. Leclerc, M.; Faid, K., Electrical and optical properties of Processable Polythiophene Derivatives: Structure-Property relationships. *Advanced Materials* **1997,** *9* (14), 1087-1094.

56. Yao, Z.; Ma, W.; Yang, Y.; Chen, X.; Zhang, L.; Lin, C.; Wu, H.-C., Colorimetric and fluorescent detection of protamines with an anionic polythiophene derivative. *Organic & Biomolecular Chemistry* **2013,** *11* (38), 6466-6469.

57. Nilsson, K. P. R.; Rydberg, J.; Baltzer, L.; Inganäs, O., Self-assembly of synthetic peptides control conformation and optical properties of a zwitterionic polythiophene derivative. *Proceedings of the National Academy of Sciences of the United States of America* **2003,** *100* (18), 10170-10174.

58. Andersson, M.; O. Ekeblad, P.; Hjertberg, T.; Wennerstroem, O.; Ingenas, O., *Polythiophene with a free amino acid side chain*. 1991; Vol. 32, p 546-548.

59. Wang, F.; Li, M.; Wang, B.; Zhang, J.; Cheng, Y.; Liu, L.; Lv, F.; Wang, S., Synthesis and Characterization of Water-Soluble Polythiophene Derivatives for Cell Imaging. *Scientific Reports* **2015,** *5*, 7617.

60. Nilsson, K. P. R.; Inganäs, O., Chip and solution detection of DNA hybridization using a luminescent zwitterionic polythiophene derivative. *Nature Materials* **2003,** *2*, 419.

61. Yao, Z.; Feng, X.; Hong, W.; Li, C.; Shi, G., A simple approach for the discrimination of nucleotides based on a water-soluble polythiophene derivative. *Chemical Communications* **2009,** (31), 4696-4698.

62. Moore, L. D.; Le, T.; Fan, G., DNA Methylation and Its Basic Function. *Neuropsychopharmacology* **2012,** *38*, 23.

63. Robertson, K. D., DNA methylation and human disease. *Nature Reviews Genetics* **2005,** *6*, 597.

64. Suzuki, M. M.; Bird, A., DNA methylation landscapes: provocative insights from epigenomics. *Nature Reviews Genetics* **2008,** *9*, 465.

65. Bernstein, B. E.; Meissner, A.; Lander, E. S., The Mammalian Epigenome. *Cell* **2007,** *128* (4), 669-681.

66. Pan, S.; Xu, J.; Shu, Y.; Wang, F.; Xia, W.; Ding, Q.; Xu, T.; Zhao, C.; Zhang, M.; Huang, P.; Lu, S., Double recognition of oligonucleotide and protein in the detection of DNA methylation with surface plasmon resonance biosensors. *Biosensors and Bioelectronics* **2010,** *26* (2), 850-853.

67. Xu, Y.; Wu, F.; Tan, L.; Kong, L.; Xiong, L.; Deng, J.; Barbera, A. J.; Zheng, L.; Zhang, H.; Huang, S.; Min, J.; Nicholson, T.; Chen, T.; Xu, G.; Shi, Y.; Zhang, K.; Shi, Yujiang G., Genome-wide Regulation of 5hmC, 5mC, and Gene Expression by Tet1 Hydroxylase in Mouse Embryonic Stem Cells. *Molecular Cell* **2011,** *42* (4), 451-464.

68. Bird, A., DNA methylation patterns and epigenetic memory. *Genes & Development* **16,** *16*, 6-21.

69. Bestor, T. H., The DNA methyltransferases of mammals. *Human Molecular Genetics* **2000,** *9* (16), 2395-2402.

70. Okano, M.; Bell, D. W.; Haber, D. A.; Li, E., DNA Methyltransferases Dnmt3a and Dnmt3b Are Essential for De Novo Methylation and Mammalian Development. *Cell* **1999,** *99* (3), 247-257.

71. Bird, A.; Taggart, M.; Frommer, M.; Miller, O. J.; Macleod, D., A fraction of the mouse genome that is derived from islands of nonmethylated, CpG-rich DNA. *Cell* **1985,** *40* (1), 91-99.

72. Saxonov, S.; Berg, P.; Brutlag, D. L., A genome-wide analysis of CpG dinucleotides in the human genome distinguishes two distinct classes of promoters. *Proceedings of the National Academy of Sciences* **2006,** *103* (5), 1412.

73. Craig, J. M.; Bickmore, W. A., The distribution of CpG islands in mammalian chromosomes. *Nature Genetics* **1994,** *7*, 376.

74. Illingworth, R. S.; Bird, A. P., CpG islands – 'A rough guide'. *FEBS Letters* **2009,** *583* (11), 1713-1720.

75. Carninci, P.; Sandelin, A.; Lenhard, B.; Katayama, S.; Shimokawa, K.; Ponjavic, J.; Semple, C. A. M.; Taylor, M. S.; Engström, P. G.; Frith, M. C.; Forrest, A. R. R.; Alkema, W. B.; Tan, S. L.; Plessy, C.; Kodzius, R.; Ravasi, T.; Kasukawa, T.; Fukuda, S.; Kanamori-Katayama, M.; Kitazume, Y.; Kawaji, H.; Kai, C.; Nakamura, M.; Konno, H.; Nakano, K.; Mottagui-Tabar, S.; Arner, P.; Chesi, A.; Gustincich, S.; Persichetti, F.; Suzuki, H.; Grimmond, S. M.; Wells, C. A.; Orlando, V.; Wahlestedt, C.; Liu, E. T.; Harbers, M.; Kawai, J.; Bajic, V. B.; Hume, D. A.; Hayashizaki, Y., Genome-wide analysis of mammalian promoter architecture and evolution. *Nature Genetics* **2006,** *38*, 626.

76. Tryndyak, V.; Kovalchuk, O.; Pogribny, I. P., Identification of differentially methylated sites within unmethylated DNA domains in normal and cancer cells. *Analytical Biochemistry* **2006,** *356* (2), 202-207.

77. Ducasse, M.; Brown, M. A., Epigenetic aberrations and cancer. *Molecular Cancer* **2006,** *5* (1), 60.

78. Shenker, N.; Flanagan, J. M., Intragenic DNA methylation: implications of this epigenetic mechanism for cancer research. *British Journal Of Cancer* **2011,** *106*, 248.

79. Tryndyak, V. P.; Kovalchuk, O.; Pogribny, I. P., Loss of DNA methylation and histone H4 lysine 20 trimethylation in human breast cancer cells is associated with aberrant expression of DNA methyltransferase 1, Suv4-20h2 histone methyltransferase and methyl-binding proteins. *Cancer Biology & Therapy* **2006,** *5* (1), 65-70.

80. Jones, P. A.; Baylin, S. B., The Epigenomics of Cancer. *Cell* **2007,** *128* (4), 683-692.

81. Myöhänen, S.; Baylin, S. B., Sequence-specific DNA Binding Activity of RNA Helicase A to thep16INK4a Promoter. *Journal of Biological Chemistry* **2001,** *276* (2), 1634-1642.

82. Hedman, M.; Bergqvist, M.; BrattstrÖM, D.; Brodin, O. L. A., Fractionated Irradiation of Five Human Lung Cancer Cell Lines and Prediction of Survival According to a Radiobiology Model. *Anticancer Research* **2011,** *31* (4), 1125-1130.

83. Levenson, V. V., DNA methylation as a universal biomarker. *Expert Review of Molecular Diagnostics* **2010,** *10* (4), 481-488.

84. Gonzalgo, M. L.; Liang, G.; Spruck, C. H.; Zingg, J.-M.; Rideout, W. M.; Jones, P. A., Identification and Characterization of Differentially Methylated Regions of Genomic DNA by Methylation-sensitive Arbitrarily Primed PCR. *Cancer Research* **1997,** *57* (4), 594.

85. Leshchenko, V. V.; Kuo, P.-Y.; Shaknovich, R.; Yang, D. T.; Gellen, T.; Petrich, A.; Yu, Y.; Remache, Y.; Weniger, M. A.; Rafiq, S.; Suh, K. S.; Goy, A.; Wilson, W.; Verma, A.; Braunschweig, I.; Muthusamy, N.; Kahl, B. S.; Byrd, J. C.; Wiestner, A.; Melnick, A.; Parekh, S., Genomewide DNA

methylation analysis reveals novel targets for drug development in mantle cell lymphoma. *Blood* **2010,** *116* (7), 1025-1034.

86. Dahl, C.; Guldberg, P., DNA methylation analysis techniques. *Biogerontology* **2003,** *4* (4), 233-250.

87. Wang, J.; Zhu, Z.; Ma, H., Label-Free Real-Time Detection of DNA Methylation Based on Quartz Crystal Microbalance Measurement. *Analytical Chemistry* **2013,** *85* (4), 2096-2101.

88. Flusberg, B. A.; Webster, D. R.; Lee, J. H.; Travers, K. J.; Olivares, E. C.; Clark, T. A.; Korlach, J.; Turner, S. W., Direct detection of DNA methylation during single-molecule, real-time sequencing. *Nature Methods* **2010,** *7*, 461.

89. Tost, J.; Gut, I. G., DNA methylation analysis by pyrosequencing. *Nature Protocols* **2007,** *2*, 2265.

90. El-Maarri, O.; Herbiniaux, U.; Walter, J.; Oldenburg, J., A rapid, quantitative, non-radioactive bisulfite-SNuPE- IP RP HPLC assay for methylation analysis at specific CpG sites. *Nucleic acids research* **2002,** *30* (6), e25-e25.

91. Goedecke, S.; Schlosser, S.; Mühlisch, J.; Hempel, G.; Frühwald, M. C.; Wünsch, B., Determination of DNA methylation by COBRA: A comparative study of CGE with LIF detection and conventional gel electrophoresis. *ELECTROPHORESIS* **2009,** *30* (17), 3063-3070.

92. Chen, H.-C.; Chang, Y.-S.; Chen, S.-J.; Chang, P.-L., Determination of the heterogeneity of DNA methylation by combined bisulfite restriction analysis and capillary electrophoresis with laser-induced fluorescence. *Journal of Chromatography A* **2012,** *1230*, 123-129.

93. Ehrich, M.; Nelson, M. R.; Stanssens, P.; Zabeau, M.; Liloglou, T.; Xinarianos, G.; Cantor, C. R.; Field, J. K.; van den Boom, D., Quantitative high-throughput analysis of DNA methylation patterns by base-specific cleavage and mass spectrometry. *Proceedings of the National Academy of Sciences of the United States of America* **2005,** *102* (44), 15785.

94. Kim, H. N.; Ren, W. X.; Kim, J. S.; Yoon, J., Fluorescent and colorimetric sensors for detection of lead, cadmium, and mercury ions. *Chemical Society Reviews* **2012,** *41* (8), 3210-3244.

95. Lin, Y.-Z.; Chang, P.-L., Colorimetric Determination of DNA Methylation Based on the Strength of the Hydrophobic Interactions between DNA and Gold Nanoparticles. *ACS Applied Materials & Interfaces* **2013,** *5* (22), 12045-12051.

96. Young, D. C., Computational Chemistry: A Practical Guide for Applying Techniques to Real-World Problems. *John Wiley & Sons* **2001,** *1*, 1-370.